Doctoral Dissertation

Department of Advanced Materials Science
Graduate School of Frontier Sciences, The University of Tokyo

Precise Analyses of High Performance Polymer Gels

2011

Takuro Matsunaga

Acknowledgements

This thesis is based on the study carried out in the research group of Professor Mitsuhiro Shibayama at Department of Advanced Materials Science, Graduate School of Frontier Sciences, The University of Tokyo from 2006 to 2011.

First of all, I would like to express my sincere gratitude to **Professor Mitsuhiro Shibayama** for kind guidance and for giving many opportunities throughout my life in laboratory. He guided me into polymer physics and has given me his knowledge generously. Especially, he taught me about attitudes towards science. I really appreciate his instruction.

I would also like to thank **Dr. Hitoshi Endo** and **Dr. Hiroki Iwase** for their advices on small-angle neutron scattering experiments. With their helps, I could accomplish this study. I am very grateful for their generosity.

I would like to acknowledge valuable advices and helpful discussions given by **Professor Ung-il Chung** and **Dr. Takamasa Sakai** at The University of Tokyo. I could not accomplish this thesis without their cooperations. **Ms. Yuki Akagi**, **Ms. Manami Kurakazu** and **Mr. Kengo Nishi**; all of who are students of Chung and Sakai laboratory, for supplying the nice samples of Tetra-PEG gel.

I would like to thank all the members of Shibayama Laboratory, especially, **Dr. Satoshi Okabe** for teaching me basic experimental techniques and attitudes towards research. The present and past members of Shibayama group are also appreciated for their helpful cooperations.

My special thanks go to the staff of Neutron Science Laboratory for their kind supports in neutron scattering experiments.

I would like to thank all the members of Neutron Science Laboratory, especially, **Dr. Yosuke Moriya**, **Dr. Takeshi Yamada**, **Mr. Norihiro Inomoto**, **Mr. Rei Morinaga**, **Mr. Ryo Yonamine**, **Mr Takenori Someya**, **Mr. Takamasa Suzuki**, **Ms. Keiko Ninomiya**, **Ms. Naomi Inoue**, **Ms. Yukari Mitsui** and **Ms. Akiko Goto** for their friendship and encouragements. I was so happy to spend with them in laboratory.

In addition to my personal acknowledgements, I can not forget to recognize the fol-

lowing financial supports during my postgraduate life: a Grant-in-Aid for the Global COE program "Global Center of Excellence for Physical Sciences Frontier, The University of Tokyo", MEXT, Japan (2008-2009), and Research Fellowships of the Japan Society for the Promotion of Science for Young Scientists(2010).

Last but not least, I am deeply grateful to my parents, **Mamoru Matsunaga**, **Kayoko Matsunaga** and my brother, **Soichiro Matsunaga** for their continuous support, encouragement and understanding.

March, 2011
Takuro Matsunaga

Contents

Chapter 1

General Introduction

1.1 Polymer gels and "Inhomogeneities" in gels

Hydrogels are defined as three-dimensional polymer networks swollen in water. Most hydrogels are composed of more than 90% of water. Initially, taking advantage of their high water absorption and retention properties, hydrogels were applied to diapers, contact lenses, drug reservoirs, etc. After the volume-phase transition behavior was discovered by Tanaka in 1978,[1] a variety of functional materials such as sensors and actuators were developed based on their stimulus-responsiveness.[2–6] Despite these unique characteristics, practical applications of hydrogels, especially as structural materials, are restricted because of their low mechanical strength, which results from their micro-inhomogeneities of polymeric topological structure created by cross-linking.[7] These inhomogeneities are inevitably introduced to a network, and are categorized into three types, i.e., spatial, connectivity, and topological inhomogeneities (Figure 1.1).[8] The spatial inhomogeneity is an inhomogeneous distribution of polymer segments in the network, and is observed as an excess scattering in small-angle light scattering (SALS) as well as small-angle neutron scattering (SANS) measurements.[9–11] The connectivity inhomogeneity includes dangling chains and elastically redundant loops, while the topological inhomogeneity includes trapped entanglements. The connectivity and topological inhomogeneities are generally discussed in the context of the theory of tree-like structure and elastically effective chains.[12,13] Because the connectivity and topological inhomogeneities have opposite effect on the elastically effective chains, these contributions cannot be decomposed. Therefore, the understanding of the rubber elasticity remains a controversial issue in polymer

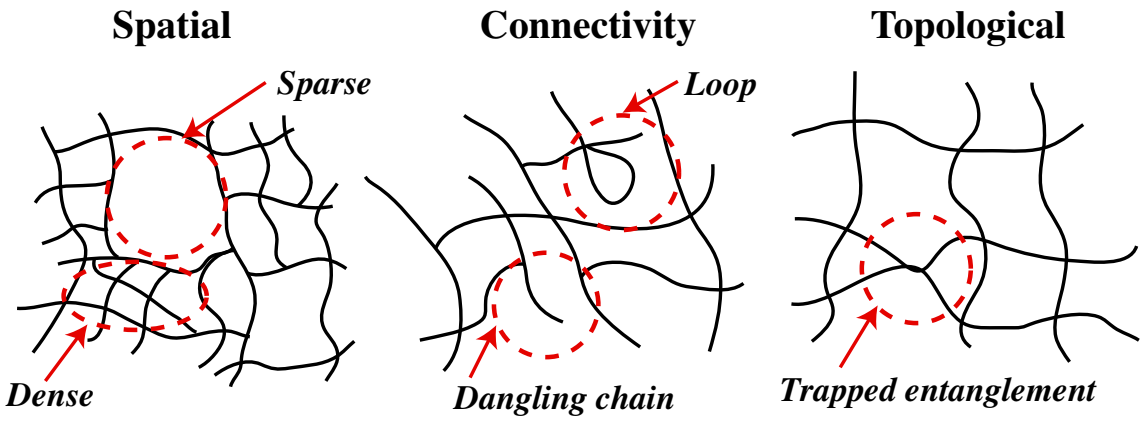

Figure 1.1: Schematic illustration of various types of inhomogeneities for polymer gels: (a) spatial inhomogeneities, (b) connectivity inhomogeneities, and (c) topological inhomogeneities.

science. In the history of the development of polymer networks, primitive randomly cross-linked networks were formed by radical polymerization using monomers and cross-linkers or by the vulcanization of polymer melts. Although these cross-linking methods are easy to perform and have been used widely up to now, they yield networks with a large number of inhomogeneities.[14] As mentioned above, three types of inhomogeneities affect the macroscopic properties of the network structure. Especially, trapped entanglements affect the extensibility of the network, which is one of the most important properties of polymer materials. As for the ideal network, the polymerization degree between neighboring chemical cross-links (N_x) determines the maximum extensibility ($\lambda_{\max}$). Theoretically, the value of $\lambda_{\max}$ is given by the ratio of the fully extended length to the initial end-to-end length of the polymer with polymerization degree of N_x.[15] Therefore, the $\lambda_{\max}$ increases as N_x increases. On the other hand, in the case of real networks, trapped entanglements, i.e., pseudo-crosslinks, exist. Because the degree of polymerization between neighboring entanglements (N_e) is smaller than N_x, the value of $\lambda_{\max}$ is given by the ratio of the fully extended length to the initial end-to-end length of the polymer with polymerization degree of N_e.[16] Because the N_e varies depending on the polymer species and concentrations, it is difficult to control $\lambda_{\max}$. In addition, N_e has inhomogeneous distribution, because entanglements are trapped at random. Therefore, an external load applied to an inhomogeneous network concentrates on the weakest regions, leading to microscopic

fracture. Then, the stress is stepwisely concentrated on the next weakest region, eventually leading to macroscopic fracture. Therefore, the mechanical properties of the conventional networks become much lower than those of the corresponding ideal network; usually the $\lambda_{\max}$ is approximately $2 \sim 5$.[16]

Recently, however, some exceptions are reported. For example, polymer gels which do not exhibit nonergodicity are reported by Wu.[17] They demonstrated that inhomogeneities in an assembly of microgels were strongly suppressed if individual swollen microgels were closely packed to each other. On the basis of this experimental evidence, they concluded that static nonergodic behavior originated from large "voids" formed during sol-gel transition in polymerization process. It should be noted, however, that the gels reported by Wu were microgels, and the absence of inhomogeneities was exclusively observed in jam-packed state where the concentration fluctuations are strongly suppressed. Here, the "voids" mean polymer-poor region in a gel. Inhomogeneities are also found even in physical gels, which spontaneously tune their network by "detachable" cross-links so as to minimize the free energy of entropy elasticity.[18,19] Here, a frozen component in the concentration fluctuations starts to appear as soon as a sol-gel transition occurs. Therefore, in general, polymer gels inherently possess inhomogeneities because of the presence of cross-links.

1.2 High performance gel and "ideal" network

Since the physical properties of gels strongly depend on the structure, it is extremely important to clarify the relationship between structure and mechanical properties. The understanding of cross-link inhomogeneities is vital from both scientific and engineering points of view since they affect the physical properties of the network polymer.[20] Especially, it is important to consider the relationship between inhomogeneities and physical properties. As the networks cannot behave cooperatively due to inhomogeneities in a network structure, they begin to break from the weakest link, thus reducing the whole mechanical strength. In order to achieve the cooperativeness, various types of hydrogels with unique network structure have been developed, e.g., a topological gel with sliding cross-linkers,[21] a nano-composite gel synthesized by polymerizing with dispersed clay disks,[22] and a double network gel containing

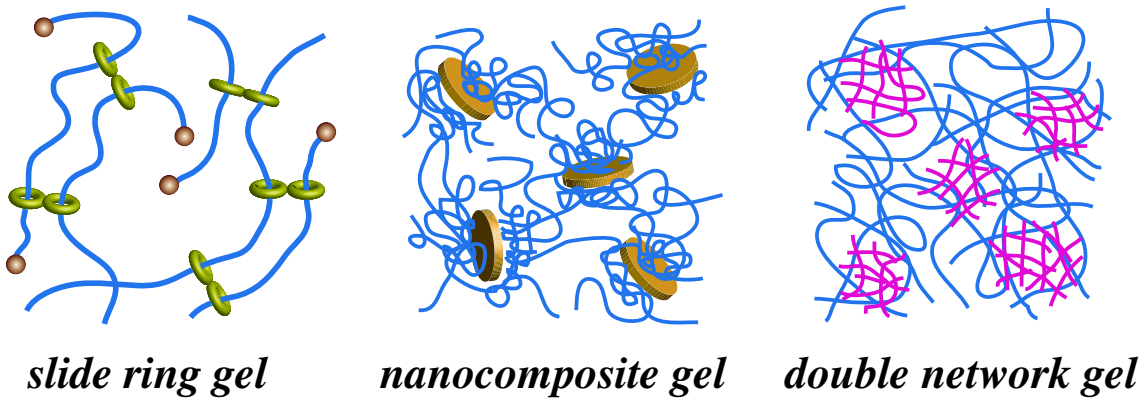

Figure 1.2: Schematic illustration of various types of high performance polymer gels: (a) slide ring gel, (b) nanocomposite gel, and (c) double network gel.

two types of independent networks.[23] Figure 1.2 shows the schematic illustration of these high performance gels. In contrast to these unique gels, other researchers have pursued ideally homogeneous network structure for a long time. If a polymer network were an infinite series of uniform meshes connected by cross-links and had no inhomogeneities, the macroscopic properties of the network would be precisely controlled by the polymerization degree and the first order structure of the mesh chains. Such a perfectly cooperative network is called an "ideal" network. In reality, however, inhomogeneities do exist and affect the cooperativeness between the meshes, compromising the macroscopic properties. The ideally homogeneous gel network is expected to have high mechanical properties including modulus and breaking strength.[24] In an attempt at realizing an ideal network, model networks were formed by using a modular construction method, that is, by using monodispersed chain extenders and multifunctional cross-linkers.[24,25] Due to the use of the preprogrammed and monodispersed chain extenders, the degree of polymerization between chemical cross-links was precisely controlled. However, it was revealed that the obtained model networks did contain a substantial number of inhomogeneities.[26,27]

1.3 Previous studies on "ideal" polymer network

In order to obtain an ideal gel network along with its resultant high mechanical properties, many attempts were made, including gelation by physical cross-linking,

gelation from macro-monomers,[26] gelation from polymers by gamma-ray irradiation,[28] etc. Homogeneity could be relatively easily obtained by physical cross-linking. However, the homogeneity cannot be controlled strictly in physical gels because cross-linking occurs at random. In addition, physical cross-linking was generally weak, and the resulting physical gels became soft and weak. Gelation from macro-monomers seemed more promising than the others because the detailed network structure was controllable by designing constitutional units, and the gelation process was predicted easily by the tree-approximation of Flory and the cascade model of Gordon.[29,30] He et al. reported the synthesis of jungle-gym-type polyimide organogels using trifunctional cross-linkers and telechelic rigid aromatic oligomers as backbones, which had a high compression modulus.[31] However, there has been no success to prepare defect-free networks so far.[32–34] No matter how precisely one controlled the architecture, the obtained "model network" had strong forward scattering at low q region and or exhibited double shoulder scattering curves. For example, Mendes et al. classified gel structures to (I) the one-correlation length gels, (II) the soft order gels that have a scattering maximum, and (III) the two-correlation length gels.[33] As for hydrogels, there were numerous studies to obtain the homogeneous biocompatible hydrogels.[35–38] To the best of our knowledge, however, no hydrogels formed from macromonomers have compressive strength reaching a MPa-range; most of the papers did not discuss the compressive strength, which is one of the most important parameters for practical use. The fragility may come from micro-inhomogeneity of the network structure. Focusing the spotlight on constitutional unit of the network, most of gels from macromonomers were formed from asymmetrical components such as multifunctional cross-linkers and telechelic polymers. These asymmetrical combinations should give the network a high degree of freedom, allowing various micro-structure including loops and defects. These various micro-inhomogeneities deprive network of the cooperativeness, resulting in weakening the gels.

1.4 Tetra-PEG gel

Sakai et al. developed a novel class of hydrogels that meet all of these criteria, i.e., high mechanical strength and toughness, easy preparation, and biocompatibil-

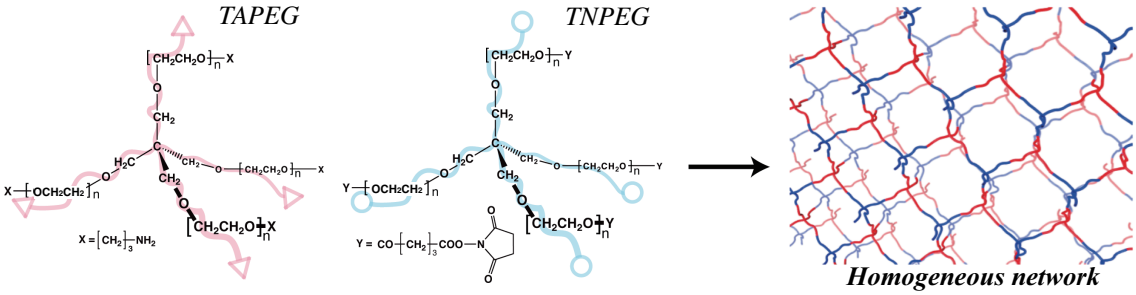

Figure 1.3: Molecular structure of Tetra-PEG and model illustration of Tetra-PEG gel.

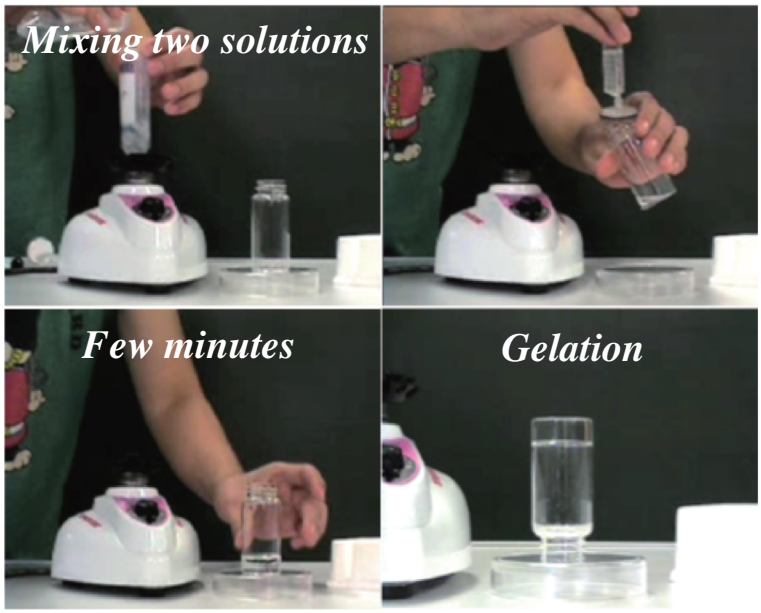

Figure 1.4: Preparation process of Tetra-PEG gels.

ity. The gel, called Tetra-PEG gel, consists of two kinds of four-arm polyethylene glycol (PEG) macromers of the same size, tetra-amine-terminated PEG (TAPEG) and tetra-NHS-glutarate-terminated PEG (TNPEG). Here, NHS represents for N-hydroxysuccinimide (Figure 1.3).

By mixing TAPEG and TNPEG aqueous solutions, Tetra-PEG gel can be instantaneously formed not only in laboratory but also in vitro (Figure 1.4 and in vivo). The mechanical properties are remarkably high (of the order of a few to tens MPa for the strength at break for 120 mg/mL Tetra-PEG gel made of 10kDa macromers), being comparable to those of native articular cartilage (approximately 6-10 MPa).

Tetra-PEG gel seems to have an extremely homogeneous network structure with very low degrees of defects in the network.

1.5 Outline of the Dissertation

By considering the above discussion, I intended to study the relationship between micro-structure and physical properties of the new-type hydrogel, Tetra-PEG gel. The following is the lineup of the contents of this dissertation.

Chapter 2;

A simple but reasonably accurate method for incoherent neutron scattering intensity evaluation for hydrogen-containing materials is proposed. An evaluation of incoherent scattering is very important especially for precise analysis for softmatter systems. Hydrogen atom has a large incoherent scattering cross section and is a major source of the incoherent scattering intensity, $(\mathrm{d}\Sigma/\mathrm{d}\Omega)_{\mathrm{inc}}$, in small-angle neutron scattering (SANS). The structure information is obtained from the coherent scattering, whereas the incoherent scattering provides a scattering-angle-independent background. By taking account of multiple scattering from hydrogen atoms, we propose a useful method (the transmission method; T-method) for the estimation of $(\mathrm{d}\Sigma/\mathrm{d}\Omega)_{\mathrm{inc}}$ for various types of H-containing systems. The incoherent scattering intensity is calculated simply by the transmission, T, and the thickness of the sample, t, i.e., $(\mathrm{d}\Sigma/\mathrm{d}\Omega)_{\mathrm{inc}} \cong [\exp(\Sigma_{\mathrm{tot}}t) - 1]/(4\pi t) = (1-T)/(4\pi t T)$, where $\Sigma_{\mathrm{tot}} \equiv -(\ln T)/t$ is the macroscopic total cross section per unit volume. This method provides a reasonable approximate value of incoherent scattering intensity for various systems. The validity and the extent of applicability of the T-method are examined for several samples, including, light/heavy water mixtures, polymer gels, and surfactant aqueous dispersions.

Chapter 3;

As a new class of high-strength hydrogels, we designed a tetra-PEG gel by combining two symmetrical tetrahedron-like macromonomers of the same size. Because the nanostructural unit of the gel network was defined by the length of the tetrahe-

dral PEG arm, the gel had a homogeneous structure and resultant high mechanical strength comparable to that of native articular cartilage. Furthermore, since the gel was formed by mixing two biocompatible macromonomer solutions, the gelation reaction itself and the resultant gel were also biocompatible.We successfully designed and fabricated a high-strength hydrogel by controlling the homogeneity of network structure for the first time, which will lead to multiplied effects, i.e., contributing to the understanding of ideal networks, providing a universal strategy for designing high-strength gels, and opening up the biomedical application of hydrogels.

Chapter 4;

In order to elucidate the relationship between physical properties and structure, we carried out the small-angle neutron scattering (SANS) experiments of the Tetra-PEG gel, as well as the precursor macromers, i.e., TAPEG and TNPEG, in aqueous solutions. The molecular weights (M_{w}) of TAPEG and TNPEG were matched to be either 10 k or 20 k g/mol. The initial macromer concentrations were varied from 5 to 160 mg/mL. Moreover, we carried out SANS and mechanical testing experiments for nonstoichiometric Tetra-PEG gels that were prepared with nonstoichiometric compositions. Structural models of macromer solutions and of Tetra-PEG gels, which account for the advanced mechanical properties of Tetra-PEG gels, are proposed.

Chapter 5;

The structure and dynamics of Tetra-PEG gels have been investigated by SANS and static light scattering (SLS). The Tetra-PEG gels were prepared by cross-end coupling of two types of tetra-arm PEG macromers with molecular weights, M_{w}, of (5 to 40) kg/mol. SANS experiments were carried out for the swollen gel in swelling equilibrium, as well as the precursor macromer solutions and the as-prepared gels. we discuss the structure of Tetra-PEG gels in more details with the scattering intensity data in a wide q range covering not only SANS ($0.003 \leq q \leq 0.2$ Å^{-1}) but also light scattering (LS) regime ($0.0008 \leq q \leq 0.002$ Å^{-1}).

Chapter 6;

Studies on deformation mechanism of polymer networks with small-angle neutron scattering (SANS) were carried out for near-"ideal" polymer networks consist-

ing of narrow-dispersed inter-cross-linked polymer chains free from dangling chains and entanglements. The polymer networks, Tetra-PEG gels, were prepared from tetra-functional A- and B-type macromers consisting of poly(ethylene glycol)(PEG) with the molecular weights of 20k and 40k by A-B cross-end-coupling. Though the SANS patterns of deformed Tetra-PEG gel-20k showed small anisotropy, i.e., prolate and oblate patterns with respect to the stretching direction at low and large-q regions, respectively, Tetra-PEG gel-40k exhibited no inhomogeneities at all even in a gel stretched by 5 times. We discuss the microscopic deformation mechanism of Tetra-PEG gels by comparing experimental results with some theoretical models (i.e., affine, junction-affine, and phantom model). Focuses are placed on (1) the relationship of spatial inhomogeneities and the gel structure and (2) deformation mechanism of Tetra-PEG gels.

Chapter 7;

Following the discussion in Chapters 2-6, we discussed the relationship between microscopic structure and macroscopic mechanical properties in Chapter 7. We carried out the dynamic viscoelastic, stretching, and compressive properties of the Tetra-PEG gels in order to compare them with those of the ideal network. The mechanical energy dissipation was extremely low ($\tan \delta \sim 10^{-4}$). The macroscopic stress-strain relationship of the Tetra network was in good agreement with that of microscopic "elastic blobs".

References

[1] Tanaka, T. *Polymer* 1979, 20, (11), 1404-1412.

[2] Miyata, T.; Uragami, T.; Nakamae, K. *Advanced Drug Delivery Reviews* 2002, **54**, (1), 79-98.

[3] Nakayama, D.; Takeoka, Y.; Watanabe, M.; Kataoka, K. *Angew. Chem.* 2003, **42**, (35), 4197-4200.

[4] Osada, Y.; Okuzaki, H.; Hori, H. *Nature* 1992, **355**, (6357), 242-244.

[5] Okuzaki, H.; Kunugi, T. *Journal of Polymer Science Part B-Polymer Physics* 1996, **34**, (10), 1747-1749.

[6] Zrinyi, M.; Feher, J.; Filipcsei, G. *Macromolecules* 2000, **33**, (16), 5751-5753.

[7] Shibayama, M. *Bulletin of the Chemical Society of Japan* 2006, **79**, (12), 21.

[8] M. Shibayama, *Macromol. Chem. Phys.* 1998, **199**, 1.

[9] J. Bastide, L. Leibler, *Macromolecules* 1988, **21**, 2647.

[10] E. Mendes, R. Oeser, C. Hayes, F. Boue, J. Bastide, *Macromolecules* 1996, **29**, 5574.

[11] M. Shibayama, Y. Shirotani, Y. Shiwa, *J. Chem. Phys.* 2000, **112**, 442.

[12] M. Rubinstein, S. Panyukov, *Macromolecules* 2002, **35**, 6670.

[13] K. Dusek, V. Vojta, Br. *Polym. J.* 1977, **9**, 164.

[14] E. Mendes, A. Hakiki, J. Herz, F. Boue, J. Bastide, *Macromolecules* 2004, **37**, 2643.

[15] W. Kuhn, *J. Polym. Sci.* 1946, **1**, 380.

[16] K. Urayama, T. Kawamura, S. Kohjiya, *Polymer* 2009, **50**, 347.

[17] Zhao, Y.; Zhang, G.; Wu, C. *Macromolecules* 2001, **34**, 7804-7808.

[18] Ikkai, F.; Shibayama, M. *Phys. Rev. Lett.* 1999, **82**, 4946-4949.

[19] Shibayama, M.; Tsujimoto, M.; Ikkai, F. *Macromolecules* 2000, **33**, 7868-7876.

[20] Shibayama, M.; Takata, S.; Norisuye, T. *Physica A* 1998, **249**, 245-252.

[21] Okumura, Y.; Ito, K. *Advanced Materials* 2001, **13**, (7), 485-+.

[22] Haraguchi, K.; Takehisa, T. *Advanced Materials* 2002, **14**, (16), 1120-1124.

[23] Gong, J. P.; Katsuyama, Y.; Kurokawa, T.; Osada, Y. *Advanced Materials* 2003, **15**, (14), 1155-+.

[24] Mark, J. E.; Erman, B., *Rubberlike Elasticity - A Molecular Primer.* Wiley: 1988.

[25] G. Hild, *Prog. Polym. Sci.* 1998, **23**, 1019.

[26] M. Shibayama, H. Takahashi, S. Nomura, *Macromolecules* 1995, **28**, 6860.

[27] W. Michalke, M. Lang, S. Kreitmeier, D. Goritz, *J. Chem. Phys.* 2002, **117**, 6300.

[28] Norisuye, T.; Masui, N.; Kida, Y.; Ikuta, D.; Kokufuta, E.; Ito, S.; Panyukov, S.; Shibayama, M. *Polymer* 2002, **43**, (19), 5289-5297.

[29] Flory, P. J. *Journal of the American Chemical Society* 1941, **63**, 14.

[30] Gordon, M. *Proceedings of the Royal Society of London Series a-Mathematical and Physical Sciences* 1962, **268**, (1333), 240.

[31] He, J. H.; Machida, S.; Kishi, H.; Horie, K.; Furukawa, H.; Yokota, R. *Journal of Polymer Science Part a-Polymer Chemistry* 2002, **40**, (14), 2501-2512.

[32] Geissler, E.; Horkay, F.; Hecht, A. M.; Rochas, C.; Lindner, P.; Bourgaux, C.; Couarraze, G. *Polymer* 1997, **38**, 15.

[33] Mendes, E.; Hakiki, A.; Herz, J.; Boue ´ , F.; Bastide, J. *Macromolecules* 2004, **37**, 2643-2649.

[34] Sukumaran, S. K.; Beaucage, G.; Mark, J. E.; Viers, B. *Eur. Phys. J. E* 2005, **18**, 29-36.

[35] Martens, P.; Anseth, K. S. *Polymer* 2000, **41**, (21), 7715-7722.

[36] Lutolf, M. P.; Hubbell, J. A. *Biomacromolecules* 2003, **4**, (3), 713-722.

[37] Azab, A. K.; Orkin, B.; Doviner, V.; Nissan, A.; Klein, M.; Srebnik, M.; Rubinstein, A. *Journal of Controlled Release* 2006, **111**, (3), 281-289.

[38] Malkoch, M.; Vestberg, R.; Gupta, N.; Mespouille, L.; Dubois, P.; Mason, A. F.; Hedrick, J. L.; Liao, Q.; Frank, C. W.; Kingsbury, K.; Hawker, C. *J. Chemical Communications* 2006, **26**, 2774-2776.

Chapter 2

Evaluation of Incoherent Scattering Intensity by Transmission and Sample Thickness

2.1 Introduction

Small-angle neutron scattering (SANS) has been a powerful tool for structural characterization of polymeric materials, colloidal dispersions, protein solutions, surfactants, vesicles, gels, etc.[1–4] The scattering intensity in absolute scale, i.e., the differential scattering cross section, $(d\Sigma/d\Omega)(q)$, consists of differential coherent scattering, $(d\Sigma/d\Omega)_{coh}(q)$, and incoherent scattering cross sections, $(d\Sigma/d\Omega)_{inc}$, i.e.,

$$\left(\frac{d\Sigma}{d\Omega}\right)(q) = \left(\frac{d\Sigma}{d\Omega}\right)_{coh}(q) + \left(\frac{d\Sigma}{d\Omega}\right)_{inc}, \tag{2.1}$$

where $(d\Sigma/d\Omega)(q)$ is the differential scattering cross section, q is the momentum transfer. $(d\Sigma/d\Omega)_{coh}(q)$ contains the structural information, such as, the size and shape of the scattering particles, the inter-particle distance, and the scattering contrast between the domains and the matrix. On the other hand, $(d\Sigma/d\Omega)_{inc}$ provides no information about structures and is unnecessary background. Hence, the incoherent scattering subtraction is one of important procedures in data reduction of SANS data and quantitative analyses. The incoherent scattering is mainly originated from the large incoherent scattering cross section of H atom, $\sigma_{inc,H} = 82.26$ barn, which is much larger than its isotope D, $\sigma_{inc,D} = 2.05$ barn and those of other major elements for soft matter systems, i.e., $\sigma_{inc,C} = 0.001$ barn, $\sigma_{inc,O} = 0.0008$ barn, and

$\sigma_{\mathrm{inc,N}} = 0.5$ barn.[5] Because of this large value of $\sigma_{\mathrm{inc,H}}$, multiple scattering takes place which makes it difficult to evaluate $(\mathrm{d}\Sigma/\mathrm{d}\Omega)_{\mathrm{inc}}$ precisely.

In the case of pure light water, no structure is present in the SANS region, i.e., $q < 0.3$ Å, the scattering is given by incoherent scattering. Jacrot et al.[6,7] obtained an empirical equation for the scattering intensity for water,

$$I_{\mathrm{H2O}} = I_{\mathrm{inc,H2O}} = \frac{I_0}{4\pi}(1 - T), \tag{2.2}$$

where I_0 is the incident beam intensity and T is the transmission. The derivation of Eq. (2.2) is based on the following intuitive discussion: The scattering intensity can be assumed to be due solely to incoherent scattering from H-atoms in water, and the fraction of scattering is the rest of transmission, i.e., $(1 - T)$. Since the scattering is isotropic, I_{H2O} is obtained by dividing it by the full solid angle, i.e., 4π. According to Jacrot, Eq. (2.2) is valid for $\lambda \geq 10$ Å. When λ becomes smaller, incoherent scattering of H-atoms becomes anisotropic and is significant in the forward scattering. Therefore, a correction factor has to be included,

$$I_{\mathrm{H2O}} = \frac{I_0}{4\pi} g_\lambda (1 - T). \tag{2.3}$$

Here, g_λ is a correction factor for the anisotropy of the incoherent scattering of H_2O, and is approximately given by,[6]

$$g_\lambda \approx \frac{1}{1 - \exp(-0.6\lambda^{0.5})}. \tag{2.4}$$

May et al.[8] extended the above discussion to mixtures of light/heavy water.

In structural analyses by SANS, samples are usually designed to consist of a large fraction of deuterated component and a small fraction of hydrogeneous component ϕ_{H}. In principle, the incoherent scattering intensity can be calculated based on the incoherent scattering cross sections of individual atoms comprising the samples. In most cases, however, the calculated values are not equal to those determined experimentally. This is mainly due to multiple scattering and inelastic scattering from H atoms in the sample[9] and wavelength dependence of the absorption cross sections. Because of these reasons, incoherent scattering intensity subtraction methods used in the literature are not unique and various empirical methods are proposed. For example, in the case of polymer blends with the volume fraction of the H-component, ϕ_{H},

$(\mathrm{d}\Sigma/\mathrm{d}\Omega)_{\mathrm{inc}}$s of pure H- and D-materials are measured and the incoherent scattering is estimated by a simple addition,[10,11]

$$\Big(\frac{\mathrm{d}\Sigma}{\mathrm{d}\Omega}\Big)_{\mathrm{inc}} = \phi_{\mathrm{H}}\Big(\frac{\mathrm{d}\Sigma}{\mathrm{d}\Omega}\Big)^{0}_{\mathrm{inc,H}} + (1-\phi_{\mathrm{H}})\Big(\frac{\mathrm{d}\Sigma}{\mathrm{d}\Omega}\Big)^{0}_{\mathrm{inc,D}}, \tag{2.5}$$

where the superscript 0 denotes the pure H- or D-component. Because of $\sigma_{\mathrm{inc,H}} \gg \sigma_{\mathrm{inc,D}}$, Eq. (2.5) can be approximated to

$$\Big(\frac{\mathrm{d}\Sigma}{\mathrm{d}\Omega}\Big)_{\mathrm{inc}} = \phi_{\mathrm{H}}\Big(\frac{\mathrm{d}\Sigma}{\mathrm{d}\Omega}\Big)^{0}_{\mathrm{inc,H}}. \tag{2.6}$$

This equation is also often used for polymer solutions, micelles dispersions, and so on. As will be discussed later, however, Eqs. (2.5) and (2.6) are not correct since $(\mathrm{d}\Sigma/\mathrm{d}\Omega)^{0}_{\mathrm{inc,H}}$ is strongly sample-thickness dependent.

Dubner et al.[11] proposed an estimation method of incoherent background intensity for isotope mixtures of poly(ethylene terephthalate), which uses the incoherent component of the transmission, T_{inc},

$$\begin{aligned} \Big(\frac{\mathrm{d}\Sigma}{\mathrm{d}\Omega}\Big)_{\mathrm{inc}} &\cong \frac{\Sigma_{\mathrm{inc}}}{4\pi}(1-T_{\mathrm{inc}}), \\ T_{\mathrm{inc}} &= \exp\,[-\Sigma_{\mathrm{inc}}t], \\ \Sigma_{\mathrm{inc}} &= \sum_i \rho_i \sigma_{\mathrm{inc},i} f_i, \end{aligned} \tag{2.7}$$

where Σ_{inc} is the macroscopic incoherent cross section, t [cm] is the sample thickness and $\sigma_{\mathrm{inc},i}$ and f_i are the incoherent cross section and the volume fraction of the i-component, respectively. Here, the summation runs over the incoherent cross sections of H and D. The agreement was reasonably good for 0.1 cm thick sample with low concentrations of H component for the neutron with the wavelength $\lambda = 4.75$ Å. Carsughi and coworkers[12] discussed sample geometry effects on incoherent scattering of H_2O. They reported that $(\mathrm{d}\Sigma/\mathrm{d}\Omega)_{\mathrm{inc}}$ collected with different ratios of sample-to-beam dimension shows large difference as a function of sample thickness. This is due to multiple scattering. Brûlet et al.,[13] and Rubinson et al.[14] also proposed the importance of multiple scattering effect on the estimation of $(\mathrm{d}\Sigma/\mathrm{d}\Omega)_{\mathrm{inc}}$. However, these discussions were limited to be semi-qunatitative level. Another method, which is more phenomenological, is to use a theoretical scattering function, $(\mathrm{d}\Sigma/\mathrm{d}\Omega)_{\mathrm{the}}(q)$, to fit an observed intensity function, $(\mathrm{d}\Sigma/\mathrm{d}\Omega)_{\mathrm{obs}}(q)$,

$$\Big(\frac{\mathrm{d}\Sigma}{\mathrm{d}\Omega}\Big)_{\mathrm{obs}}(q) = \Big(\frac{\mathrm{d}\Sigma}{\mathrm{d}\Omega}\Big)_{\mathrm{the}}(q) + \Big(\frac{\mathrm{d}\Sigma}{\mathrm{d}\Omega}\Big)_{\mathrm{inc}}. \tag{2.8}$$

This method is applicable when the theoretical function well represents the system to be investigated. However, there is no definite reason why it can be applied. Therefore, the incoherent intensity subtraction has yet been an ill-posed problem in SANS analyses.

In our previous papers,[15,16] we reported sample-thickness dependence of incoherent scattering intensity from H_2O and low-density polyethylene slabs. The scattering intensity predominantly consists of multiple scattering of incoherent scattering from H atoms, which turns out a strong sample thickness dependence. We then proposed an incoherent scattering intensity function which was a function of sample thickness as well. On the basis of this theory, we propose here a method to evaluate $(\mathrm{d}\Sigma/\mathrm{d}\Omega)_{\mathrm{inc}}$ without using values in the table for the scattering lengths/cross sections[5] nor reference samples, such as a pure hydrogeneous sample, $(\mathrm{d}\Sigma/\mathrm{d}\Omega)^0_{\mathrm{inc,H}}$. This method, hereafter we call "the transmission method (T-method)", simply uses the transmission T and the thickness t of the sample. Since both T and t are values routinely obtained in a SANS measurement for data reduction, the T-method is quite useful. The validity and applicability of the T-method are examined from theoretical and experimental viewpoints. As will be demonstrated, effects of multiple scattering on incoherent scattering have to be taken into account even for thin samples, e.g., 0.1 or 0.2 cm-thick samples.

2.2 Theoretical Background

In a scattering experiment, the transmission, T, is simply obtained by taking the ratio of the transmitted, I_{tr}, and the incident beam intensities, I_0, and it is related to the Lambert-Beer law, i.e.,

$$T \equiv \frac{I_{\mathrm{tr}}}{I_0} = \exp[-\Sigma_{\mathrm{tot}} t], \tag{2.9}$$

where Σ_{tot} [cm^{-1}] is the macroscopic total cross section per unit volume. In the case of neutron scattering, Σ_{tot} is related to the total scattering cross section,

$$\Sigma_{\mathrm{tot}} = \sum_i \rho_i \sigma_{\mathrm{tot},i}, \tag{2.10}$$

where $\rho_{\rm i}$ [cm^{-3}] and $\sigma_{{\rm tot},i}$ [cm^2] are the number density and the total cross section of the scattering element i. For compound i, ρ_i is given by

$$\rho_{\rm i} = \frac{d_i N_{\rm A}}{m_i}, \tag{2.11}$$

where d_i [g·cm^{-3}] and m_i [g·mol^{-1}] are the mass density and molecular weight of compound i, and $N_{\rm A}$ is the Avogadro's number. The total cross section is the sum of the coherent scattering cross section, $\sigma_{{\rm coh},i}$, the incoherent scattering cross section, $\sigma_{{\rm inc},i}$, and the absorption cross section, $\sigma_{{\rm abs},i}$. Hence, $\sigma_{{\rm tot},i}$ is given by

$$\sigma_{{\rm tot},i} = \sigma_{{\rm coh},i} + \sigma_{{\rm inc},i} + \sigma_{{\rm abs},i}. \tag{2.12}$$

The mean-free path of neutron beam Λ [cm] is obtained by $\Lambda = 1/\Sigma_{\rm tot}$. According to our previous work, the mean-free paths of 7 Å-neutron in H_2O and in D_2O are $\Lambda =$ 0.16 cm ($\Sigma_{\rm tot,H2O} = 6.22$ cm^{-1}) and 1.70 cm ($\Sigma_{\rm tot,D2O} = 0.588$ cm^{-1}), respectively.[15] This means that strong multiple scattering occurs in a SANS experiment for H-containing objects.

After the treatment of Schelten & Schmatz,[9] the scattering intensity, $J_1(q)$ [s^{-1}], from a H-containing object with a thin parallel-plate shape is given by,

$$\begin{aligned} \frac{J_1(q)}{\varepsilon A \Delta\Omega} &= \Phi_0 \int_0^t \exp(-\Sigma_{\rm tot} x) \frac{{\rm d}\Sigma_{\rm inc}}{{\rm d}\Omega} \exp[-\Sigma_{\rm tot}(t-x)] {\rm d}x \\ &= \Phi_0 \exp(-\Sigma_{\rm tot} t) t \frac{\Sigma_{\rm inc}}{4\pi}, \end{aligned} \tag{2.13}$$

where Φ_0 [cm^{-2}s^{-1}], ε, A [cm^2], and $\Delta\Omega$ [sr] are the incident neutron flux, the counting efficiency, the irradiated sample area, and the solid angle of the detector pixel, respectively. Here, it is assumed that the scattering is dominated by incoherent scattering from H-atoms in the object. The subscript 1 in $J_1(q)$ indicates single-scattering. Eq. (2.13) means that the second (and subsequent) scattering is likely to give a roughly isotropic distribution of scattered neutron, and the effect of scattering of the once-scattered neutrons can be ignored.[17] However, as mentioned above, multiple scattering is not negligible in the case of H-atom containing materials, such as soft matter and biological systems. As discussed in the previous paper,[15] Eq. (2.13) can be easily extended to n–times scattering, i.e.,

$$\frac{J_{\rm n}(q)}{\varepsilon A \Delta\Omega} = \Phi_0 \exp(-\Sigma_{\rm tot} t) \frac{1}{n!} t^n \frac{1}{4\pi} \left(\Sigma_{\rm inc}\right)^n. \tag{2.14}$$

By summing up the n–times scattering, one obtains

$$\begin{aligned}\frac{J(q)}{\varepsilon A\Delta\Omega} &= \Phi_0 \exp(-\Sigma_{\rm tot}t)\frac{1}{4\pi}\sum_{n=1}^{\infty}\frac{1}{n!}\left(\Sigma_{\rm inc}t\right)^n \\ &= \Phi_0 \exp(-\Sigma_{\rm tot}t)\frac{1}{4\pi}(\mathrm{e}^{\Sigma_{\rm inc}t}-1). \end{aligned} \tag{2.15}$$

The differential cross section is obtained by taking account of the transmission, $T = \exp(-\Sigma_{\rm tot}t)$, and the sample thickness, t, and is given by,

$$\left(\frac{\mathrm{d}\Sigma}{\mathrm{d}\Omega}\right)(q) = \frac{J(q)}{\varepsilon A\Delta\Omega\Phi_0 \exp(-\Sigma_{\rm tot}t)t}. \tag{2.16}$$

By substituting Eq. (2.15) into Eq. (2.16), one obtains,

$$\left(\frac{\mathrm{d}\Sigma}{\mathrm{d}\Omega}\right)_{\rm inc} = \frac{(\mathrm{e}^{\Sigma_{\rm inc}t}-1)}{4\pi t} = \frac{\Sigma_{\rm inc}}{4\pi}\frac{(\mathrm{e}^{\Sigma_{\rm inc}t}-1)}{\Sigma_{\rm inc}t}. \tag{2.17}$$

In the thrid formula of Eq. (2.17), the term $\Sigma_{\rm inc}/(4\pi)$ represents the differential incoherent scattering cross section of the sample ($\equiv \mathrm{d}\Sigma_{\rm inc}/\mathrm{d}\Omega$) at the zero-thickness limit, and the term $(\mathrm{e}^{\Sigma_{\rm inc}t}-1)/(\Sigma_{\rm inc}t)$ is the correction term for multiple scattering with finite sample thickness of the sample.

If the sample is a H-containing sample, $\Sigma_{\rm inc}$ is very close to $\Sigma_{\rm tot}$. Hence,

$$\begin{aligned}\left(\frac{\mathrm{d}\Sigma}{\mathrm{d}\Omega}\right)_{\rm inc} &\cong \frac{\Sigma_{\rm tot}}{4\pi}\frac{(\mathrm{e}^{\Sigma_{\rm tot}t}-1)}{\Sigma_{\rm tot}t} = \frac{1}{4\pi}\frac{(\mathrm{e}^{\Sigma_{\rm tot}t}-1)}{t} \\ &= \frac{1}{4\pi}\frac{1-T}{tT}. \end{aligned} \tag{2.18}$$

Eq. (2.18) means that the incoherent scattering intensity can be determined solely by the sample transmission, T, and thickness, t. We call this T-method which stands for the transmission method. Note that Eq. (2.18) is essentially the same as that obtained by Jacrot,[6] i.e., Eq. (2.2).

Note that Eq. (2.18) is independent of absolute intensity calibration. Hence, it is important for incoherent intensity evaluation to measure accurately the scattering intensity of a sample in the absolute intensity scale. It should also be noted that Eq. (2.18) is a generalized form of Eq. (2.2) by taking account of multiple scattering with the assumption of $\Sigma_{\rm tot} = \Sigma_{\rm inc}$. In general, the transmission is related not only multiple scattering but also absorption. For example, Eq. (2.17) has to be used when absorption is not negligible, e.g., vanadium ($\Sigma_{\rm inc,V} = 0.348$ cm^{-1}, $\Sigma_{\rm abs,V} = 0.350$ cm^{-1}). In the following sections, we examine the applicability and validity of Eq. (2.18).

2.3 Experimental Section

2.3.1 Samples

Four sets of samples were used to examine the T-method, (1) light/heavy water (H_2O/D_2O) mixtures, (2) nanometer-size oil emulsions, (3) polymer gels, and (4) a concentrated ternary surfactant solution. (1) Firstly, we prepared mixtures of H_2O and D_2O with different compositions. Here, D_2O with purity of 99.6 % and deionized H_2O were used. The sample thicknesses were (0.1, 0.2, 0.3, and 0.4) cm. (2) The nanometer-size oil emulsion (nanoemulsion; NE) was prepared by high-pressure emulsification of a solution consisting of mass fractions of 30 % glycerol, 3 % ethanol, 16 % oil (dimethylpolysiloxane with the viscosity of 6 mPa·s), 5 % fatty acid (N-(hexadecyloxyhydroxypropyl)-N-hydroxyethylhexadecanamide), 1.5 % anionic surfactant (n-stearoyl-L-glutamic acid monosodium) in deuterated water. Those samples were coded as NEx, where x is the dilution ratio with respect to the as-prepared NE. The details of the samples are given elsewhere.[18] (3) Well defined tetra-arm polyethylene glycol gels (tetra-PEG) and the corresponding macromers were prepared.[19,20] The molecular weights of the macromers before cross-linking were (5k, 20k, and 40k) g/mol. These samples were swollen or dissolved in D_2O at various polymer volume fractions, $\phi_p = \phi_H$. (4) A ternary mixture of water, oil and surfactant is known to form various types of structures depending on concentration, temperature, etc. Here we used D_2O, n-octane-d18, and pentaethylene glycol dodecyl ether ($C_{12}E_5$), respectively. The volume fraction of the components were 0.65, 0.08, and 0.27 to form randomly packed spherical oil droplet dispersed in water medium.

2.3.2 SANS

SANS-U@JAEA

SANS experiments were carried out at the SANS-U,[16,21] a small-angle neutron scattering instrument with a 64 cm x 64 cm–wide position sensitive area detector (PSD) for all the samples except for sample (4). SANS-U is owned by Institute for Solid State Physics (ISSP), The University of Tokyo, and is located at the guide hall of the JRR-3 20 MW research reactor, Japan Atomic Energy Agency (JAEA), Tokai, Japan. The incident neutron wavelength λ was 7.0 Å with the wavelength distribution of 10 % (FWHM), and the sample-to-detector distances were chosen to be 2

m, 4 m, and 8 m dependent on the experiments. The covered momentum transfer, q, was ranged from 0.003 $Å^{-1}$ to 0.2 $Å^{-1}$. The transmission of neutron beam was counted with a ^{3}He detector placed at the center of the transmitted beam in front of the PSD. The transmission of the samples with various thicknesses was obtained by measuring the transmitted neutrons with and without the samples for 30 s. The measurements were carried out three times each and arithmetic averages were taken. The scattered neutrons detected on the area detector were circularly averaged and the scattering intensity function, $(d\Sigma/d\Omega)_{obs}(q)$, was obtained as a function of q. The absolute intensity calibration was carried out by using a secondary standard sample of a low-density polyethylene slab with $t = 2.03$ mm calibrated with vanadium.[16] The scaling factor was 0.0695.

NG7@NIST

For the sample (4) the NG7 30m SANS instrument at the National Institute of Standards and Technology (NIST) was used.[22] The sample-to-detector distance was selected to 1 m and 6.2 m with the incident wavelength of 6.0 Å, so that the accessible q range was from 0.008 $Å^{-1}$ to 0.49 $Å^{-1}$. The neutron transmission was measured using an area detector without beam stop irradiated by the appropriately attenuated incident neutrons. The measurements were performed for 3 min. each with and without sample. In order to reduce the observed data, the software package developed at NIST was used.[23]

2.4 Results and Discussion

2.4.1 H_2O and D_2O mixture: strong incoherent scattering

A series of SANS measurements were carried out for H_2O and D_2O mixtures with different sample thicknesses and the data were analyzed using the T-method. Figure 2.1(a) shows the thickness dependence of the transmission, T for H_2O and D_2O mixtures. Here, ϕ_H is the fraction of H_2O. This figure shows that Lambert-Beer law holds in the whole range of water compositions at least up to $t = 0.4$ cm. Figure 2.1(b) is the plot of total cross sections per unit volume, Σ_{tot}, obtained by $\Sigma_{tot} = -\ln T/t$. As shown in the figure, all the plots with different sample thicknesses fall on a single-

master curve given by,

$$\Sigma_{\rm tot} = -\frac{\ln T}{t} = \phi_{\rm H}\Sigma_{\rm tot,H2O} + (1-\phi_{\rm H})\Sigma_{\rm tot,D2O}, \tag{2.19}$$

where $\Sigma_{\rm tot,H2O}$ and $\Sigma_{\rm tot,D2O}$ are the total cross sections per unit volume of H_2O and D_2O, respectively. Evaluated total cross sections per unit volume are $\Sigma_{\rm tot,H2O}$ = (6.71±0.02) cm^{-1} and $\Sigma_{\rm tot,D2O}$ = (0.634±0.003) cm^{-1}. While, the value of $\Sigma_{\rm tot,D2O}$ is in good agreement with the value calculated from the table of cross sections ($\Sigma_{\rm tot,D2O}$ = 0.646 cm^{-1}), the value of $\Sigma_{\rm tot,H2O}$ is somewhat larger than the calculated value ($\Sigma_{\rm tot,H2O}$ = 5.65 cm^{-1}). This is probably due to wavelength dependence of inelastic scattering and anisotropic scattering (stronger in the forward direction for $\lambda \leq 10$Å) of water observed at $\lambda = 7$Å.

The differential incoherent scattering cross sections were evaluated in the q-range of $0.02 \geq q \geq 0.15$ Å^{-1}, similarly to the case reported in the previous paper.[21] The results (open symbols) are shown in Figure 2.2 as well as those evaluated by the T-method (filled symbols with solid lines). The agreement between the observed values and those evaluated by the T-method is remarkably good for $\phi_{\rm H} \geq 0.05$. However, for lower $\phi_{\rm H}$s (≤ 0.025), agreement becomes poor. To compare the SANS-U result with NG7 result, 0.2 cm-thick pure D_2O data obtained at NG7 are also shown in the inset, which is an enlarged figure of a part of Fig. 2.2 around t = 0.2 cm. This shows a comparison of $(d\Sigma/d\Omega)_{\rm inc}$s for 0.2-cm thick D_2O obtained by NG7 at NIST (open double-triangle) and by SANS-U (open circle). The estimated value of $(d\Sigma/d\Omega)_{\rm inc,NIST}$ from the T-method is 0.0571 cm^{-1} and the value observed directly from the scattering profile is (0.0500 ± 0.0002) cm^{-1}. This agreement supports the validity of the T-method to estimate the differential incoherent scattering cross section. The solid line and filled circle in the inset denotes the value for SANS-U obtained by the T-method, which is also in excellent agreement with $(d\Sigma/d\Omega)_{\rm inc,NIST}$. This means that the observed value at SANS-U (open circle) must be underestimated. This underestimation is probably due to a low statistics of neutron scattering from D_2O measurement at SANS-U compared with that from a block beam measurement. That is, $I_{\rm D2O}$ was not high enough with respect to $I_{\rm B4C}$, a low statistics in $(I_{\rm D2O} - I_{\rm B4C})$ led to a nontrivial error. Here, B4C was boron carbide used for dark current scattering measurement. As a result, it turns out that the T-method is a more powerful and useful method to evaluate the incoherent scattering intensity for quantitative analyses

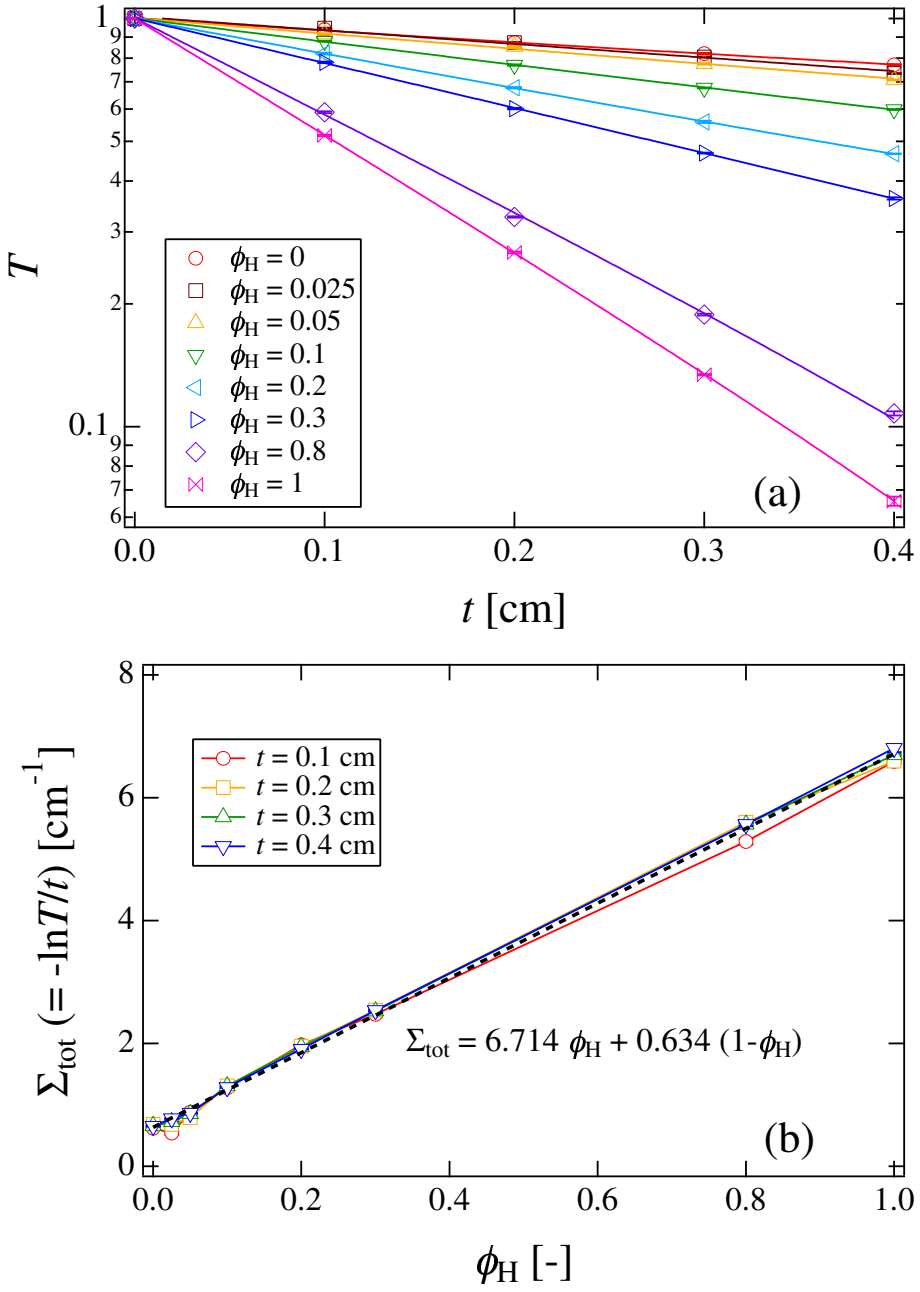

Figure 2.1: (a) Sample thickness dependence of the transmission, T, for mixtures of D_2O and H_2O, and (b) the total cross sections per unit volume, Σ_{tot}. Error bars shown in this paper indicate ± 1 standard deviation.

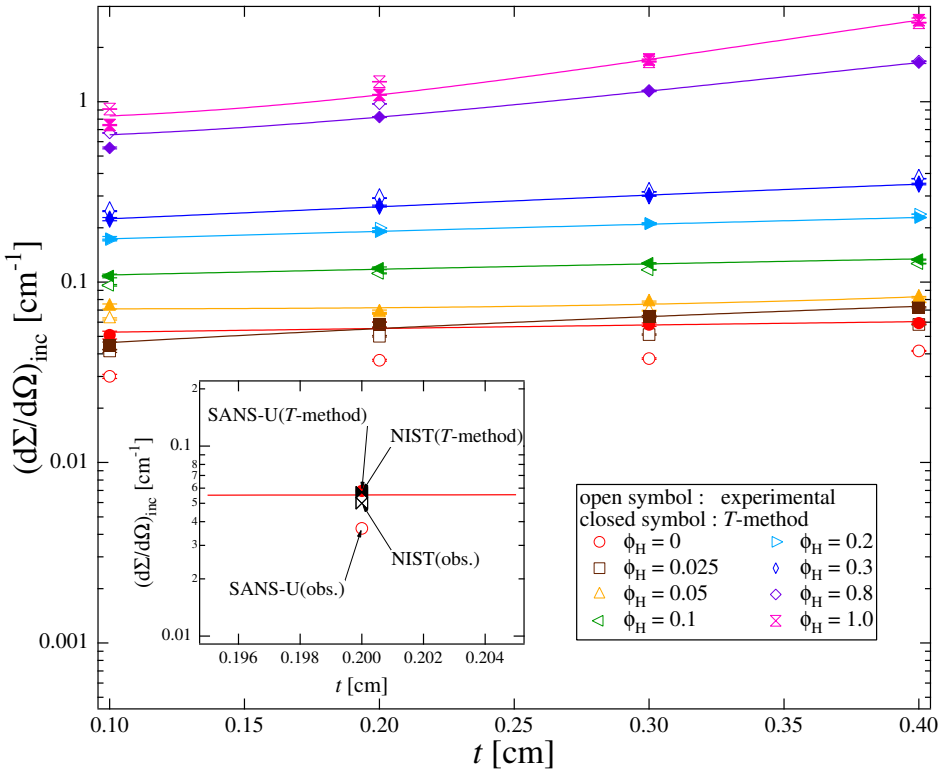

Figure 2.2: Sample thickness dependence of $(\mathrm{d}\Sigma/\mathrm{d}\Omega)_{\mathrm{inc}}$ in the mixtures of D_2O and H_2O. Open symbols denote the observed values, while filled symbols with solid lines are values evaluated by the T-method, i.e., Eq. (2.18). The inset shows an expanded figure around $t = 0.2$ cm as well as NIST data.

of SANS data for $\phi_{\mathrm{H}} \geq 0.025$. This method to estimate $(\mathrm{d}\Sigma/\mathrm{d}\Omega)_{\mathrm{inc}}$ is of particular importance in contrast-variation SANS experiments, where ϕ_{H} has to be varied in a wide range between 0 and 1.

Figure 2.3 shows the H-fraction dependence of the zero-thickness differential cross section, $(\mathrm{d}\Sigma/\mathrm{d}\Omega)_{\mathrm{inc}}(t \to 0) \equiv (\mathrm{d}\Sigma(t=0)/\mathrm{d}\Omega)_{\mathrm{inc}}$. As shown in Fig. 2.3, $(\mathrm{d}\Sigma(t=0)/\mathrm{d}\Omega)_{\mathrm{inc}}$ is a linear function of ϕ_{H}. The dashed line was obtained by fitting the observed data with Eq. (2.20) by adjusting the Jacrot's parameter g_λ, i.e.,

$$\left(\frac{\mathrm{d}\Sigma(t=0)}{\mathrm{d}\Omega}\right)_{\mathrm{inc}} = \frac{g_\lambda}{4\pi}\left[\phi_{\mathrm{H}}\Sigma^{\mathrm{tbl}}_{\mathrm{inc,H2O}} + (1-\phi_{\mathrm{H}})\Sigma^{\mathrm{tbl}}_{\mathrm{inc,D2O}}\right]. \tag{2.20}$$

The values of the incoherent cross sections per unit volume for H_2O and D_2O are calculated from the data[5] and are $\Sigma^{\mathrm{tbl}}_{\mathrm{inc,H2O}} = 5.369$ cm^{-1} and $\Sigma^{\mathrm{tbl}}_{\mathrm{inc,D2O}} = 0.136$ cm^{-1}. For $g_\lambda = 1.0$, the calculated values of $(\mathrm{d}\Sigma(t=0)/\mathrm{d}\Omega)_{\mathrm{inc}}$ shown by the chain line is much lower than the observed ones (dashed line). This is partially due to the

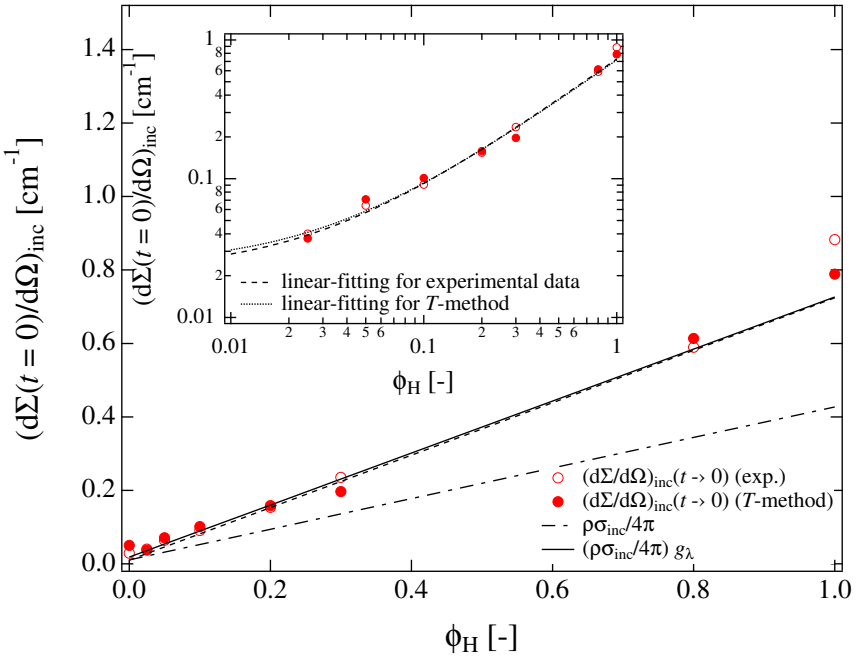

Figure 2.3: Sample thickness dependence of $(\mathrm{d}\Sigma(t=0)/\mathrm{d}\Omega)_{\mathrm{inc}}$ in the mixtures of D_2O and H_2O. Lines indicate the fit results according to Eq. (2.17).

anisotropic scattering of incoherent scattering for $\lambda \leq 10$Å as discussed by Jacrot. Another possible reason is an error of the absolute intensity calibration for SANS-U. Since the reason is unclear at this stage, we simply take into account these unknown error by the g_λ factor in this work. The best fit was obtained with $g_\lambda = 1.7$, as shown by the solid lines in Fig. 2.3 and in the inset. This value is somewhat larger than the value calculated by Eq. (2.4) i.e., $g_\lambda \cong 1.3$ for $\lambda = 7$ Å. The dashed line with filled circles in Fig. 2.3 and in the inset denote $(\mathrm{d}\Sigma(t=0)/\mathrm{d}\Omega)_{\mathrm{inc}}$s evaluated by the T-method, which shows excellent agreement between the observed ones and those evaluated by the T-method. Note that the incoherent signal arising from composition fluctuations is not negligible compared with the pure incoherent cross sections of H and D solvents as is discussed by Brûlet et al.[13]

Figure 2.4 shows the relative error of $(\mathrm{d}\Sigma(t=0)/\mathrm{d}\Omega)_{\mathrm{inc}}$ obtained by the T-method with respect to the observed ones. Here, the relative error is defined by,

$$\text{error} \equiv \frac{\mathrm{d}\Sigma(t=0)/\mathrm{d}\Omega)_{\mathrm{inc,T-method}} - \mathrm{d}\Sigma(t=0)/\mathrm{d}\Omega)_{\mathrm{inc,obs}}}{\mathrm{d}\Sigma(t=0)/\mathrm{d}\Omega)_{\mathrm{inc,obs}}} \tag{2.21}$$

As shown in the figure, the error evaluated by the T-method lie within 17 % of the observed ones. The disagreement at low $\phi_{\mathrm{H}}(\leq 0.025)$ is due to low statistics of

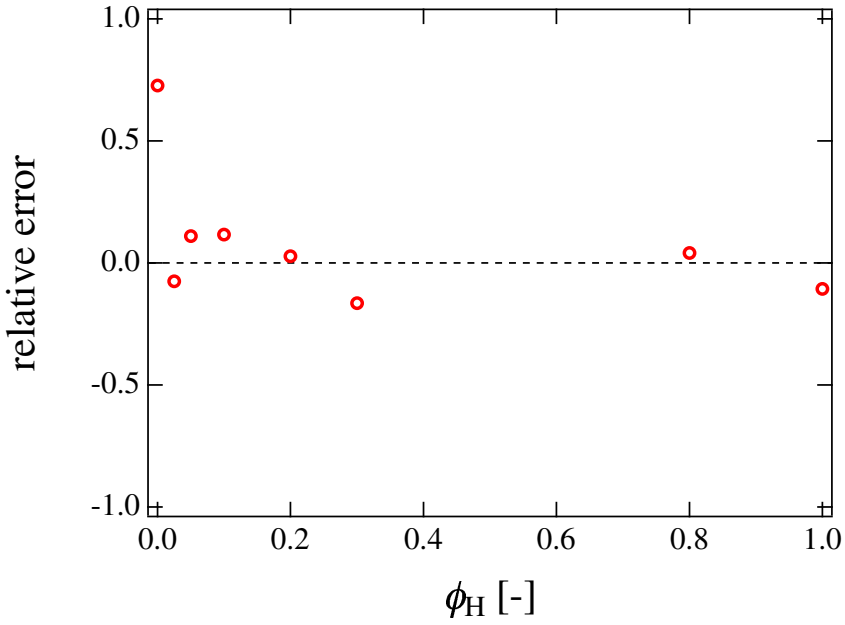

Figure 2.4: Relative error of $(d\Sigma(t = 0)/d\Omega)_{inc}$ obtained by the T-method with respect to the observed ones.

scattering counts as discussed above.

2.4.2 Nanoemulsions: strong particle scattering

Figure 2.5 shows SANS curves of a series of nanoemulsions having different concentrations. Even the volume fractions of the solute are 20 % or less, $(d\Sigma/d\Omega)_{obs}(q)$s show distinct inter-particle scattering peaks (for $x < 16$). The asymptotic behavior of $(d\Sigma/d\Omega)_{obs}(q)$s is well reproduced by Porod's law, i.e., $(d\Sigma/d\Omega)_{obs}(q) \propto q^{-4}$ as shown by the dashed lines. $(d\Sigma/d\Omega)_{inc}$ was evaluated by both (a) the T-method and (b) by fitting with Eq. (2.8) and $(d\Sigma/d\Omega)_{the} \propto q^{-4}$. Figure 2.6 (a) shows the dilution ratio dependence of $(d\Sigma/d\Omega)_{inc}$ of the nanoemulsions. $(d\Sigma/d\Omega)_{inc}$ was evaluated by the T-method (filled circles) and by fitting with a q^{-4} function (open circles). Figure 2.6 (b) shows the relative error of $(d\Sigma/d\Omega)_{inc}$ for nanoemulsions obtained by the T-method with respect to the theoretical curve fitting. The $(d\Sigma/d\Omega)_{inc}$s obtained by the T-method agree well with those obtained by Porod curve fitting. Note that this is rather a special case where the fitting function is well defined for the system. In general, systems to be investigated are more complicated and no decisive theoretical scattering functions are assumed. Hence, the agreement in this model system is

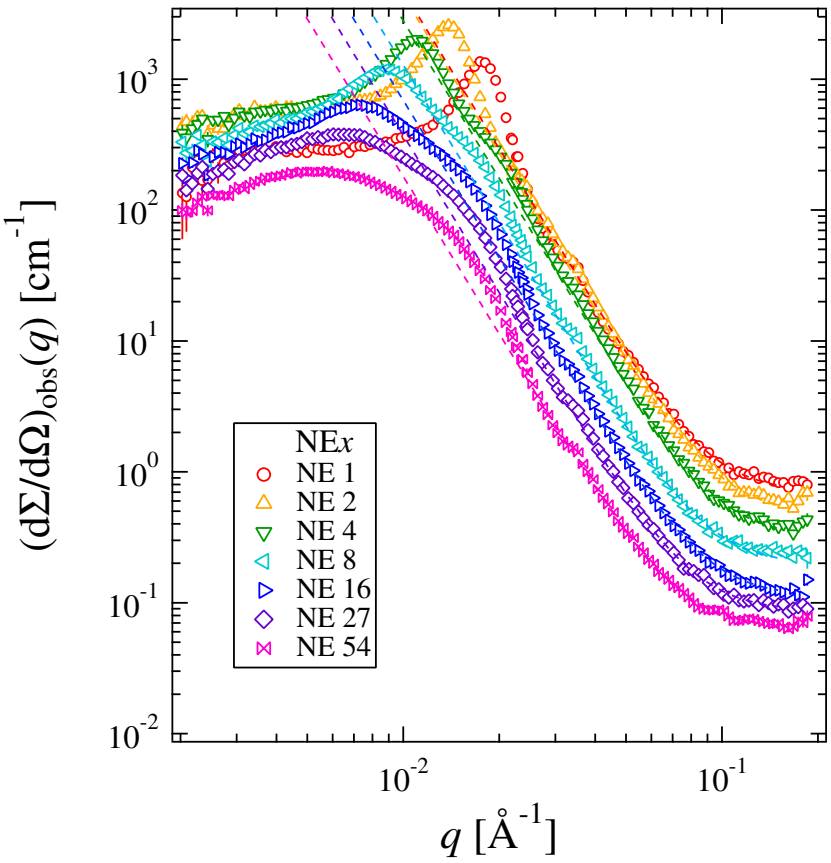

Figure 2.5: Scattering intensity functions of nanoemulsions with various dilution ratios xs. The dashed lines indicate lines with slope = -4. The error bar is exclusively smaller compared with other figures. This is because that the circular averaging of $(d\Sigma/d\Omega)_{obs}(q)$ in a two-dimensional detector was taken in the logarithmic scale of q, which gave better statistics with increasing q.

quite meaningful because it guarantees the validity of the T-method. It should be also noted here that the scattering intensity from nanoemulsion is very strong of the order of 10^3 cm^{-1}. The T-method seems to apply even to such a strong scattering system.

2.4.3 Polymer gels: weak scattering

Scattering intensity from semi-dilute polymer solutions are given by the so-called Ornstein-Zernike function,[24]

$$\left(\frac{d\Sigma}{d\Omega}\right)_{OZ}(q) = \left(\frac{d\Sigma}{d\Omega}\right)_{q=0} \frac{1}{1+\xi^2 q^2}, \tag{2.22}$$

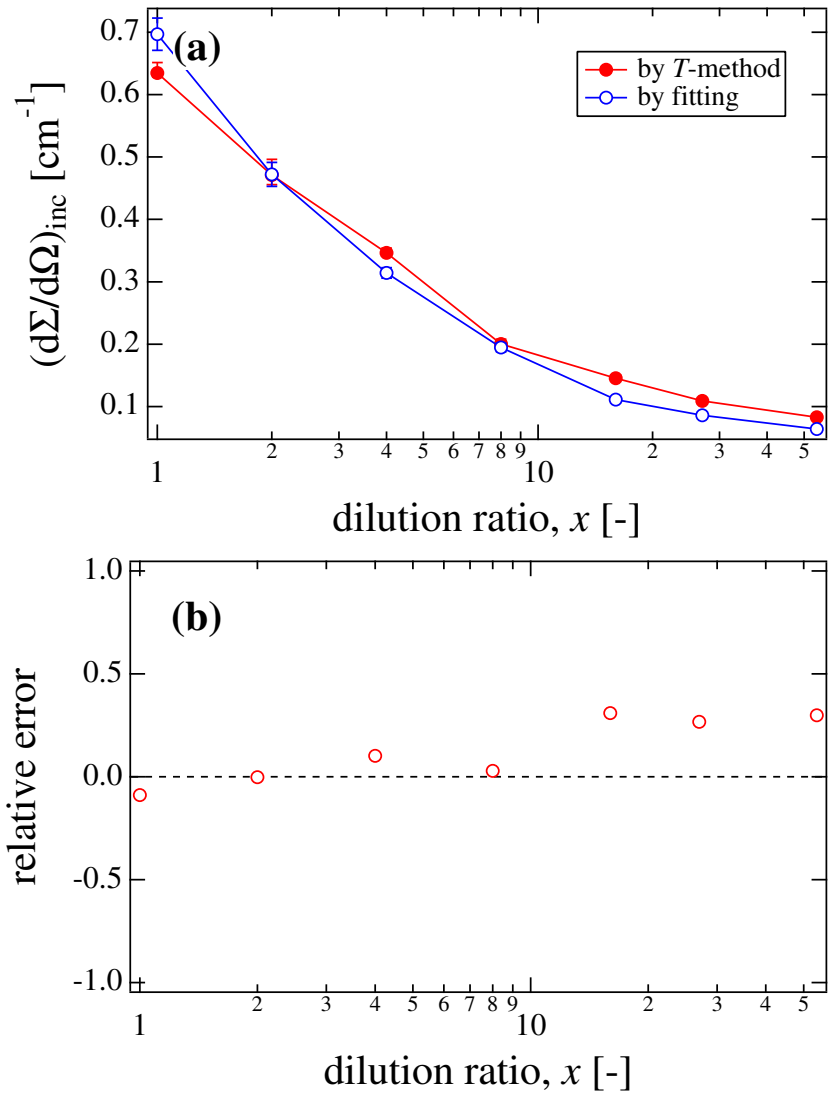

Figure 2.6: (a) Comparison of $(d\Sigma/d\Omega)_{inc}$s for nanoemulsions obtained by the T-method and by Porod's law fitting. (b) Relative error of $(d\Sigma/d\Omega)_{inc}$ obtained by the T-method with respect to the curve-fitting ones. Lines are drawn for the eye.

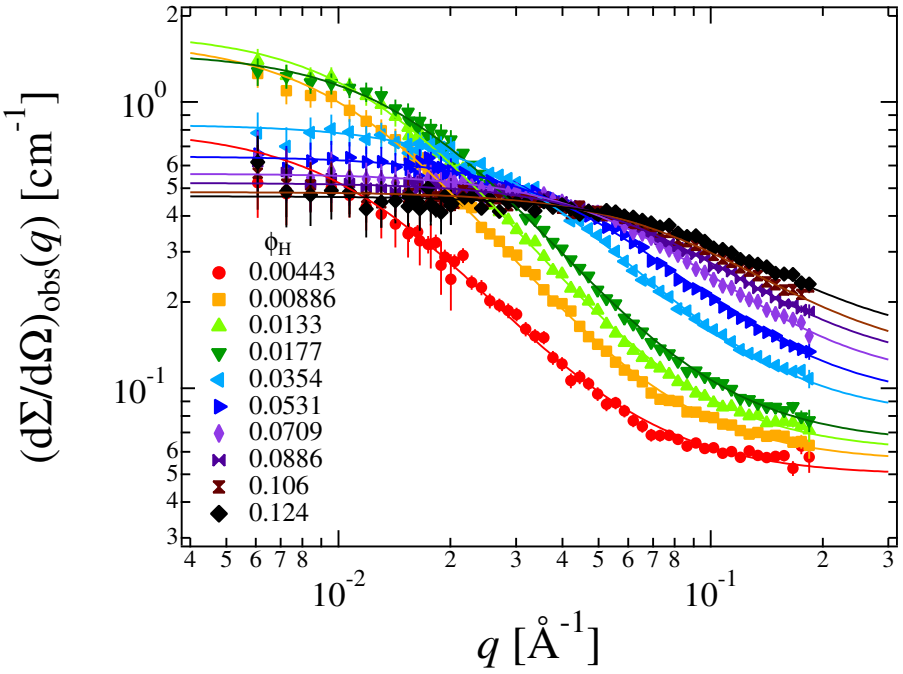

Figure 2.7: Observed scattering intensity, $(d\Sigma/d\Omega)_{obs}(q)$, for tetra-PEG gels(20 kg/mol) prepared from different polymer concentrations.

where ξ is the correlation length. In the case of polymer gels, additional scattering intensity is often observed due to cross-linking inhomogeneities.[25] However, we recently investigated a series of gels called tetra-PEG gels which did not exhibit excess scattering in SANS regime.[20] Figure 2.7 shows the observed scattering intensity $(d\Sigma/d\Omega)_{obs}(q)$ for tetra-PEG gels (20 kg/mol). The solid lines are the fits with Eq. (2.8) and $(d\Sigma/d\Omega)_{the} = (d\Sigma/d\Omega)_{OZ}$. As shown in the figure, $(d\Sigma/d\Omega)_{obs}(q)$s are strongly dependent on ϕ_H. The incoherent scattering intensities were extracted by subtracting the fitted-theoretical functions, $(d\Sigma/d\Omega)_{OZ}(q)$, from $(d\Sigma/d\Omega)_{obs}(q)$. Figure 2.8 shows the relative error of $(d\Sigma/d\Omega)_{inc}$ for tetra-PEG gels(20 kg/mol). The larger deviation for $\phi_H \leq 0.02$ is due to a misuse of the fitting function as will be discussed below. The relative error except for $\phi_H \leq 0.02$ is less than 13 %. Therefore, the error is also acceptably small for weak scattering system.

Figure 2.9 shows polymer concentration dependence of $(d\Sigma/d\Omega)_{inc}$ for tetra-PEG gels made from samples having different molecular weights, i.e., (5k, 20k, and 40k) g/mol. The sample thickness was $t = 0.4$ cm. The filled symbols denote $(d\Sigma/d\Omega)_{inc}$s obtained by curve fitting with Eq. (2.22). Note that $(d\Sigma/d\Omega)_{inc}$s at the same concen-

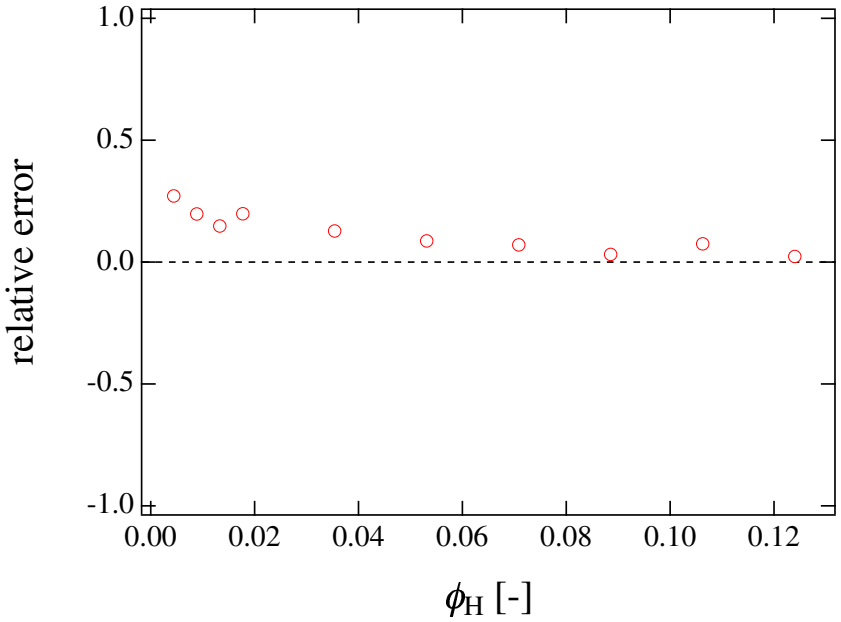

Figure 2.8: Relative error for tetra-PEG gels(20 kg/mol) of $(d\Sigma/d\Omega)_{inc}$ obtained by the T-method with respect to the curve-fitted ones.

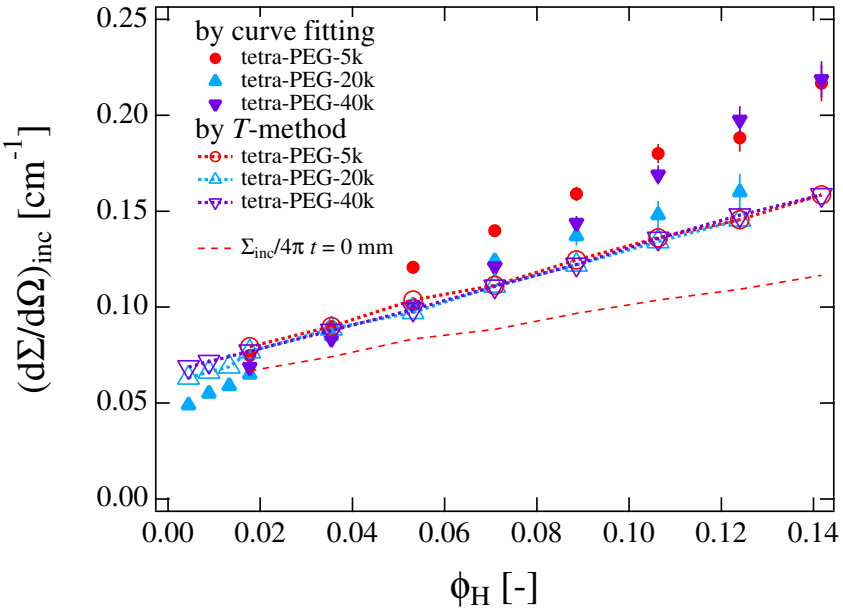

Figure 2.9: Polymer concentration dependence of $(d\Sigma/d\Omega)_{inc}$ for tetra-PEG gels prepared from different molecular weight prepolymers. $(d\Sigma/d\Omega)_{inc}$s obtained by curve fitting (filled symbols) are scattered, while those from the T-method (open symbols) do not.

tration should be equal. As shown in the figures, however, the data points obtained by curve fitting (closed symbols) do not merge onto a single value for each concentration, but increase and scatter larger with increasing $\phi_{\rm H}$. This is due to uncertainty of curve fitting. The open symbols with dotted curves, on the other hand, are $({\rm d}\Sigma/{\rm d}\Omega)_{\rm inc}$s evaluated from the T-method. The values obtained by the T-method seem to be more relevant. Another interesting feature is the deviation of the data points for $\phi_{\rm H} \leq 0.02$ (filled triangles) evaluated by curve fitting. It was found that these samples were found to be not gels but polymer solutions. Therefore, the use of Eq. (2.22) was not appropriate. Due to insufficient polymer concentrations, these samples could not undergo gelation and remained as polymer solutions.[20] Hence, an erroneous use of a curve fitting with Eq. (2.22) led to wrong values of $({\rm d}\Sigma/{\rm d}\Omega)_{\rm inc}$. The T-method, on the other hand, gave reasonable values (open triangles) throughout the whole concentration range studied here. It is interesting to note that the T-method clearly indicates such misuse of theoretical function. The dashed line is the value of $\Sigma_{\rm tot}/4\pi$, i.e., the observed differential incoherent cross section at the limit of $t = 0$. Note that the deviation of $({\rm d}\Sigma/{\rm d}\Omega)_{\rm inc}$ obtained by curve fitting becomes larger with increasing $\phi_{\rm H}$. This is probably an erroneous evaluation of multiple scattering by curve fitting. Therefore, one has to be careful to estimate $({\rm d}\Sigma/{\rm d}\Omega)_{\rm inc}$ from a curve fitting, particularly for the case with large H-content or for thick samples.

2.4.4 Concentrated surfactant system: NG7@NIST

Figure 2.10 shows the SANS profile from the $C_{12}E_5$, water, and oil system. The circles and triangles indicate the SANS profile before and after subtraction of the incoherent scattering intensity. The subtraction was done by the T-method. The sample thickness was 0.2 cm. Since the system forms rather densely packed oil droplet structure, a clear scattering peak is observed at $q \approx 0.07$ Å^{-1}. The peak at $q \approx 0.15$ Å^{-1} originates from the core-shell shape of the oil droplet. At high-q, since the contribution of the structure factor to $I(q)$ is expected to be unity, the polydisperse core-shell model form factor is applied to fit the high-q data at $q > 0.1$ Å^{-1}. The observed $({\rm d}\Sigma/{\rm d}\Omega)_{\rm inc}$ by the fitting was (0.3445 ± 0.0006) cm^{-1}, while the T-method gives the value of (0.33810 ± 0.0001) cm^{-1}. The difference is only 2 %. The after-subtracted data slightly show another dip at $q \approx 0.35$ Å^{-1} and the fit function follows

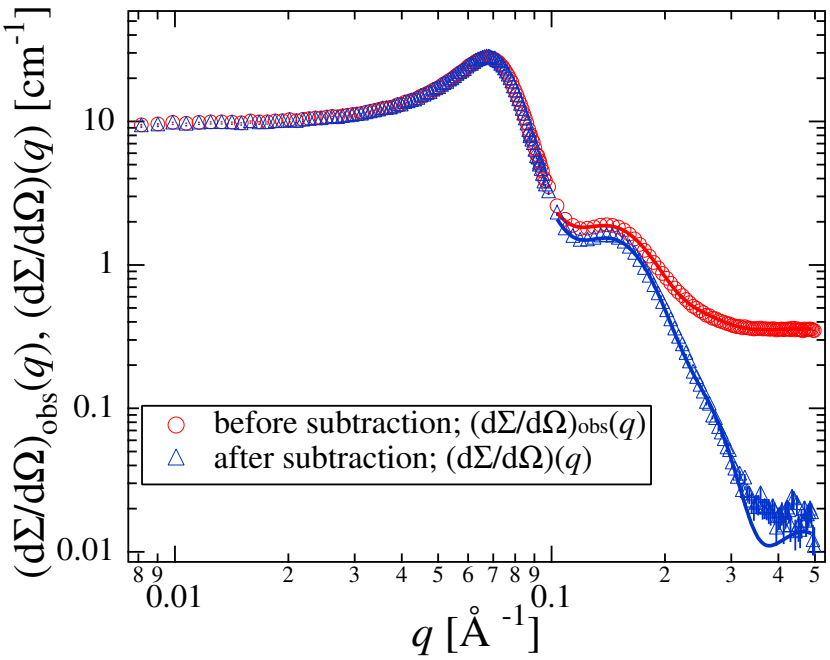

Figure 2.10: SANS profile from $C_{12}E_5$, water, and octane microemulsion system before and after the subtraction of $(d\Sigma/d\Omega)_{inc}$. Solid lines are the fit results according to a core-shell-model form factor by taking the size polydispersity and instrumental smearing into consideration.

the scattering profile quite well up to $q \approx 0.30$ Å^{-1}. This means that the hindered weak scattering can be emphasized after accurate subtraction of the incoherent signal.

2.4.5 The sample-to-beam size dependence

The sample-to-beam dimension dependence reported by Carsughi et al. Carsughi et al.[12] can be explained by multiple scattering discussed in this work. The multiple scattering is related to the mean-free path, $\Lambda = 1/\Sigma_{tot}$. As already discussed above, the mean-free paths of 7 Å-neutron in H_2O and in D_2O are $\Lambda = 0.149$ cm ($\Sigma_{tot,H2O} = 6.714$ cm^{-1}) and 1.58 cm ($\Sigma_{tot,D2O} = 0.634$ cm^{-1}). Hence, not only the sample thickness but also the beam dimension (typically of the order of 0.1 cm to 1 cm) is crucial for incoherent scattering evaluation since incoherent scattering is isotropic. However, the T-method should give a beam-size independent incoherent scattering because the transmission measurement itself includes the effect of multiple scattering along the lateral direction of the sample, i.e., the beam-size direction.

2.5 Conclusion

A simple but reasonably-accurate method for incoherent scattering intensity evaluation for H-containg materials is proposed. This method (the T-method) requires only transmission and thickness of the sample and is given by,

$$\left(\frac{\mathrm{d}\Sigma}{\mathrm{d}\Omega}\right)_{\mathrm{inc}} = \frac{1}{4\pi}\frac{1-T}{tT}. \tag{2.23}$$

In order to apply, the following three conditions have to meet, (1) negligible absorption, (2) incoherent scattering is predominant, and (3) inapplicable to strong coherent scattering, such as critical phenomena. It is needless to mention that absolute intensity calibration is inevitable to apply this method for quantitative analyses of SANS data. It is demonstrated that multiple scattering of incoherent scattering from H-atoms cannot be ignored for most cases of SANS measurements. The validity and applicability of the T-method were carefully examined for (1) mixtures of H_2O and D_2O (strong incoherent scatterers), (2) nanoemulsion (strong coherent scatterers), (3) gels (weak coherent scatterers), and (4) a concentrated surfactant system (strong coherent scatter with inter-particle interference), and were found to be quite successful, particularly for H-rich samples of sample thicknesses being 0.1 cm to 0.4 cm. This method might not work for systems with critical concentration fluctuations because forward scattering is extraordinarily dominated not by incoherent scattering but by coherent scattering.

References

[1] Kirste, R.G., Kurse, W. A. & Schelten, J. (1973). *Macromol. Chem.* **162**, 299–865.

[2] Benoit, H., Decker, D., Higgins, J. S., Picot, C., Cotton, J. P., Farnoux, B., Jannink, G. & Ober, R. (1973). *Nature Phys. Sci.* **245**, 13–15.

[3] Wignall, G. D., Ballard, D .G. H. & Schelten, J. (1974). *Eur. Polym. J.* **10**, 861–865.

[4] Higgins, J. & Benoit, H. (1994). *Polymers and Neuron Scattering*, Oxford Univ. Press, Oxford.

[5] Sears, V. F. (1992) *Neutron News* **3**, 29–37.

[6] Jacrot, B. (1976), *Rep. Prog. Phys.*, **39**, 911–953.

[7] Jacrot, B. & Zaccai, G. (1981), *Biopolymers*, **20**, 2413–2426.

[8] May, R. P., Ibel, K. & Haas, J. (1982), *J. Appl. Cryst.*, **15**, 15-19.

[9] Schelten, J. & Schmatz, W. (1980). *J. Appl. Cryst.* **13**, 385–390.

[10] Shibayama, M., Yang, H. J. & Stein, R. S. (1985). *Macromolecules* **18**, 2179–2187.

[11] Dubner, W. S., Schultz, J. M. & Wignall, G. D. (1990). *J. Appl. Cryst.* **23**, 469–475.

[12] Carsughi, F., May, R. P. & Plenteda, R. (2000). *J. Appl. Cryst.* **33**, 112–117.

[13] Brûlet, A., Lairez, D., Lapp, A. & Cotton, J. P. (2007). *J. Appl. Cryst.* **40**, 165–177.

[14] Rubinson, K., Stanley, C. & Krueger, S. (2008). *J. Appl. Cryst.* **41**, 456–465.

[15] Shibayama, M., Nagao, M., Okabe, S. & Karino, T. (2005). *J. Phys. Soc. Jpn.* **74**, 2728–2736.

[16] Okabe, S., Karino, T., Nagao, M. & Shibayama, M. (2007). *Nuclear Inst. and Methods in Physics Research, A* **572**, 853-858.

[17] Brockhouse, B. N. (1955). *Phys. Rev.* **95**, 1721–1727.

[18] Shibayama, M., Kawada, H., Kume, T., Sano, T., Matsunaga, T., Osaka, N., Miyazaki, S., Okabe, S. & Endo, H. (2007). *J. Chem. Phys.* **127**, 14450.

[19] Sakai, T., Matsunaga, T., Yamamoto, Y., Ito, C., Yoshida, R., Suzuki, S., Sasaki, N., Shibayama, M. & Chung, U. (2008). *Macromolecules* **41**, 5379–5384.

[20] Matsunaga, T., Sakai, T., Akagi, Y., Chung, U. & Shibayama, M. (2009). *Macromolecules* **42**, 1344–1351.

[21] Okabe, S., Nagao, M., Karino, T., Watanabe, S., Adachi, T., Shimizu, H. & Shibayama, M. (2005). *J. Appl. Cryst.* **38**, 1035-1037.

[22] Glinka, C. J., Barker, J. G., Hammouda, B., Krueger, S., Moyer, J. J. & Orts, W. J. (1998). *J. Appl. Cryst.* **31**, 430-445.

[23] Kline, S. R. (2006). *J. Appl. Cryst.* **39**, 895-900.

[24] de Gennes, P. G. (1979). *Scaling Concepts in Polymer Physics*, Cornell Univ. Press, NY.

[25] Shibayama, M. (1998). *Macromol. Chem. Phys.* **199**, 1-30.

Chapter 3

Design and Fabrication of a High-Strength Hydrogel with Ideally Homogeneous Network

3.1 Introduction

Hydrogels are defined as 3D polymer networks, in which aqueous solution exists as a solvent. Most hydrogels are composed of more than 90% of water.A variety of functional materials such as sensors and actuators were developed based on their stimulus-responsiveness.[1–5] Despite these unique characteristics, practical applications of hydrogels, especially as structural materials, are restricted because of their low mechanical strength, which results from the micro-inhomogeneities of polymeric topological structure created by cross-linking.[6] In order to resolve these problems, many researchers have pursued the ideally homogeneous network structure for a long time. The ideally homogeneous gel network is expected to have high mechanical properties including modulus and breaking strength.[7]

In Chapter 2, we show the new strategy for forming a homogeneous network by decreasing the degree of freedom of the micro-network structure. We formed the gel by combining two well-defined symmetrical tetrahedron-like macromonomers of the same size (Figure 3.1). As each macromonomer has four end-linking groups reacting each other, these two macromonomers must connect alternately with avoiding the self-reaction. This gelation process is simple A-B type reaction going along with Flory's classical theory; the gel was formed by mixing two macromonomer solutions within several minutes. We named this hydrogel Tetra-PEG gel. The constitutional macromonomers and the reaction were biocompatible, and the compressive strength

of resulting gel was in a MPa-range which was much superior to those of agarose gels or acrylamide gels having the same network concentrations (Figure 3.2). We discuss the relation between the mechanical properties and homogeneity of the network structure.

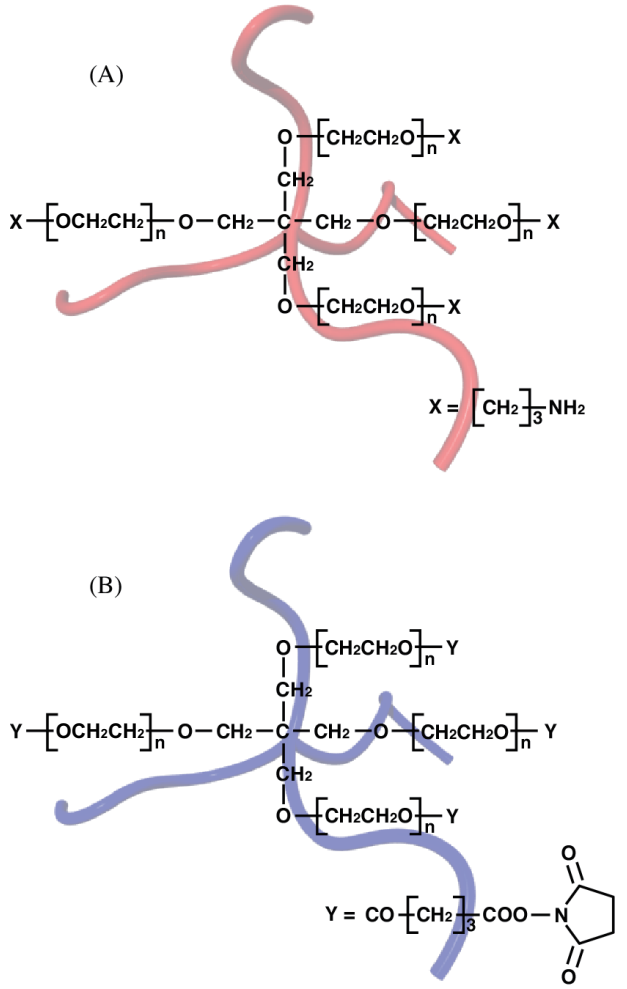

Figure 3.1: Molecular structures of TAPEG (A) and TNPEG (B).

3.2 Experimental

Preparation of Tetra-hydroxyl teminated PEG (THPEG)

THPEGs were synthesized by successive anionic polymerization reaction of ethylene oxide from sodium alkoxide of pentaerythritol. The molecular weight was estimated

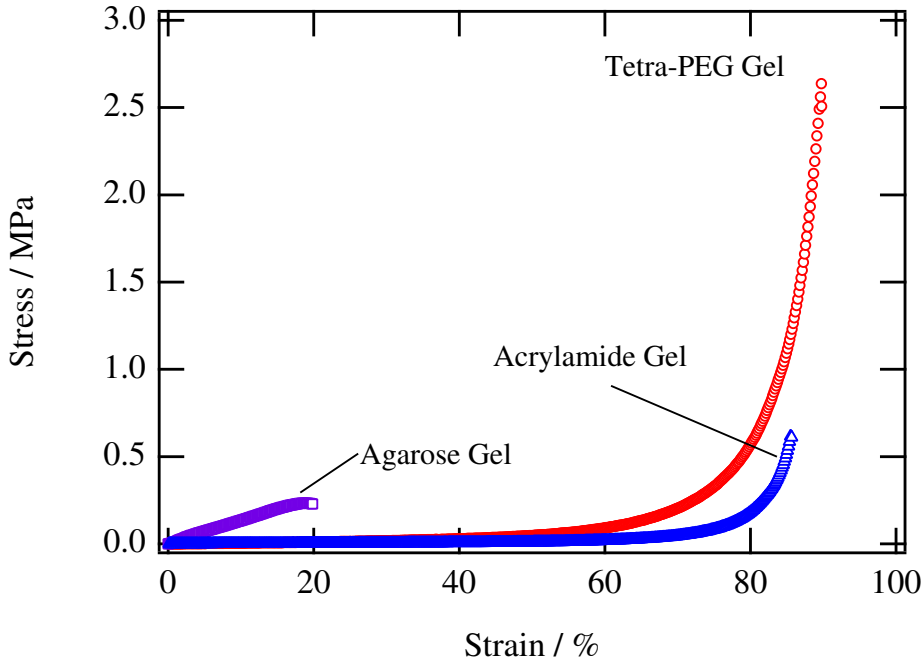

Figure 3.2: Stress-strain curves of agarose gel, acrylamide gel, and tetra-PEG gel.

from the hydroxyl value. The hydroxyl value was determined by an esterification reaction with phthalic anhydride in a pyridine solution; subsequently, excess of phthalic acid was estimated by alkaline titration using sodium hydrate solution according to a method (JIS K 1557) filed in Japan Industrial Standards (JIS).

Preparation of Tetra-amine terminated PEG (TAPEG)

One hundred grams of THPEG was dissolved in 100 g of KOH aqueous solution. Then, acrylonitrile was added, followed by reaction for 4 hours. After neutralization, the product was extracted from the aqueous solution into chloroform, and then concentrated by evaporation. The extract was purified by a repeated crystallization using ethyl acetate and hexane; via drying in vacuum, the Tetra-nitrile terminated PEG was recovered. Ninety grams of the tetra-nitrile terminated PEG dissolved in 360 g of toluene was hydrated with 9 g of Ni/Carbon catalysis under NH_3 and H_2 pressure. The toluene solution was filtrated and crystallized by adding an excess amount of hexane. After filtration and drying, TAPEG was obtained. Molecular weight (M_w) was estimated from the hydroxyl value of raw THPEGs. The molec-

ular weight distribution (MWD) was measured by gel permeation chromatography (GPC) (LC-10Avp, Shimadzu). The activity of the functional group was estimated using NMR.

Preparation of Tetra-NHS-glutarate terminated PEG (TNPEG)

One hundred grams of THPEG were dissolved in 150 g of toluene. After dehydration, 6.9 g of Glutaric anhydride and sodium acetate (0.5 g) were added to the solution. The reaction was performed under reflux condition ($\sim$ 110 °C) for 12 hours. The reaction solution containing tetra-glutaric acid terminated PEG was cooled down to 40 °C. Then, 13.8 g of N-Hydroxysuccinimide and 17 g of N,N'-Dicyclohexyl carbodiimide were added and reacted at 40 °C for 3 hours. The mixture was purified by a repeated crystallization process from a solvent system comprised of toluene, ethyl acetate and hexane. The crystalline precipitate was dried in vacuum, and TNPEG was recovered. The M_{w}, MWD, and activity of the functional group were measured by the same method as TAPEG.

Viscometric measurement of TAPEG and TNPEG aqueous solution

Constant amounts of TAPEG and TNPEG ranging from 50 mg to 3000 mg were resolved in 20 mL of water. The relative viscosity of the solutions was measured with a rheometer (MCR501, Anton Paar), using the concentric double cylinder at a constant shear rate of 100 s^{-1}. All experiments were carried out at 25 °C.

DLS measurement of TAPEG and TNPEG

TAPEG and TNPEG (100 mg) were resolved into 10 mL of water. For resultant solutions, dynamic light scattering (DLS) measurements were taken at a 90 ° angle by using a static/dynamic compact goniometer (SLS/DLS-5000, ALV). A He-Ne laser with a power of 22 mW emitting a polarized light at $\lambda = 632.8$ nm was used as the incident beam. All the measurements were carried out at 20 °C. The characteristic decay time distribution function, $G(\Gamma^{-1})$, was obtained from $g^{(2)}(\tau)$ with an inverse Laplace transform program (a constrained regularization program, CONTIN provided

by ALV).

TRDLS measurement of Tetra-PEG gel

TAPEG and TNPEG (600 mg) were resolved into 0.1 M phosphate buffer (10 mL), pH 7.4 and 7.2, respectively. After mixing two solutions in 10-mm pyrex test tube, DLS measurements were taken at an interval of 30 s at a 90 ° angle by using a static/dynamic compact goniometer (SLS/DLS-5000, ALV). All the measurements were carried out at 20 °C.

Compression test of agarose gel and acrylamide gel

Agarose (600 mg) was dissolved into 10 mL of water at 85 °C. The solution was poured into an acryl cylinder that was 15 mm in diameter and 7.5 mm in height. Then, agarose gel was obtained by cooling it at room temperature for 2 hours. Acrylamide (600 mg) and N,N'-Methylenebis(acrilamide) (9.2 mg) (one crosslinker per 10,000 dalton) were resolved into 10 mL of water at room temperature. Then, 50 μL of aqueous solution of Ammonium persulfate (100 mg/mL) and 6 μL of N,N,N',N'-tetramethylenediamine were added to the solution. The acrylamide gel was synthesized in an acryl cylinder that was 15 mm in diameter and 7.5 mm in height. The compression test was carried out using a mechanical testing apparatus (INSTRON 3365, Instron Corporation) at a velocity of 0.75 mm/min.

Compression test of Tetra-PEG gel

Constant amounts of TAPEG and TNPEG ranging from 400 mg to 1600 mg were resolved into 0.1 M phosphate buffer (10 mL), pH 7.4 and pH 7.2, respectively. Two equal amounts of polymer solutions were mixed under room temperature, and the gelation was initiated in an acryl cylinder that was 15 mm in diameter and 7.5 mm in height for 2 hours. The compression test was carried out using a mechanical testing apparatus (INSTRON 3365, Instron Corporation) at a velocity of 0.75 mm/min. More than 10 samples were tested for each network concentration.

Stoichiometric study of Tetra-PEG gel

Constant total amounts of TAPEG and TNPEG (total amount of precursors = 600 mg) with a TAPEG to TNPEG ratio ranging from 0.33 to 3.0 were dissolved into 0.1 M phosphate buffer (10 mL), pH 7.2 and pH 7.4, respectively. Two equal volumes of polymer solutions were mixed under room temperature, and the gelation was initiated in an acryl cylinder that was 15 mm in diameter and 7.5 mm in height for 2 hours. The compression test was carried out using a mechanical testing apparatus (INSTRON 3365, Instron Corporation) at a velocity of 0.75 mm/min.

DLS measurement of Tetra-PEG gel

Tetra-PEG gels containing polymer networks ranging from 20 to 140 mg/mL were prepared by the above-mentioned method in 10-mm pyrex test tubes. DLS measurements were performed at a 90 ° angle using SLS/DLS-5000 at 20 °C. In order to obtain the ensemble average, the intensity time correlation function, $g^{(2)}(\tau)$, was measured at 100 different sample positions.

Table 3.1: Molecular Weight (M_{W}) Estimated from Hydroxyl Value, Polydispersity($M_{\mathrm{W}}/M_{\mathrm{n}}$) Measured by Gel Permeation Chromatography, and Activity of the Functional Groups Estimated by NMR

properties	TAPEG	TNPEG
molecular weight (M_{W})	9617	11091
polydispersity($M_{\mathrm{W}}/M_{\mathrm{n}}$)	1.05	1.01
functionality of end group(%)	92.7	92.9

3.3 Results and Discussion

3.3.1 Design and fabrication of Tetra-PEG gel

In order to form a homogeneous network structure, we designed a novel hydrogel synthesized in situ by mixing solutions of two kinds of macromonomers with different reactive terminal groups. As constitutional units, two types of 4-armed polyethyleneg-

lycol (PEG) were synthesized with a tetrahedron-like structure (Tetra-amine terminated PEG (TAPEG) and Tetra-NHS-glutarate terminated PEG (TNPEG)). The terminal groups of TAPEG and TNPEG were propylamine and succinimidylglutarate, respectively (Figure 3.1 (a) and (b), Table 3.1). TAPEG and TNPEG were monodisperse, and the M_{w} were approximately 10,000 Da; the molecular weight of one arm was about 2,500 Da (Table 3.1). Four arms had a fixed-bond angle (109.47 °), and the motility of the arms was likely restricted by steric repulsion. Thus, the shape of the macromonomer was assumed to be tetrahedron-like, having a spatial symmetry capable of filling the 3D space. Figure 3.3 shows the characteristic distribution function, $G(\Gamma^{-1})$, for the TAPEG and TNPEG measured by DLS. Note that there are two modes, i.e., fast and slow modes. The fast mode corresponds to the translational diffusion of individual TAPEG or TNPEG chains. On the other hand, the slow mode appearing between Γ^{-1} = 100 and 101 ms indicates that some polymer chains are clustered, as are often observed in water-soluble polymers.[8] Although the slow mode looks comparable to the fast mode, it is emphasized by the factor of the sixth power of the size ratio of the individual polymer chains to the clusters, i.e., $(R_{\mathrm{h,chian}}/\ R_{\mathrm{h,cluster}})^5$ due to the nature of scattering, i.e., the scattering intensity being proportional to the sixth power of the size of the scatterers. Here, R_{h} is the hydrodynamic radius. In our case, the cluster fraction is of the order of a few percent at most. Hence, this contribution can be neglected in this work. The values of Rh for the TAPEG and TNPEG were evaluated to be 2.42 and 2.85 nm, respectively.[9]

Figure 3.4 shows the specific viscosity of the solutions measured by a rheometer as a function of polymer concentration [TAPEG] (circle) and [TNPEG] (square). From the crossover of the two straight lines, the overlap concentrations (C^*) of the macromonomers were estimated to 60 mg/mL, and the hydrodynamic radius calculated from the intrinsic viscosity using Flory-Fox equation was 3.8 nm. The simulation result showed that the conformation of the star polymer depends on the arm length; when the polymer chain is short enough to be affected by self-avoiding condition, the chain take more elongated conformation than random coil.[10] Compared with the radius calculated under the assumption of random coil (3.45 nm), each arm has elongated conformation compared with random coil. When these two polymer solutions were mixed under the biological pH, amide bonds were formed between amino groups and succinimidyl ester groups, forming a network structure. The time course of gela-

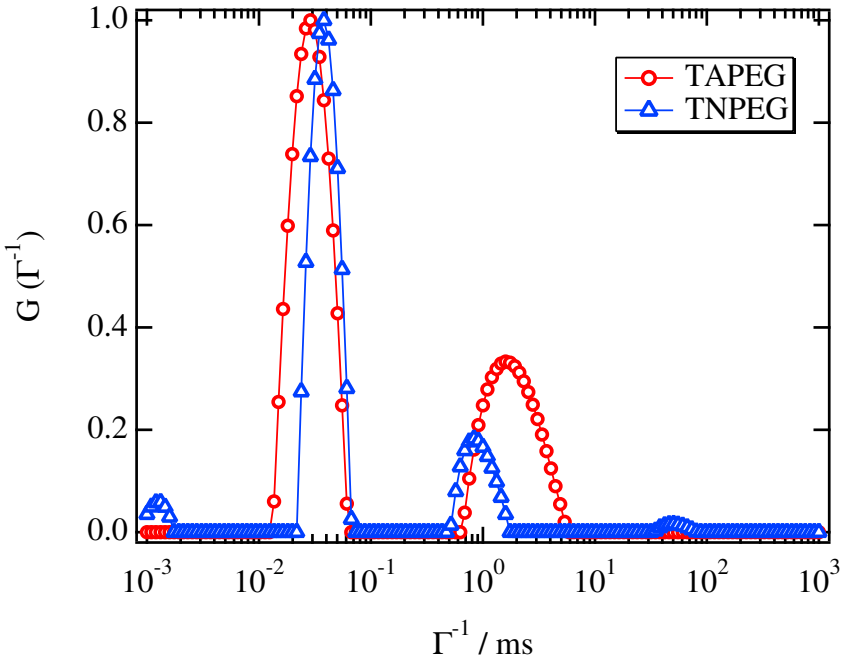

Figure 3.3: Characteristic distribution function, $G(\Gamma^{-1})$, for the TAPEG and TNPEG measured by dynamic light scattering. The characteristic distribution function was obtained from the intensity-time correlation function.

tion can be monitored by the time resolved DLS measurement (TRDLS). Figure 3.5 is a typical example showing time course of $G(\Gamma^{-1})$s of Tetra-PEG gel during gelation process. In the cases of curves 1 to 5, there appeared two shoulders in $G(\Gamma^{-1})$. The first shoulder (the fast mode) corresponds to the translational diffusion of individual polymer chains and/or corrective diffusion, while the second shoulder (the slow mode) does to the translational diffusion of clusters. The characteristic time of the slow mode disappear when an infinite cluster is formed. In other word, the slow mode disappears when a sol-gel transition occurs as a result of divergence of the characteristic time for the slow mode. Thus, the gelation time was estimated to be ca. 4 minutes. The important message here is that gelation takes place in a few minutes. As this reaction is a simple polymer-to-polymer one, it can be performed in situ, with no toxic residual monomers. The dissociating succinimidyl group, which is a citric acid derivative, can be easily metabolized by the citric cycle.[11]

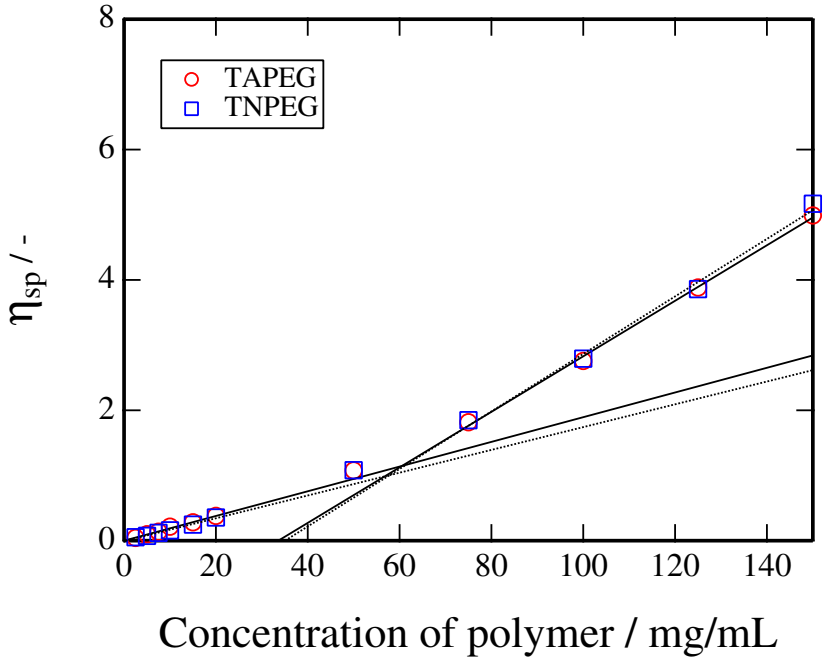

Figure 3.4: Relative viscosity of the solutions measured by a rheometer as a function of polymer concentration [TAPEG] and [TNPEG]. From the point at the intersection of the fitting lines of higher concentration and lower concentration, the overlap concentration (C^*) was estimated.

3.3.2 Influence of macromonomer concentration on mechanical properties

In order to investigate the breaking strength of Tetra-PEG gel, we performed the compression test for gels having stoichiometric amounts of TAPEG and TNPEG. Figure 3.6 shows the mean breaking strength and breaking strain obtained from the stress-strain curve. There was a good correlation between the breaking stress and breaking strain, because the compression stress increased dramatically in the larger strain region (Figure 3.2). The maximum breaking stress of Tetra-PEG gel was 9.6 MPa at 120 mg/mL. This value was extremely high, surpassing that of conventional hydrogels (several tens to hundreds of kPa), and was comparable to native articular cartilage (approximately 6-10 MPa). As seen in Figure 3.6, the breaking stress and breaking strain had two peculiar peaks unlike conventional gels. This unique mechanical property could be interpreted by using C^* as follows. The network with [Net] = 40 mg/mL was weak because the [Net] was below C^*, leading to the forma-

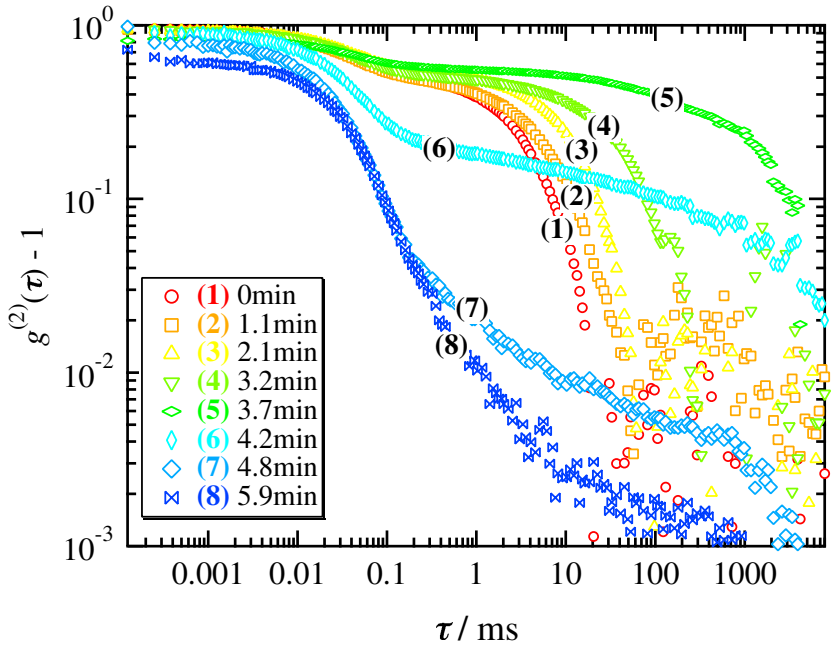

Figure 3.5: Time evolution of ICFs for tetra-PEG gel(60 mg/mL) in gelation process.

tion of an underdeveloped network with defects such as clusters and dangling chains. When [Net] became C* (60 mg/mL), as macromonomers were perfectly packed in the solution, a homogeneous structure was obtained, giving the first peak. Then, both the breaking stress and breaking strain decreased dramatically at [Net] = 70 and 80 mg/mL. This suggested that an excess of polymers introduced defects into the gel network. However, when [Net] was increased to 90 mg/mL, both the breaking stress and breaking strain began to increase again. At [Net] = 120 and 140 mg/mL, the second peak of the breaking stress and breaking strain appeared. Because these values were equal or close to $2C^*$, the formation of another homogeneous structure, i.e., the double network structure, was indicated. The network formed here was probably not a real double network structure but pseudo one; an apparent interpenetrating network existed, but all building blocks belonged to one network. When [Net] became 160 mg/mL, breaking stress and breaking strain decreased again, indicating that defects were introduced into the network again. In order to investigate the effect of the stoichiometry of two macromonomers on mechanical properties, we measured the compression modulus and breaking strength at several stoichiometric ratios r with the total macromonomer concentration being equal to C^*, where r equals the molar ratio

of TAPEG to TNPEG (Figure 3.7 and 3.8). The maximum value of the compression modulus and breaking strength were obtained at $r = 1.0$, indicating that equimolar macromonomers reacted with each other, and that even a slight excess or shortage of one component weakened the gel. Furthermore, the values of the compression modulus among reciprocal r ' s were almost the same; no matter which component was in excess or shortage, the reductions in the compression modulus were similar, suggesting a similarity in their network structures. This highly stoichiometrical and symmetrical gelation process is unprecedented, strongly suggesting the formation of a homogeneous network structure of Tetra-PEG gel. The optimal quantity and optimal ratio of macromonomers were needed to form the homogeneous network structure.

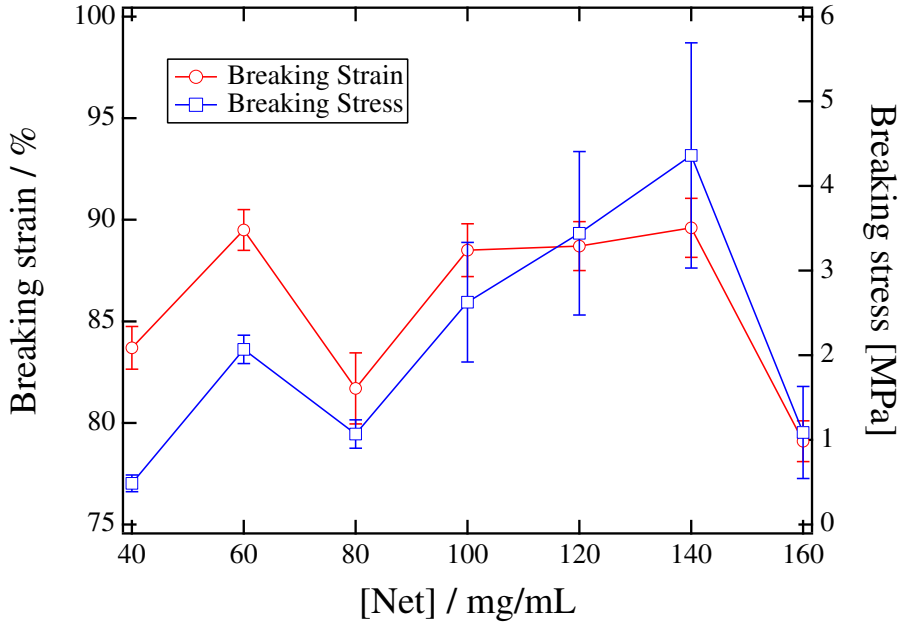

Figure 3.6: Network concentration dependence of breaking strain (left axis) and breaking stress (right axis).

3.3.3 Structural analyses by DLS

To directly analyze the network structure, we performed DLS measurement. The scattered light from gels is composed of the fluctuation component that originates from the Brownian motion of the solution and/or solute and the frozen concentration inhomogeneities introduced by cross-linking. Shibayama et al. proposed a method

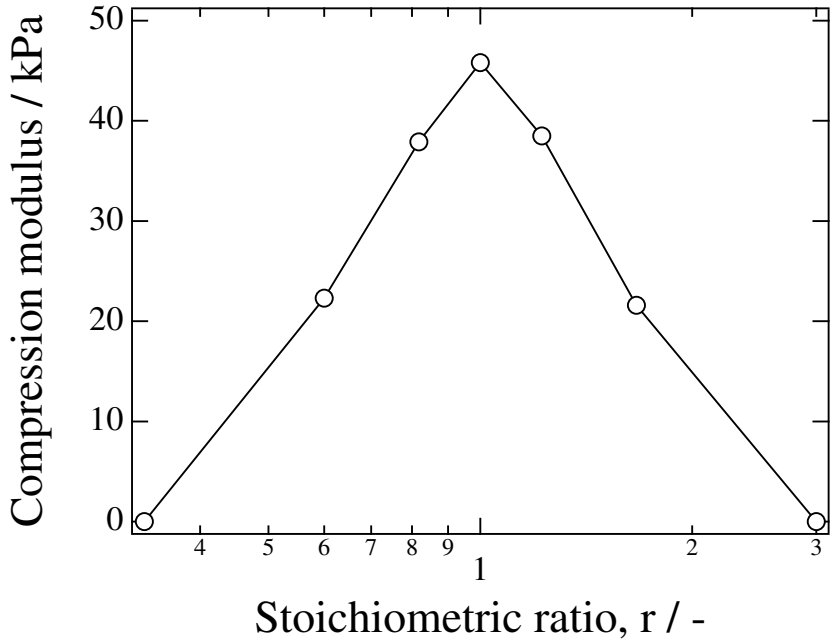

Figure 3.7: Dependence of compression modulus on stoichiometric ratio of two macromonomers. Total network concentration was kept at C^* (60 mg/mL).

for decomposing the concentration fluctuation in gels into the dynamic fluctuations and the static inhomogeneities through statistical analysis of intensity-time correlation functions (ICF) obtained from different sampling points.[12–15] From the analysis, the ensemble-average scattering intensity $< I >_{\mathrm{E}}$, indicating the inhomogeneity of the network, and the fluctuating component $< I_{\mathrm{F}} >_{\mathrm{T}}$, indicating the motility of the network, were obtained. In order to investigate the influence of [Net] on the network structure, we performed DLS analysis of gels at several network concentrations ranging from 20 to 160 mg/mL. The obtained $< I >_{\mathrm{E}}$ was very low, being comparable to that of dilute gelatin gel representative of physical gels with a homogeneous network structure. In addition, the optical transmittance of Tetra-PEG gel was approximately 100%, also indicating the homogeneous network structure.[12,16] Figures 3.9 show the $< I >_{\mathrm{E}}$ and $< I_{\mathrm{F}} >_{\mathrm{T}}$ as functions of [Net]. When [Net] = 20 mg/mL, both $< I >_{\mathrm{E}}$ and $< I_{\mathrm{F}} >_{\mathrm{T}}$ were at a maximum, suggesting that the network is inhomogeneous and fluctuating. This result indicated that the constituent polymers were in short supply, resulting in the formation of an incomplete network including finite clusters.[17,18] When [Net] was increased to C^* (60 mg/mL), both $< I >_{\mathrm{E}}$ and $< I_{\mathrm{F}} >_{\mathrm{T}}$ were dra-

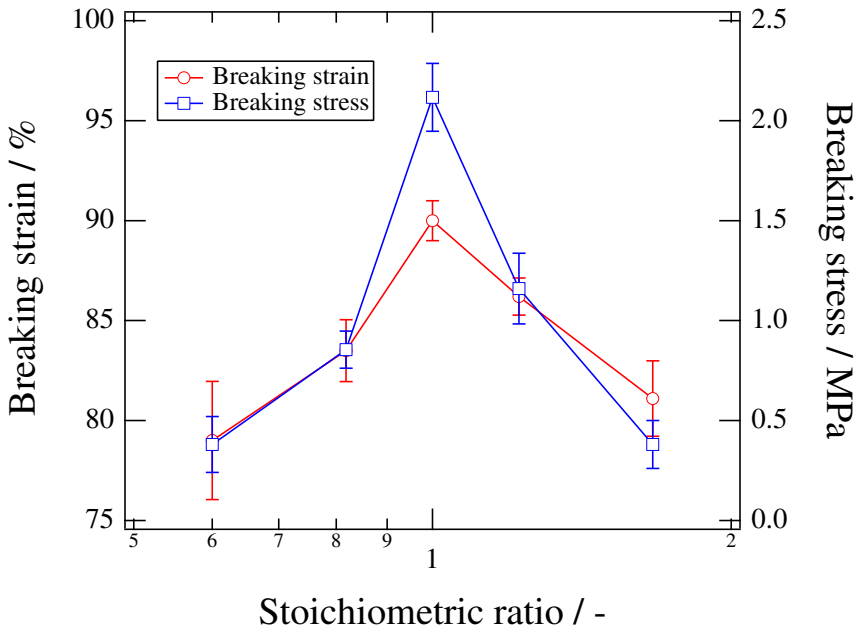

Figure 3.8: Dependence of breaking strain (left axis) and breaking stress (right axis) on stoichiometric ratio of two macromonomers. Total network concentration was kept at C^* (60 mg/mL).

matically decreased, and $< I >_{\mathrm{E}}$ reached the minimum value. These results suggest that completely packed macromonomers formed a single homogeneous network. This concentration corresponds to first local maximum of compression breaking stress. When [Net] = 80 mg/mL, both $< I >_{\mathrm{E}}$ and $< I_{\mathrm{F}} >_{\mathrm{T}}$ were almost the same as those of C^*, despite the drastic change in mechanical properties. Although the mechanism was unclear, we speculated that the existence of excess constituent polymers affected the mechanical properties. When [Net] was further increased, $< I >_{\mathrm{E}}$ became larger, because the excess network was formed. Although the network became inhomogeneous in this region, $< I_{\mathrm{F}} >_{\mathrm{T}}$ continued to decrease, reaching a minimum at [Net] = 120 mg/mL. When [Net] was further increased, $< I_{\mathrm{F}} >_{\mathrm{T}}$ became larger again. These results suggested that the network at 120 mg/mL was the most rigid. Because this concentration coincided with the second local maximum of breaking strength and was $2C^*$, we deduced that excess constituent polymers formed the second homogeneous network. Taken together, we conclude that Tetra-PEG gel formed at C^* has extremely homogeneous structure. From the DLS measurement, the characteristic length of the network formed at C^* was estimated to 5.3 nm which corresponds

to the double of the PEG arm length. Considering the fact that these tetrahedral macromonomers are connected alternately with small inhomogeneity at the C^* and the network had characteristic length corresponding to two arm-length, the formation of a well-defined network structure was strongly suggested (Figure 3.10).

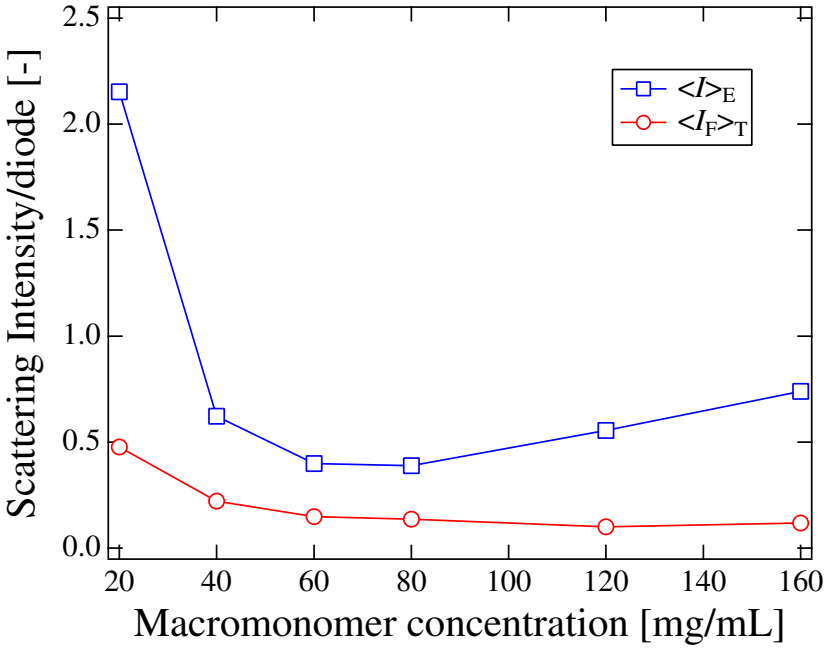

Figure 3.9: Network concentration dependence of the ensemble average$< I >_{\mathrm{E}}$ and dynamic fluctuation component $< I_{\mathrm{F}} >_{\mathrm{T}}$ of scattered light.

3.4 Conclusion

In this study, we successfully designed and fabricated a novel homogeneous hydrogel by combining two symmetrical tetrahedron-like macromonomers of the same size. Tetra-PEG gel was prepared through a highly stoichiometrical and symmetrical gelation process. The breaking strength was extremely high, being comparable to that of native articular cartilage. Local maxima of the breaking strength and local minima of $< I >_{\mathrm{E}}$ and $< I_{\mathrm{F}} >_{\mathrm{T}}$ were obtained at C^* and $2C^*$, indicating the formation of a homogeneous network structure. Judging from these data, we conclude that Tetra-PEG gel has an extremely homogeneous network structure. To the best of

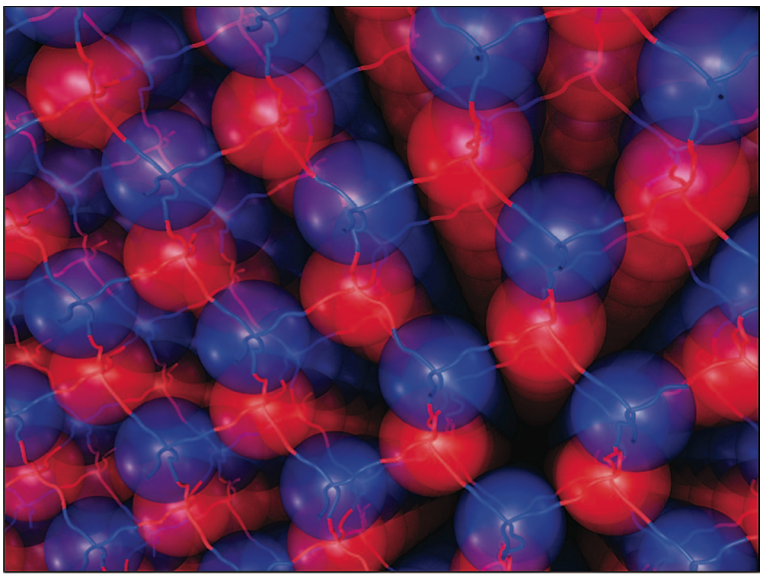

Figure 3.10: Schematic illustration of a model structure for tetra-PEG gel formed at C^*. Red and blue spheres represent TAPEG and TNPEG, respectively.

our knowledge, this is the first successful fabrication of a homogeneous chemical hydrogel having high mechanical strength. Since the mechanical properties of ideal networks can be modified by increasing the length between cross-linking points,[?] we plan to further increase the mechanical properties of Tetra-PEG gel by controlling the PEG arm length. Furthermore, we plan to fabricate stimuli-responsive hydrogels using this strategy from tetrahedron-like macromonomers. High homogeneity of the network may dramatically enhance the degree and kinetics of volume change. In addition, Tetra-PEG gel may be valuable in application for practical use. For biomedical applications, hydrogels are required to meet three criteria at the same time: high-mechanical properties, biocompatibility and an easy fabrication process. Tetra-PEG gel has successfully satisfied all three criteria. First, it has attained high-mechanical properties using symmetrical tetrahedron-like constitutional polymers to form an extremely homogeneous structure. Second, Tetra-PEG gel uses biocompatible tetrahedron-like PEG with mutually reactive terminal groups; its gel formation reaction does not use or produce any toxic substance. Third, Tetra-PEG gel can be fabricated within a few minutes through in situ gelation by simply mixing two macromonomer solutions. Because of these combined merits, we strongly believe that Tetra-PEG gel and its derivatives may be useful in the biomedical field. In con-

clusion, by combining symmetrical tetrahedron-like macromonomers, we successfully controlled gel network structure and the resultant mechanical properties. Tetra-PEG gel will not only be useful as a biomaterial but may also contribute to the understanding of ideal networks. Furthermore, as we may be able to apply this strategy regardless of polymer species, we believe that this strategy will have a strong impact on the field of gel research.

References

[1] Miyata, T.; Uragami, T.; Nakamae, K. *Advanced Drug Delivery Reviews* 2002, **54**, (1), 79-98.

[2] Nakayama, D.; Takeoka, Y.; Watanabe, M.; Kataoka, K. *Angew. Chem.* 2003, **42**, (35), 4197-4200.

[3] Osada, Y.; Okuzaki, H.; Hori, H. *Nature* 1992, **355**, (6357), 242-244.

[4] Okuzaki, H.; Kunugi, T. *Journal of Polymer Science Part B-Polymer Physics* 1996, **34**, (10), 1747-1749.

[5] Zrinyi, M.; Feher, J.; Filipcsei, G. *Macromolecules* 2000, **33**, (16), 5751-5753.

[6] Shibayama, M. *Bulletin of the Chemical Society of Japan* 2006, **79**, (12), 21.

[7] Mark, J. E.; Erman, B., *Rubberlike Elasticity - A Molecular Primer.* Wiley: 1988.

[8] Shibayama, M.; Karino, T.; Okabe, S. *Polymer* 2006, **47**, (18), 6446-6456.

[9] Matsuda, Y.; Kawata, T.; Sugihara, S.; Aoshima, S.; Sato, T. *Journal of Polymer Science Part B-Polymer Physics* 2006, **44**, (8), 1179-1187.

[10] Forni, A.; Ganazzoli, F.; Vacatello, M. *Macromolecules* 1997, **30**, (16), 4737-4743.

[11] Taguchi, T.; Saito, H.; Aoki, H.; Uchida, Y.; Sakane, M.; Kobayashi, H.; Tanaka, J. *Materials Science & Engineering C-Biomimetic and Supramolecular Systems* 2006, **26**, (1), 9-13.

[12] Shibayama, M. *Macromolecular Chemistry and Physics* 1998, **199**, (1), 1-30.

[13] Shibayama, M.; Norisuye, T.; Nomura, S. *Macromolecules* 1996, **29**, (27), 8746-8750.

[14] Shibayama, M.; Takata, S.; Norisuye, T. *Physica A* 1998, **249**, (1-4), 245-252.

[15] Shibayama, M.; Fujikawa, Y.; Nomura, S. *Macromolecules* 1996, **29**, (20), 6535-6540.

[16] Okumura, Y.; Ito, K. *Advanced Materials* 2001, **13**, (7), 485-+.

[17] Norisuye, T.; Takeda, M.; Shibayama, M. *Macromolecules* 1998, **31**, (16), 5316-5322.

[18] Herning, T.; Djabourov, M.; Leblond, J.; Takerkart, G. *Polymer* 1991, **32**, (17), 3211-3217.

Chapter 4

Structure Characterization of Tetra-PEG Gel by Small-angle Neutron Scattering

4.1 Introduction

One of major reasons for insufficient mechanical strength is cross-link inhomogeneities introduced during gel preparation. Cross-link inhomogeneities were found in vulcanized rubbers[1] and in polymer gels.[2] The understanding of cross-link inhomogeneity is very important from both scientific and engineering points of view since it affects the physical properties of the network polymer, such as mechanical and optical properties.[3] Inhomogeneous distribution of cross-links leads to stress-concentration in low cross-link density regions, resulting in mechanical breakdown. In order to circumvent this problem, various types of gels were proposed, such as networks prepared by end-linking of well-defined prepolymers,[4] gels obtained by gamma ray cross-linking of polymer solutions.[5] Recently, several novel gels having advanced mechanical properties are proposed on the basis of completely different concepts, namely slide ring gels,[6] nanocomposite gels,[7] and double network gels.[8] Though these gels meet the criterion of the mechanical properties, other criteria, such as biocompatibility and easy preparation are not satisfied.

Sakai et al. developed a novel class of hydrogels that meet all of these criteria, i.e., high mechanical strength and toughness, easy preparation, and biocompatibility.[9] Tetra-PEG gel seems to have an extremely homogeneous network structure with very low degrees of defects in the network. However, the structure-property relationship has not been fully elucidated. In this chapter , we extensively studied the

network structure of Tetra-PEG gel as well as the structure of precursor macromers, i.e., TAPEG and TNPEG, in aqueous solutions using small-angle neutron scattering (SANS).

4.2 Theoretical Background

4.2.1 Thermodynamics of polymer solutions and gels

In the context of Flory-Huggins theory for polymer solutions,[?] the osmotic pressure of the polymer solution is given by

$$\Pi = -\frac{RT}{V_1}\left[\ln(1-\phi) + \left(1 - \frac{1}{z}\right)\phi + \chi\phi^2\right] \tag{4.1}$$

where V_1 is the molar volume of the solvent, R is the gas constant, T is the absolute temperature, ϕ is the volume fraction of the polymer, and χ is the Flory-Huggins interaction parameter. z is the reduced degree of polymerization of the solute polymer normalized to the molar volume of the solvent, V_1.

$$z = \left(\frac{V_2}{V_1}\right) Z \tag{4.2}$$

Here, Z is the degree of polymerization of the polymer based on the monomer unit of the polymer and V_2 is the molar volume of the monomeric unit of the solute (polymer). The osmotic modulus is given by[11]

$$K_{\mathrm{OS}} = \phi\frac{\partial\Pi}{\partial\phi} = \frac{RT\phi}{V_2 Z}\left[1 + \left(\frac{1}{1-\phi} - 2\chi\right)\left(\frac{V_2}{V_1}\right)\phi Z\right] \tag{4.3}$$

Note that the factor (V_2/V_1) is necessary for the case where the molar volume of the monomeric unit of the solute is different from that of the solvent.

In the case of polymer gels, there are two contributions to the osmotic pressure. One is from the free energy of mixing, Π_{mix}, and the other is from the elasticity of network chains, Π_{el}. Since the degree of polymerization is infinite ($z \to \infty$ or $Z \to \infty$) for gels, Π_{mix} is given by taking $z \to \infty$ in eq 4.1, i.e.,

$$\Pi_{\mathrm{mix}} = -\frac{RT}{V_1}\left[\ln(1-\phi) + \phi + \chi\phi^2\right] \quad \text{(polymer gel)} \tag{4.4}$$

On the other hand, Π_{el} is obtained by[12]

$$\Pi_{\mathrm{el}} = \nu_{\mathrm{e}} RT\left[\frac{1}{2}\left(\frac{\phi}{\phi_0}\right) - \left(\frac{\phi}{\phi_0}\right)^{1/3}\right] \tag{4.5}$$

where ν_e is the number density of the effective elastic chains in the network and ϕ_0 is the volume fraction of the polymer at preparation. At swelling equilibrium, the following equation holds,[13]

$$\Pi = \Pi_{mix} + \Pi_{el} = 0 \tag{4.6}$$

Hence, ν_e is obtained for affine-model networks

$$\nu_{e,aff} = \frac{[\ln(1-\phi) + \phi + \chi\phi^2]}{V_1\left[\frac{1}{2}\left(\frac{\phi}{\phi_0}\right) - \left(\frac{\phi}{\phi_0}\right)^{1/3}\right]} \quad \text{(affine)} \tag{4.7}$$

This is the so-called Flory-Rehner equation and is used to determine the cross-link density (or the number density of effective polymer chains in a polymer network).[12] In the case of phantom chains, the number density of effective polymer chains is modified to[14]

$$\nu_{e,ph} = \nu_{e,aff}\left(1 - \frac{2}{f_x}\right) \tag{4.8}$$

where f_x is the functionality of the cross-link. Since the phantom network does not have the translational entropy term of cross-links, the equation for swelling equilibrium is given by[15]

$$\nu_{e,ph} = -\frac{[\ln(1-\phi) + \phi + \chi\phi^2]}{V_1\left(\frac{\phi}{\phi_0}\right)^{1/3}} \quad \text{(phantom)} \tag{4.9}$$

for $f_x = 4$ network. The phantom chain model allows that fluctuations of the displacement of cross-links after deformation are equal to those of undeformed state and are given by $\langle(\Delta\boldsymbol{r})^2\rangle = \langle(\Delta\boldsymbol{r})^2\rangle_0 = 2\langle\boldsymbol{r}^2\rangle_0/f_x$[16] Here, $\boldsymbol{r}$ and $\Delta\boldsymbol{r}$ denote the end-to-end distance of polymer chains between neighboring cross-inks and its deviation from the affine deformation, respectively, and the subscript 0 means undeformed state. This leads to $\langle(\Delta\boldsymbol{r})^2\rangle = \langle(\Delta\boldsymbol{r})^2\rangle_0 = \langle\boldsymbol{r}^2\rangle_0/2$ for $f_x = 4$, which is too large for Tetra-PEG gels as will be discussed later. Hence, we employ the affine model hereafter.
The osmotic modulus of polymer gels is given by

$$\begin{aligned} K_{OS} &= K_{OS,mix} + K_{OS,el} \\ &= \frac{RT\phi^2}{V_1}\left(\frac{1}{1-\phi} - 2\chi\right) + \nu_e RT\left[\frac{1}{2}\left(\frac{\phi}{\phi_0}\right) - \frac{1}{3}\left(\frac{\phi}{\phi_0}\right)^{1/3}\right] \end{aligned} \tag{4.10}$$

The longitudinal modulus is obtained by[17]

$$M_{OS} = K_{OS} + \frac{4}{3}G \tag{4.11}$$

Here, G is the shear modulus given by[11]

$$G = \nu_{\mathrm{e}} RT \left(\frac{\phi}{\phi_0}\right)^{1/3} \tag{4.12}$$

Hence,

$$\begin{aligned} M_{\mathrm{OS}} &= K_{\mathrm{OS}} + \frac{4}{3}G \\ &= \frac{RT\phi^2}{V_1}\left(\frac{1}{1-\phi} - 2\chi\right) + \nu_{\mathrm{e}} RT \left[\frac{1}{2}\left(\frac{\phi}{\phi_0}\right) + \left(\frac{\phi}{\phi_0}\right)^{1/3}\right] \end{aligned} \tag{4.13}$$

4.2.2 The scattering intensity functions for star-polymer solutions and polymer gels

According to the Einstein's fluctuation theory,[18] the scattering intensity at $q = 0$ (i.e., the thermodynamic limit), $I(0)$, for polymer solutions is related to the osmotic modulus by

$$I(0) = (\Delta\rho)^2 \frac{k_{\mathrm{B}} T \phi^2}{K_{\mathrm{OS}}} \tag{4.14}$$

where q is the magnitude of the scattering vector and is the scattering length density difference square between the polymer (2) and solvent (1) given by

$$(\Delta\rho)^2 = (\rho_2 - \rho_1)^2 = \left[\left(\frac{b_2}{\tilde{V}_2}\right) - \left(\frac{b_1}{\tilde{V}_1}\right)\right]^2 \tag{4.15}$$

Here, b_i and $\tilde{V}_i$ are the scattering length and the monomeric volume of component i (= 1 or 2). Since $I(0)$ is related to eq 4.3, the scattering intensity function for polymer-solvent systems is given by the single-contact theory of Zimm,[19,20]

$$I(q) = \frac{(\Delta\rho)^2}{N_{\mathrm{A}}} \frac{V_2 \phi P_{\mathrm{star}}(q)}{1 + (1-2\chi)\left(\frac{V_2}{V_1}\right)\phi P_{\mathrm{star}}(q)} \tag{4.16}$$

Here, N_{A} is the Avogadro's number, and ϕ is the volume fraction of the solute. $P_{\mathrm{star}}(q)$ is the form factor of f-arm star-polymer chains given by[21,22]

$$P_{\mathrm{star}}(q) = \frac{2Z}{fu^2}\{u - [1 - \exp(-u)] + \frac{f-1}{2}[1 - \exp(-u)]^2\} \tag{4.17}$$

where f is the number of arms of the star polymer and $u \equiv= Za^2q^2/6$. Note that

$$P_{\mathrm{star}}(0) = \frac{Z}{f} + \frac{(f-1)\,Z}{f} = Z \tag{4.18}$$

The radius of gyration of the star polymer, $R_{\mathrm{g,star}}$ is related to that of the arm polymer by

$$R^2_{\mathrm{g,star}} = \frac{(3f-2)}{f} R^2_{\mathrm{g,arm}} = \frac{(3f-2)}{f^2} \frac{Za^2}{6} \tag{4.19}$$

The scattering function for polymer gels is given as a sum of Ornstein-Zernike function (OZ)[23] and a squared-Lorentzian function (SL) as written by,[24,25]

$$I(q) = \frac{(\Delta\rho)^2 RT\phi^2}{N_{\mathrm{A}} M_{\mathrm{OS}}} \left[\frac{1}{1+\xi^2 q^2} + \frac{A_{\mathrm{inhom}}}{\left(1+\Xi^2 q^2\right)^2} \right] \tag{4.20}$$

Here, ξ is the correlation length of the network and Ξ is the characteristic size of inhomogeneities in the gel. A_{inhom} is a constant representing the contribution of frozen inhomogeneities and is independent of q. It is known that the OZ function represents thermal concentration fluctuations and the SL term represents frozen-spatial inhomogeneities. Since M_{OS} is given by eq 4.13, $I(0)$ for polymer gels is given by

$$I(0) = \frac{(\Delta\rho)^2 \phi^2}{N_{\mathrm{A}}} \frac{1}{\frac{\phi^2}{V_1}\left(\frac{1}{1-\phi} - 2\chi\right) + \nu_{\mathrm{e}}\left[\frac{1}{2}\left(\frac{\phi}{\phi_0}\right) + \left(\frac{\phi}{\phi_0}\right)^{1/3}\right]} \left[1 + A_{\mathrm{inhom}}\right] \tag{4.21}$$

4.3 Experimental

4.3.1 Sample preparation

Tetraamine-terminated PEG (TAPEG) and tetra-NHS-glutarate-terminated PEG (TNPEG) were prepared from tetrahydroxyl-terminated PEG (THPEG) having equal arm lengths. The details of TAPEG and TNPEG preparation are reported elsewhere.[9] The molecular weights (M_{w}) of TAPEG and TNPEG were matched to be either 10 k or 20 kDa. Here, NHS represents for *N*-hydroxysuccinimide. The activity of the functional group was estimated using NMR. Tetra-PEG gels were synthesized as follows. Constant amounts of TAPEG and TNPEG (5-160 mg/mL) were dissolved in phosphate buffer (pH7.4) and phosphate-citric acid buffer (pH5.8), respectively. In order to control the reaction rate, the ionic strengths of buffers were chosen to be 25 mM for lower macromer concentrations (5-100 mg/mL) and 75 mM for higher macromer concentrations (110-160 mg/mL). Two solutions were mixed and the resulting solution was poured into the mold. At least 12 hours were spent for completion of reaction before the following experiments. No noticeable sol fraction was detected by NMR.

SANS samples were prepared in quartz cell with equi-amounts (stoichiometric case) or with different compositions (non-stoichiometric case) of Tetra-PEG-10k and Tetra-PEG-20k. Note that the condition of sample preparation was significantly changed from that employed in the previous paper.[9] The pHs were carefully chosen so as not to cause hydrolysis and to optimize the coupling reaction. The gelation time was also extended from 4 h to 12 h for completion of coupling reaction. The initial macromer concentrations were varied from 5 to 160 mg/mL. The corresponding initial polymer volume fractions, ϕ_0, were in the range between 4.43×10^{-3} and 1.42×10^{-1}.

4.3.2 Mechanical and swelling measurements

Stretching measurements were carried out for rectangular-shaped films (30 mm high, 5 mm wide, and 2 mm thick) of Tetra-PEG gel using a mechanical testing apparatus (RHEO METER:CR-500DX-SII, Sun Scientific Co.) at a velocity of 0.1 mm/sec. Shear experiments were also conducted for disk shape films 25 mm in diameter and 1 mm in thickness using dynamic viscoelasticity measuring apparatus (MCR301, Anton Paar.) In the case of swelling measurements, sample specimens of the same size as those for the stretching measurements were immersed in large amount of deionized water for at least 2 days. Then, the weights of the specimens were measured in order to calculate the polymer fraction in equilibrium swelling state.

4.3.3 Small-angle neutron scattering (SANS)

Small-angle neutron scattering experiments were carried out at two-dimensional SANS instrument, SANS-U, the University of Tokyo, located at JRR-3 Research Rector, Japan Atomic Energy Agency, Tokai, Ibaraki, Japan. Monochromated cold neutron beam with the average neutron wavelength of 7.00 Å and 10 % wavelength distribution was irradiated to the samples. The scattered neutrons were counted with a two-dimensional position detector (Ordela 2660N, Oak Ridge, USA). The sample-to-detector distance was chosen to be 1 and 4 m for macromer measurements and 2 and 8 m for Tetra-PEG measurements. After necessary corrections for open beam scattering, transmission and detector inhomogeneities, the corrected scattering intensity functions were normalized to the absolute intensity scale with a polyethylene secondary standard. The details of the instrument are reported elsewhere.[26,27] Inco-

herent scattering subtraction was made with the method reported by Shibayama et al.[28]

4.4 Results and Discussion

4.4.1 Swelling and Mechanical Properties

Figure 4.1 shows the swelling degree, ϕ_0/ϕ, as a function of ϕ_0 for Tetra-PEG-10k and Tetra-PEG-20k. Here, ϕ_0 is the polymer volume fraction at sample preparation. The degree of swelling increases approximately linearly with ϕ_0. The higher the initial polymer concentration, the larger the degree of swelling is. Note that (1) ϕ_0/ϕ is in the range of 1 to 3, and (2) a uniform gel was prepared from a solution of Tetra-PEG-10k even with a half of the so-called C^* concentration evaluated by viscometry, C^* ($\approx$ 60 mg/mL), i.e., 30 mg/mL ($\phi_0 = 2.26 \times 10^{-2}$).[9] This indicates that network formation occurs by spontaneous chain-stretching and coupling of succinimidyl ester and amine groups at chain ends. In the case of Tetra-PEG-20k, a gel prepared with the concentration lower than C^* was too brittle to measure the swelling ratio.

Figure 4.2 shows the variation of Young's modulus, E, as a function of ϕ_0 for Tetra-PEG-10k and of Tetra-PEG-20k. We also measured the shear modulus, G, and confirmed the relationship, $E \approx 3G$ (valid for materials with Poisson ratio being 1/2). According eq 4.12, E is expected to scale as $E \sim G \sim \nu_e \sim \phi_0$. The dashed lines are drawn by crossing the origin and by fitting with the data for $\phi_0 \gg \phi_0^*$. As a matter of fact, E seems to scale with ϕ_0^1 at high ϕ_0 regions, while E does not cross the origin but reduces to zero by approaching ϕ_0^*. This is why E depends on ϕ_0 with a higher exponent than unity in the low ϕ_0 region as shown in the inset, i.e., $E \sim \phi_0^{1.51}$. Larger exponents than unity are reported in the literature, e.g., 1.83 for poly(diethylsiloxane) networks.[29] Such a higher exponent is explained as a result of entanglements. However, in the case of Tetra-PEG gels, it is important to note that E is essentially proportional to ϕ_0, indicating absence of entanglements. Note that E's for the two samples are co-linear in the log-log plot with the factor of 2 as expected (i.e., $\nu_{e,10k} = 2\nu_{e,20k}$). It is noteworthy that the order of E is a few-tens of kPa, which is about one order of magnitude larger than that of typical gels with similar polymer concentrations[30,31] and that of tetra-arm PEG gels made with bi-functional chain extender.[32] Lutolf and Hubbell investigated tetra-arm-PEG gels with 10 k and 20

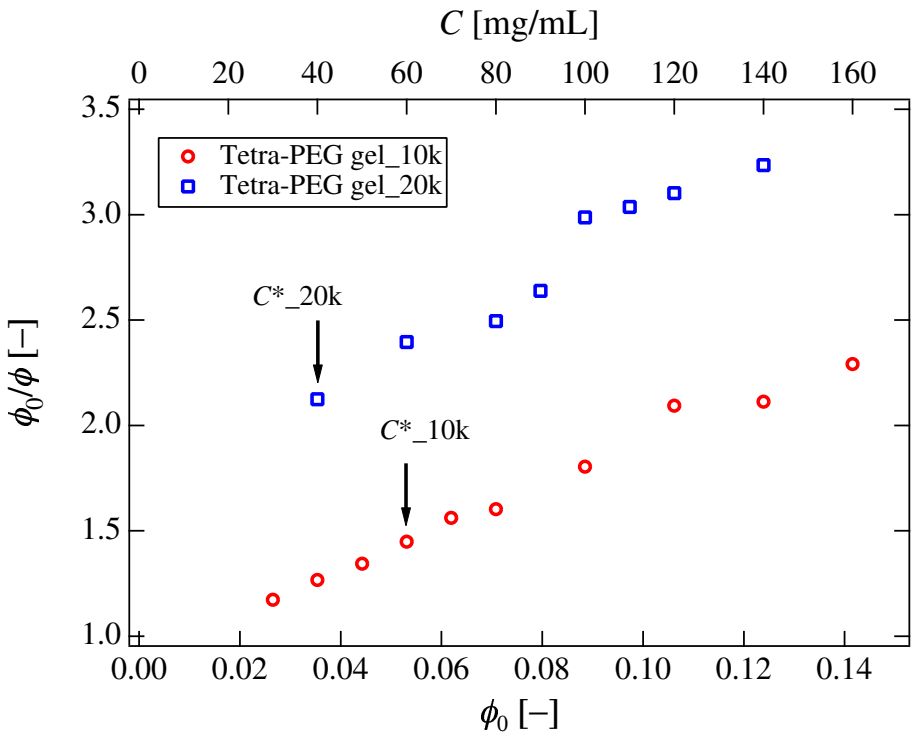

Figure 4.1: Initial polymer volume fraction, ϕ_0, dependence of the swelling degrees, ϕ_0/ϕ, for Tetra-PEG-10k and Tetra-PEG-20k. The up-arrow and down-arrow indicate the chain overlap concentrations for Tetra-PEG-10k and Tetra-PEG-20k, respectively evaluated by viscometry.

kDa. Their PEG gels were prepared from vinyl sulfonated tetra-arm PEG by Michael-type addition of thiol-containing peptides. Hence, the latter plays as a chain extender. In their case, the order of shear modulus, G, was a few kPa in the concentration range of 5 to 20 w/v%.[32] The origin of the high mechanical strength in Tetra-PEG gels results from its high yield of network formation. The linear relationship between E and ϕ_0 indicates that there are no noticeable entanglements in the network. Therefore, the higher modulus of Tetra-PEG gels is ascribed solely to a high efficiency of network formation with no or very low amount of defects. We conjecture that the superiority in the mechanical properties of Tetra-PEG gels is due to its unique sample preparation, i.e., A-B type end-coupling of tetra-arm PEG. In the following, we further report on the structures of the prepolymer (macromer) solutions and Tetra-PEG gels.

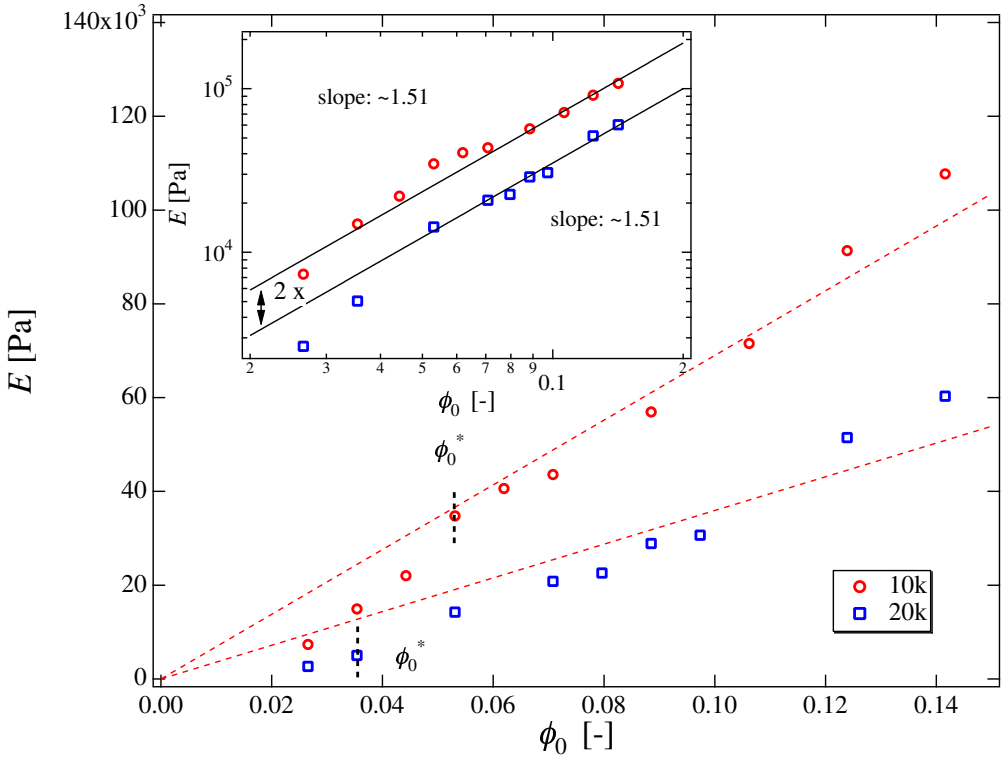

Figure 4.2: ϕ_0 dependence of Young ' s moduli, E, for Tetra-PEG-10k and Tetra-PEG-20k. The dashed lines are fitted lines by crossing the origin and by fitting the data for $\phi_0 \gg \phi_0^*$. The inset shows the log-log plots.

Figure 4.3 shows the comparison of the number densities of effective polymer chains for (a) Tetra-PEG-10k and (b) Tetra-PEG-20k, evaluated from stoichiometry ($\nu_{\mathrm{e,st}}$), swelling equilibrium (affine model; $\nu_{\mathrm{e,aff}}$), and mechanical measurements ($\nu_{\mathrm{e,el}}$). The stoichiometric number density, $\nu_{\mathrm{e,st}}$, is evaluated via

$$\nu_{\mathrm{e,st}} = \frac{f_x}{2}\frac{\phi_0}{V_2 Z} = \frac{2\phi_0}{V_2 Z} \tag{4.22}$$

Here, we set $f_x = f = 4$ and $V_2 = 39.02$ cm^3/mol (monomeric molar mass = 44.04 g, mass density = 1.129 g/cm^3). The ϕ_0 dependence of $\nu_{\mathrm{e,st}}$, is shown with a dashed line, The open circles denote $\nu_{\mathrm{e,aff}}$. The value of $\chi = 0.43$ was taken from the literature.[32] However, in order to match the values of the number densities from the swelling and mechanical measurements (open squares), it was necessary to play with χ. We fitted the swelling results using affine model with $\nu_{\mathrm{e,el}}$ by changing χ as a floating parameter. The best fit was achieved when $\chi = 0.475$ as shown with solid circles ($\nu_{\mathrm{e,aff}}$) and open squares ($\nu_{\mathrm{e,el}}$). Hence, the experimental χ value in Tetra-PEG gels for the swelling

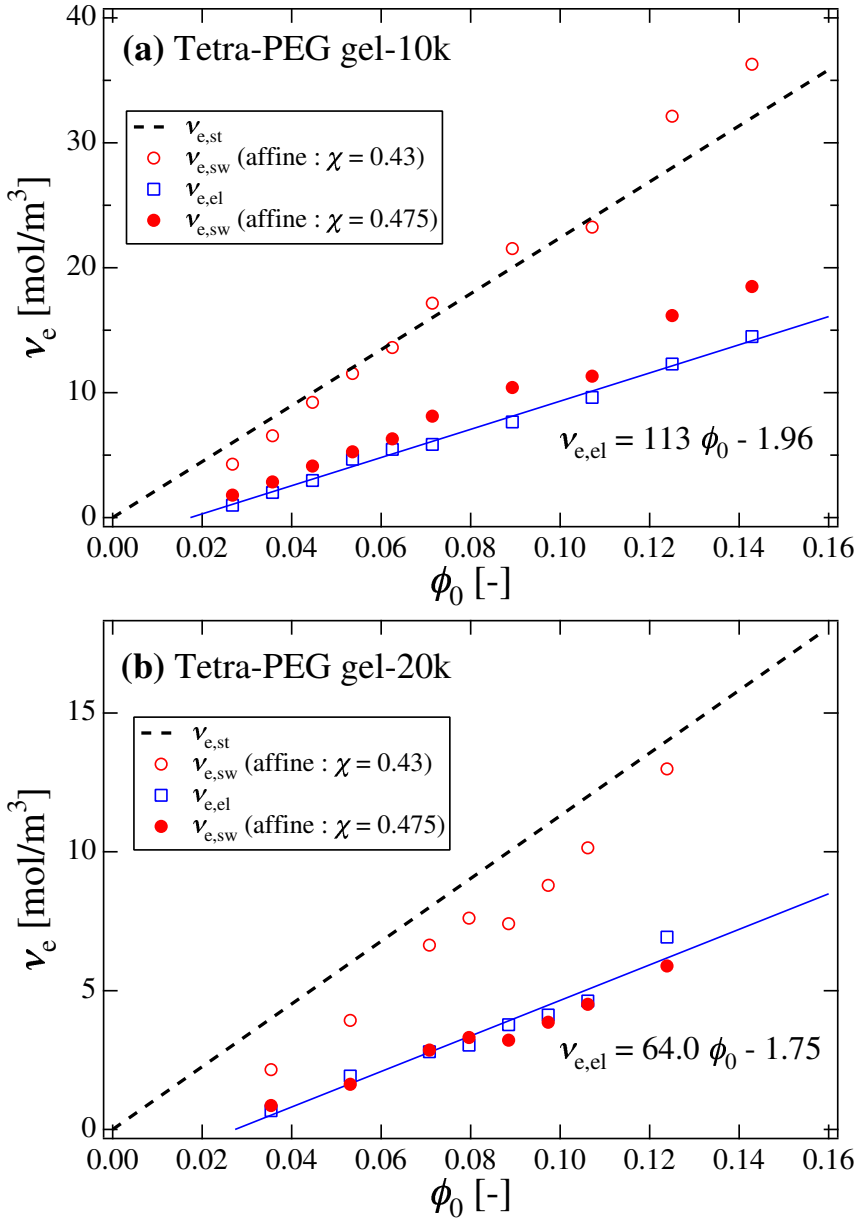

Figure 4.3: ϕ_0 dependence of the number densities of the effective polymer chains for (a) Tetra-PEG-10k and (b) Tetra-PEG-20k, evaluated from stoichiometry, ($\nu_{e,st}$; dashed line), affine model ($\nu_{e,aff}$; open circles), phantom model ($\nu_{e,ph}$; triangles), and Young ' s modulus ($\nu_{e,el}$; open squares). The solid lines were obtained with phantom model with $\chi = 0.475$ instead of $\chi = 0.43$.

measurements was slightly larger than the value written in the literature. Figure 4.3b shows the similar plots for Tetra-PEG-20k. Phenomenological equations for $\nu_{\mathrm{e,el}}$ obtained by fitting for the limited concentration range are given in the figures, i.e.,

$$\begin{aligned} \nu_{\mathrm{e,el}} &= 113\phi_0 - 1.96 \ [\mathrm{mol/m^3}] \ \ \text{(Tetra-PEG-10k)} \\ \nu_{\mathrm{e,el}} &= 64.0\phi_0 - 1.75 \ [\mathrm{mol/m^3}] \ \ \text{(Tetra-PEG-20k)} \end{aligned}$$

These phenomenological equations also indicate no or negligible entanglements in Tetra-PEG gels.

4.4.2 Tetra-PEG macromers

Before discussing the structure of Tetra-PEG gels, let us discuss the structure of Tetra-PEG macromers. Figure 4.4 shows the SANS intensity function, $I(q)$, for TAPEG-10k in deuterated solution. The concentration was $\phi_0 = 3.54 \times 10^{-2}$ (40 mg/mL), which is the one of the lowest concentrations investigated in this work. The dashed and chain lines represent the theoretical scattering functions calculated with the star-polymer (eqs 4.16 and 4.17 with $f = 4$ and $\chi = 1/2$) and OZ functions (eq 4.20 with $A_{\mathrm{inhom}} = 0$), respectively. As shown in the figure, the observed scattering function is not well reproduced by the OZ function, but by the star-polymer function. The difference is more clearly seen in the Kratky plot, i.e., $q^2 I(q)$vs q, in the inset.

Figure 4.5 shows $I(q)$s for (a) TAPEG-10k and (b) TAPEG-20k at various polymer concentrations. $I(q)$s look monotonously decreasing functions of q. $I(0)$ is expected to be proportional to ϕ_0, i.e., $I(0) \sim \phi_0 Z$, if no inter-polymer chain interaction exists (i.e., $\chi \approx 1/2$). However, it was found that $I(q)$s did not change systematically as a function of ϕ_0 and were decreasing function of ϕ_0 as shown in Figure 4.6. As a matter of fact, concentration dependence of $I(0)$ has a peak, and such phenomenon was first reported by Debye and Bueche in turbidity of polymer solutions.[33] Soni and Stein also observed a peak in light scattering intensity for end-linked poly(dimethylsiloxane) solutions.[34] The presence of the maximum in $I(0)$vs ϕ_0 plot suggests the importance to take into account of the inter-polymer chain interaction. The solid lines in Figure 4.5 were calculated by using eq 4.16, which takes into account of the inter-polymer chain interactions with $\chi = 0.475$. Accordingly, the solid lines in Figure 4.6 were also calculated with eq 4.16 with the same parameters.

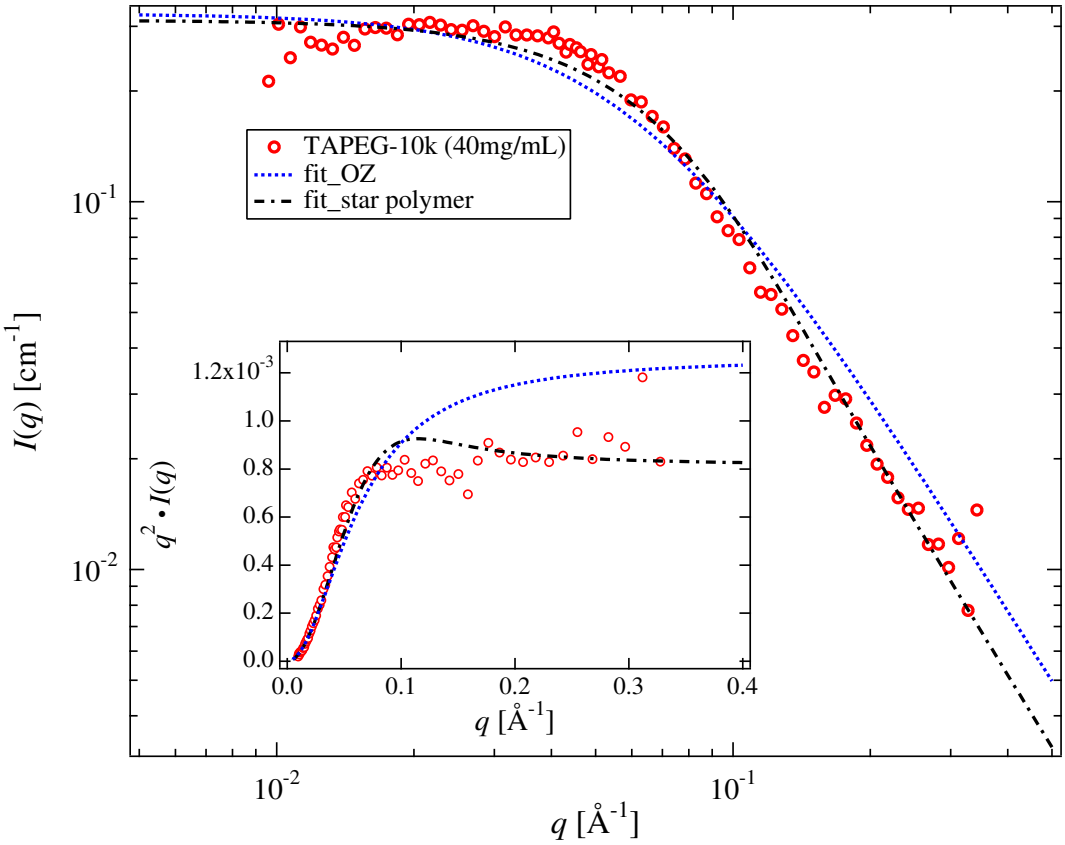

Figure 4.4: Scattering intensity function of TAPEG-10k macromer aqueous solution. The concentration was 40 mg/mL. The dashed and dotted lines are the fits with the scattering functions of star polymers and of gels, respectively.

Figure 4.7 shows the variations of R_{g},star for TAPEG-10k and TAPEG-20k as a function of ϕ_0. Note that R_{g},star is defined as the radius of gyration of the star polymer. Figure 4.7 indicates that R_{g},star is a decreasing function of ϕ_0 both for TAPEG-10k and TAPEG-20k. The value of R_{g},star was 19.1 Å for 40 mg/mL-TAPEG-10k. The hydrodynamic radius of four-arm TAPEG-10k at 10 mg/mL was obtained by dynamic light scattering (DLS). The value was $R_{\mathrm{h}} = 24.2$ Å.[9] By knowing the segment length of PEG chains to be 5.89 Å,[35] the radius of gyration can be estimated via eq 4.19. The theoretical value is 28.6 Å for the four-arm polymer in Θ condition. The ratio $\rho = R_{\mathrm{g}}/R_{\mathrm{h}}$ is 1.18. This value is reasonably in accordance to the theoretical ratio $\rho = R_{\mathrm{g}}/R_{\mathrm{h}} = 1.333$ (for $f = 4$ star polymer in Θ condition)[36] by considering that the latter is for the Θ condition. However, the values of R_{g} obtained by SANS are significantly lower than that obtained by DLS and do not

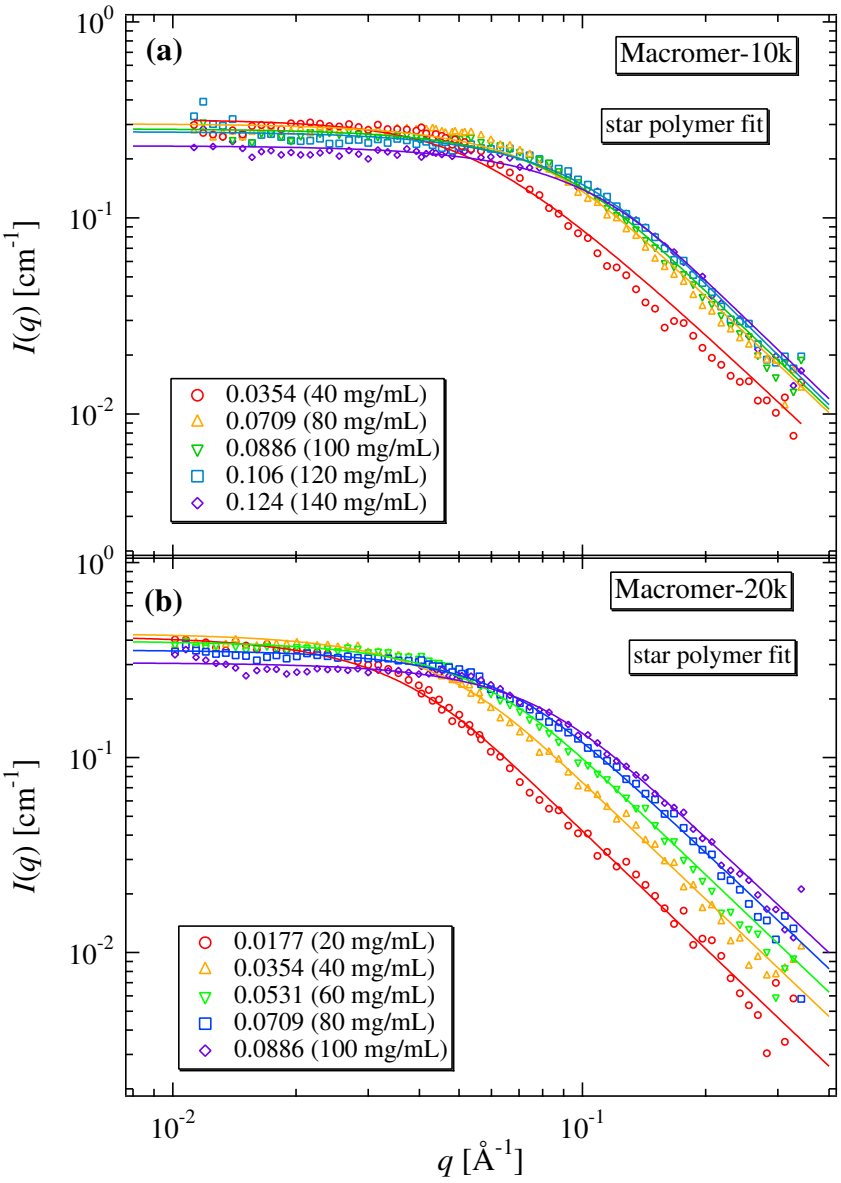

Figure 4.5: SANS intensity functions of TAPEG macromer solutions (a) TAPEG-10k and (b) TAPEG-20k. The solid lines are obtained by fitting with eq 4.16.

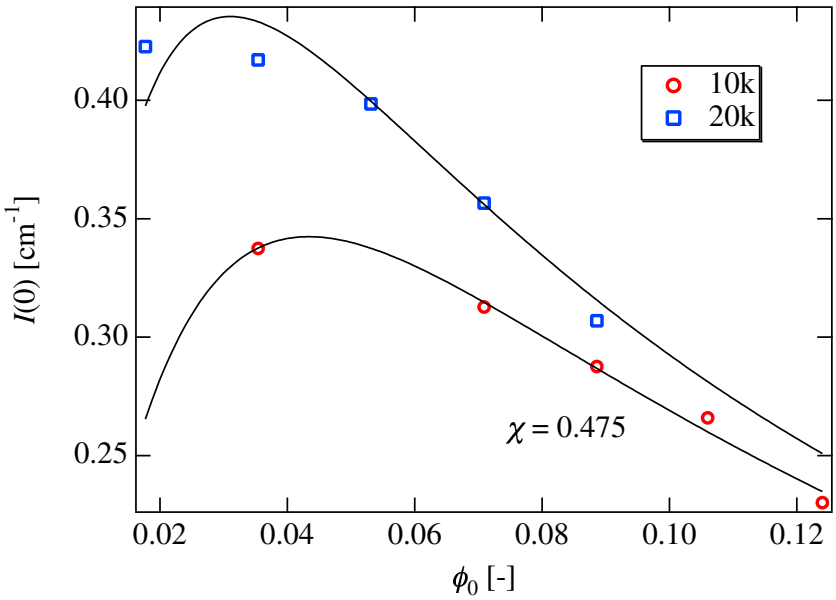

Figure 4.6: Variation of $I(0)$ as a function of ϕ_0. The solid lines are obtained with eq 4.16.

satisfy the relation. This is partially due to the difference in the concentrations, i.e., 40 mg/mL (SANS) and 10 mg/mL (DLS). By extrapolating ϕ_0 to 8.86×10^{-3} (10 mg/mL), one obtains $R_{\mathrm{g,star}} = 25.4$ Å, which is still below the expected value by the unperturbed chain calculation and by DLS. The reason is not clear at this stage. Apart from the absolute values of $R_{\mathrm{g,star}}$, $R_{\mathrm{g,star}}$ decreases roughly with a power-law fashion, i.e., $R_{\mathrm{g,star}} \sim \phi_0^{\beta}$, with $\beta = -0.293$ (Tetra-PEG-10k) and -0.325 (Tetra-PEG-20k). This indicates that Tetra-PEG macromer solutions consist of space-filled blobs of Tetra-PEG macromers and behave as $R_{\mathrm{g,star}} \sim \phi_0^{-1/3}$.

4.4.3 Tetra-PEG gel

Figure 4.8 shows SANS intensity curves for (a) Tetra-PEG-10k (b) Tetra-PEG-20k at various polymer concentrations. The solid lines represent fitting curves with OZ functions (eq 4.20)[37] with $A_{\mathrm{inhom}} = 0$ and the dashed lines are obtained with the star-polymer function (eq 4.16). Surprisingly, all the curves for gels are nicely fitted with the theoretical function (eq 4.20) without the inhomogeneitiy term (i.e., $A_{\mathrm{inhom}} = 0$). Figure 4.9 shows plots of $I(q)/\phi_0\xi^2$vs ξq. All the curves for gels are superimposed to a single master curve for (a) Tetra-PEG-10k and (b) Tetra-PEG-20k, respectively.

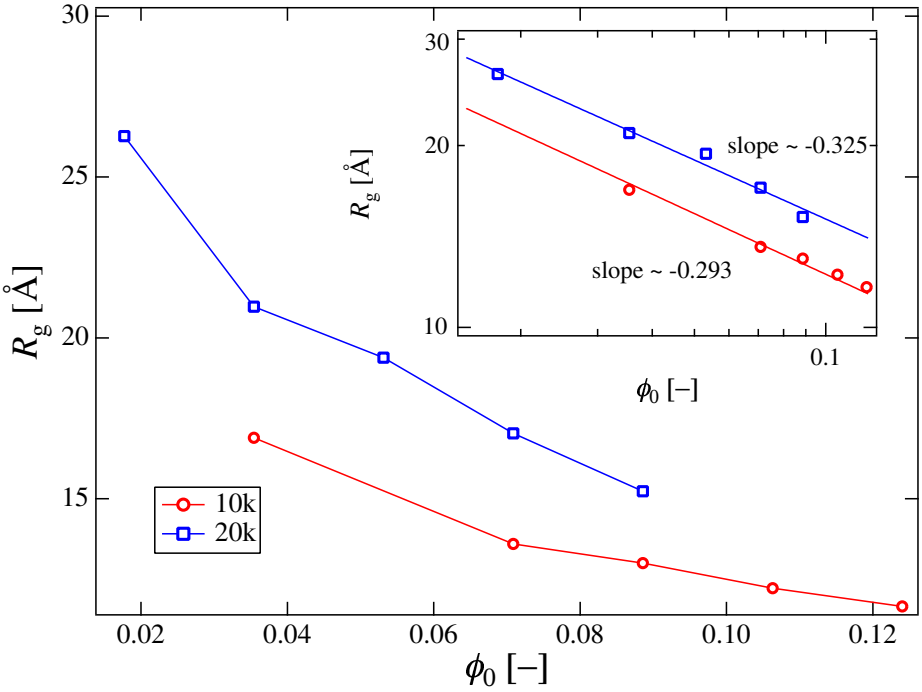

Figure 4.7: Variation of R_g as a function of ϕ_0. The inset is log-log plot of the same data.

This indicates that all the samples are in semi-dilute regime where macromer chains are connected to each other and form an infinite network. It should be noted here that the scattering intensity functions for polymer gels, in general, cannot be represented by a simple OZ function and hence cannot be superimposed by a single function, such as $I(q)/\phi\xi^2$vs ξq. Such non-universality in the scattering function is ascribed to the contribution of frozen-inhomogeneities (i.e., $A_{\text{inhom}} \neq 0$).[24,38] The experimental results for Tetra-PEG gels, however, strongly suggest that the network structure in Tetra-PEG gels is extraordinarily uniform at least up to the lower bound of the SANS experiment, i.e., 0.003 Å^{-1} ($\approx$ 2000 Å). It is known that frozen-inhomogeneities appear not in as-prepared gels but in swollen or deformed gels.[24,39] From this point of view, Figure 4.9 does not fully prove that Tetra-PEG gels have extraordinarily uniform networks. However, Figures 4.1 and 4.2 show that gelation in Tetra-PEG occurs even at lower concentrations than ϕ_0^*, probably via spontaneous stretching and coupling of the arm chains of TAPEG and TNPEG. In other words, uniform Tetra-PEG gels are also obtained even from a macromer mixture with $\phi_0 < \phi_0^*$ and these gel do not have the inhomogeneity term in the SANS function. These data strongly

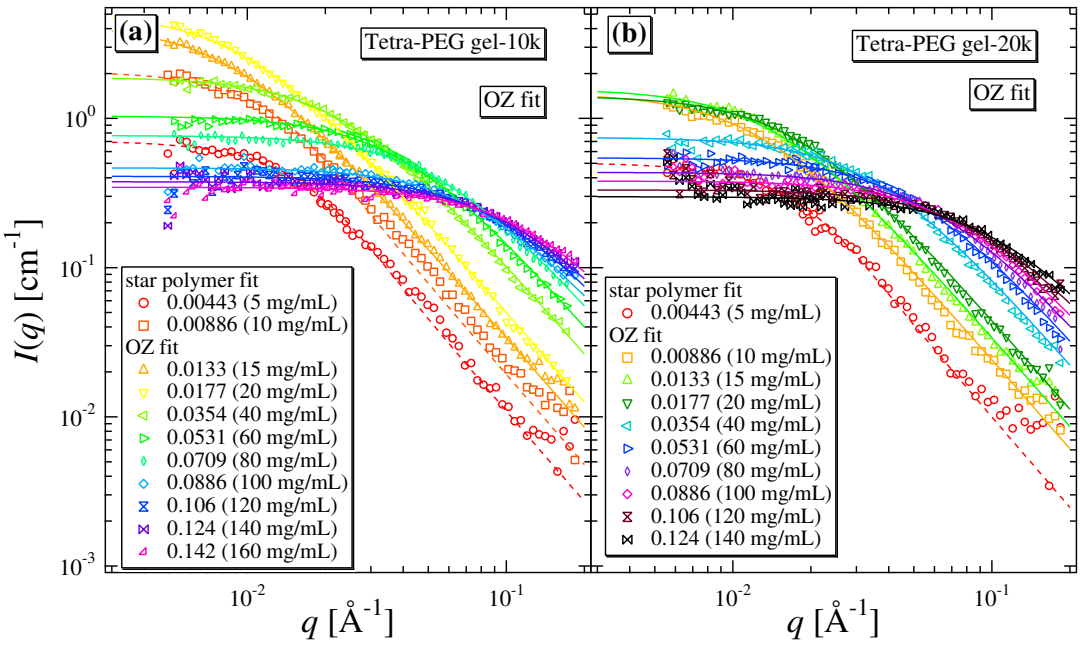

Figure 4.8: SANS intensity functions of Tetra-PEG gels. (a) Tetra-PEG -10k and (b) Tetra-PEG-20k. The solid lines are obtained by fitting with eq 4.20 with $A_{\mathrm{inhom}} = 0$. The dashed lines are fitted functions with eq 4.16 for imperfect gels prepared at low macromer concentrations.

support our argument. Furthermore, we recently carried out SANS measurements for swollen Tetra-PEG gels and observed absence of the inhomogeneity term. The details of the swollen gel systems will be reported in the forthcoming paper. In a more condensed and entangled system, Beltzung et al. reported SANS results on end-linked poly(dimethylsiloxane) network in swelling equilibrium.[4] They also observed no significant increase in scattering intensity. But in the field of hydrogels, Tetra-PEG gel is the first hydrogel having no inhomogeneities in equilibrium swollen state. It should be also mentioned that dynamic light scattering results showed nonergodicity in Tetra-PEG gels.[9] The presence of nonergodicity, in spite of high homogeneity in Tetra-PEG gels, may be ascribed to the fact that nonergodicity is not related to inhomogeneities but to topological fixation of chain motion by cross-linking. This issue will be also addressed in the forthcoming paper.

The variation of correlation length, ξ, is plotted against ϕ_0 in Figure 4.10. ξ is a decreasing function of ϕ_0. Note that the chain overlap concentrations, ϕ_0^*, of the macromer solutions, i.e., TAPEG and TNPEG, are calculated to be around 5.31×10^{-2}

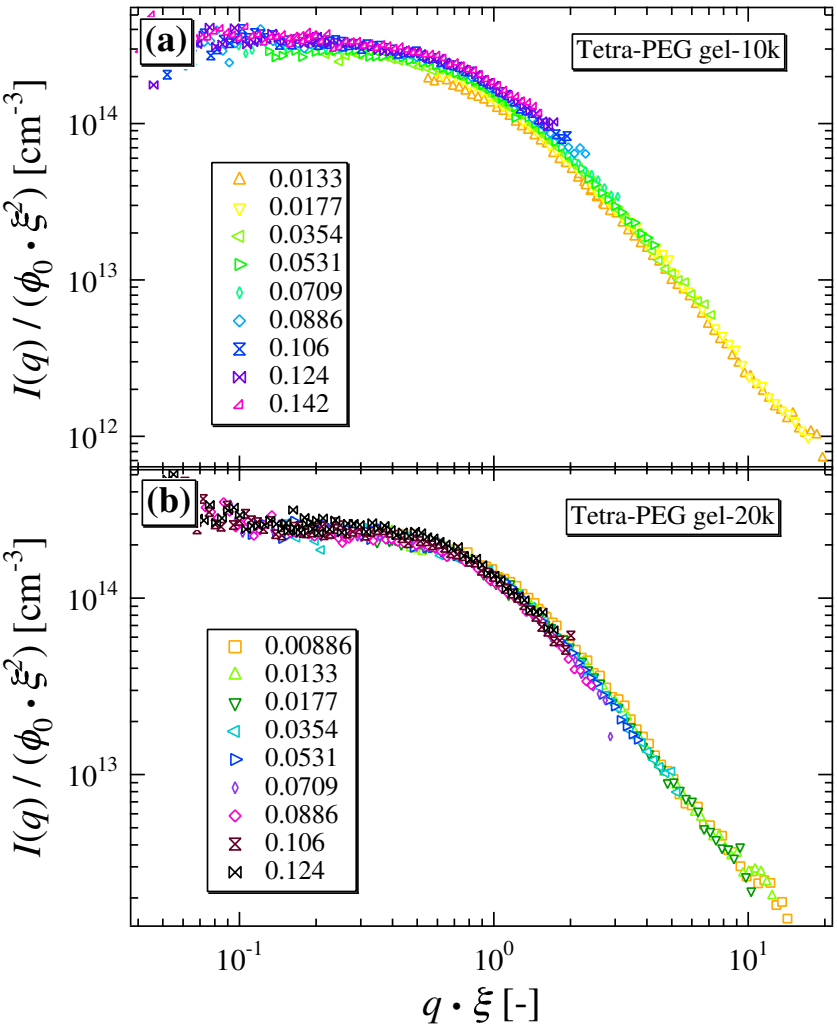

Figure 4.9: Master curve of Fig. 4.8 for (a) Tetra-PEG -10k and (b) Tetra-PEG-10k.

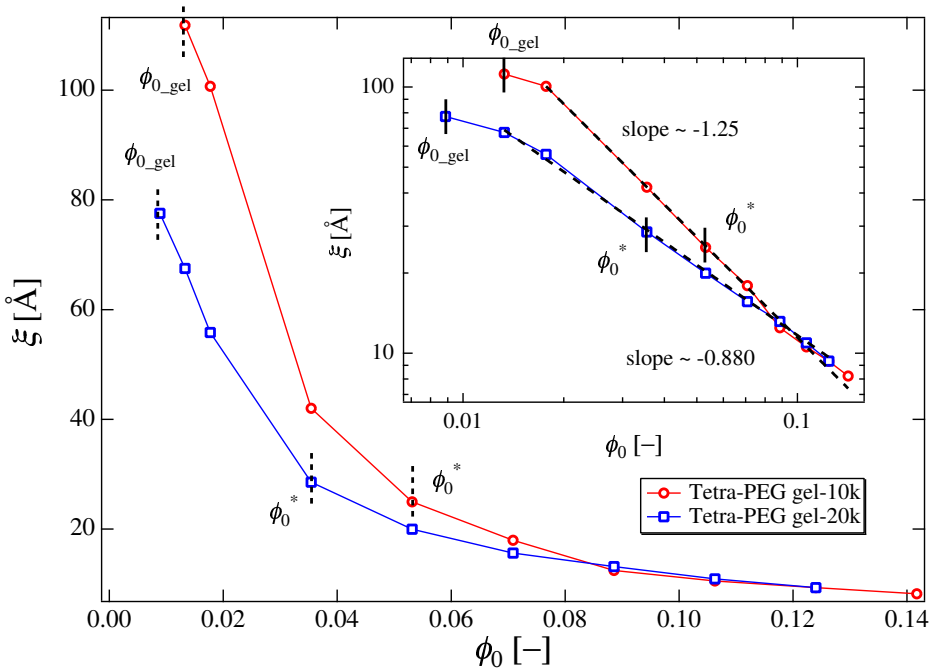

Figure 4.10: Variation of ξ as a function of ϕ_0. The inset is the log-log plot.

(60 mg/mL) and 3.54×10^{-2} (40 mg/mL) (marked with arrows) for Tetra-PEG-10k and Tetra-PEG-20k, respectively. If the concentration fluctuations in Tetra-PEG gels are the same as those in polymer solutions in a good solvent, ξ scales as $\xi \sim \phi_0^{-3/4}$ in a good solvent[37] and $\xi \sim \phi_0^{-1}$ in a Θ solvent. Therefore, the exponents shown in the inset, -1.25 (Tetra-PEG-10k) and -0.88 (Tetra-PEG-20k) may indicate that the blob chains in Tetra-PEG gels behave more likely as Gaussian chains than self-avoiding chains. This, in turn, means that the χ parameter of Tetra-PEG gels is close to 1/2.

Figure 4.11 shows $I(0)$vs ϕ_0 for Tetra-PEG-10k and Tetra-PEG-20k. $I(0)$ is a decreasing function of ϕ_0, except for the low ϕ_0 region ($\phi_0 < \phi_{0,\mathrm{gel}}$). The solid lines are the theoretical functions for $I(0)$ (eq 4.21) with $A_{\mathrm{inhom}} = 0$, with χ evaluated from the SANS analysis on the star-polymer solutions (Figure 4.5). These lines roughly reproduce the variation of $I(0)$ with ϕ_0, suggesting the validity of the SANS analysis. The results and discussion given above suggest that the network structure of Tetra-PEG gels is quite uniform and does not have noticeable defects, such as loops and dangling chains. In order to confirm these results more specifically, we carried out SANS experiments for non-stoichiometric cases.

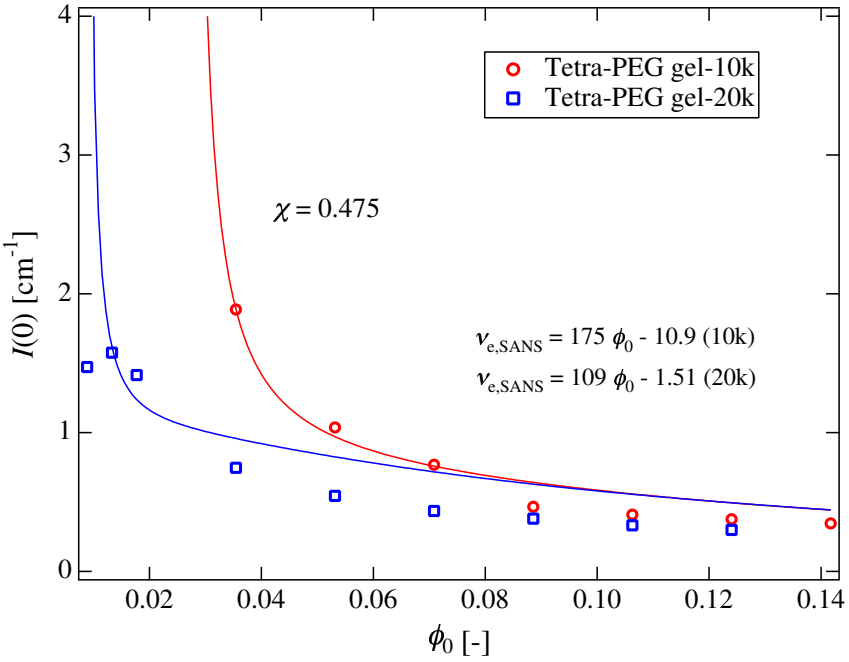

Figure 4.11: Variation of $I(0)$ as a function of ϕ_0. The solid lines are obtained with eq 4.21, where the ϕ_0 dependence of χ and ν_e are taken into account.

4.4.4 Non-stoichiometric Tetra-PEG gel

According to the discussion given above, it is of particular importance to match the concentration of TAPEG and TNPEG for achieving optimal mechanical properties of Tetra-PEG gels. In order to examine this conjecture, we carried out SANS and mechanical testing experiments for non-stoichiometric Tetra-PEG gels that were prepared with non-stoichiometric compositions, r = [TAPEG]/[TNPEG].

Figure 4.12a shows SANS intensity curves of Tetra-PEG-10k gels with TAPEG:TNPEG = 100:100 (matched) (r = 1), 90:110 (r = 0.82), 75:125 (r = 0.60), and 50:150 (r = 0.33). Interestingly, $I(q)$ is a sensitive function of the degree of asymmetry and decreases progressively when the degree of asymmetry increased. The SANS curve of the macromer (TAPEG) is also shown in the figure. The solid lines are the fits with

$$I(q) = \alpha I_{\mathrm{OZ}}(q) + (1-\alpha) I_{\mathrm{star}}(q) \tag{4.23}$$

Here, α is the ratio of the gel component. The physical meaning of eq 4.23 is that the minor component is able to couple with the same amount of the other component and forms a network, while the rest of the major component remains as star

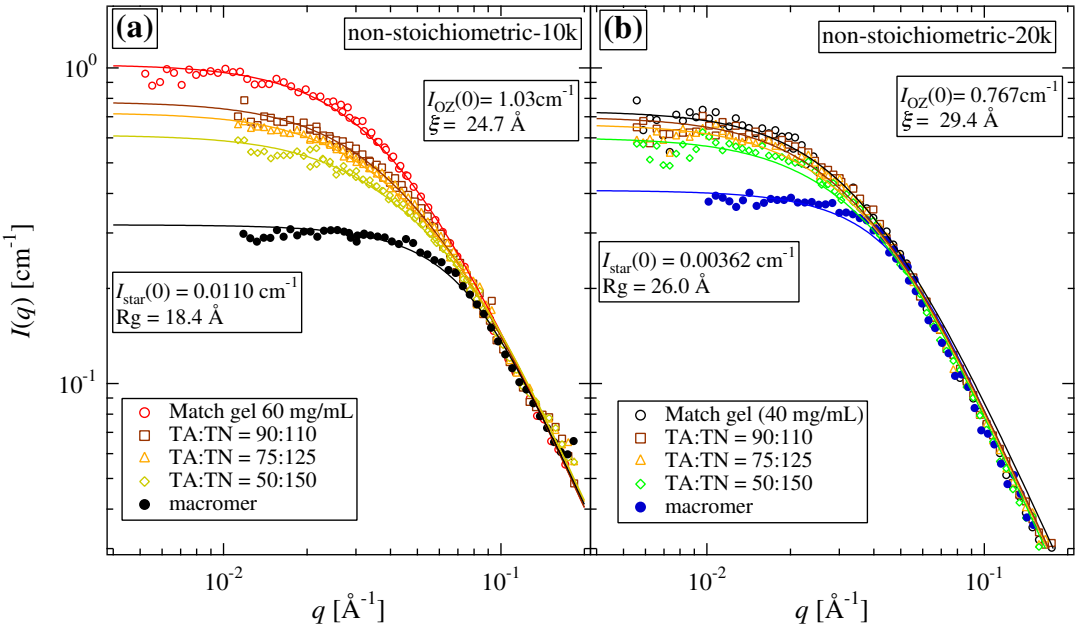

Figure 4.12: SANS intensity functions of non-stoichiometric Tetra-PEG gels, (a) Tetra-PEG-10k and (b) Tetra-PEG-20k. The solid lines are obtained by fitting with eq 4.21.

macromer chains. Curve fitting gives $\alpha = 0.65$ when $r = 0.9$. This means that simple additivity does not hold in $I(q)$. A similar result was obtained for the other side of non-stoichiometry, i.e., TAPEG:TNPEG = 110:90 ($r = 1.22$), 125:75 ($r = 1.67$), and 150:50 ($r = 3.0$). It is clear that $I(q)$ decreased when the degree of stoichiometry increased. Figure 4.12b shows the cases of Tetra-PEG-20k, resulting in the same conclusion as the case of Tetra-PEG-10k.

Figure 4.13 shows α together with (a) the breaking stress by compression and (b) the number density ratio of effective polymer chains contributing to the elasticity, $\nu_{e,w}/\nu_{e,st}$ as a function of log$r$. As clearly seen, both are symmetric function of log$r$. Figure 4.13 shows that (1) $I(q)$ and E are strong functions of the degree of stroichiometry and it becomes a maximum at $r = 1$, (2) a slight offset of composition results in a significant deviation from the simple additivity rule of $I(q)$, (3) the nonmatched TAPEG or TNPEG chains behave as defects of the network, resulting in significant depression of the mechanical properties.

Figure 4.14 shows schematic models of (a) Tetra-PEG macromer solutions and (b) Tetra-PEG gels as a function of ϕ_0. Due to the presence of a bulky end-group (NHS-

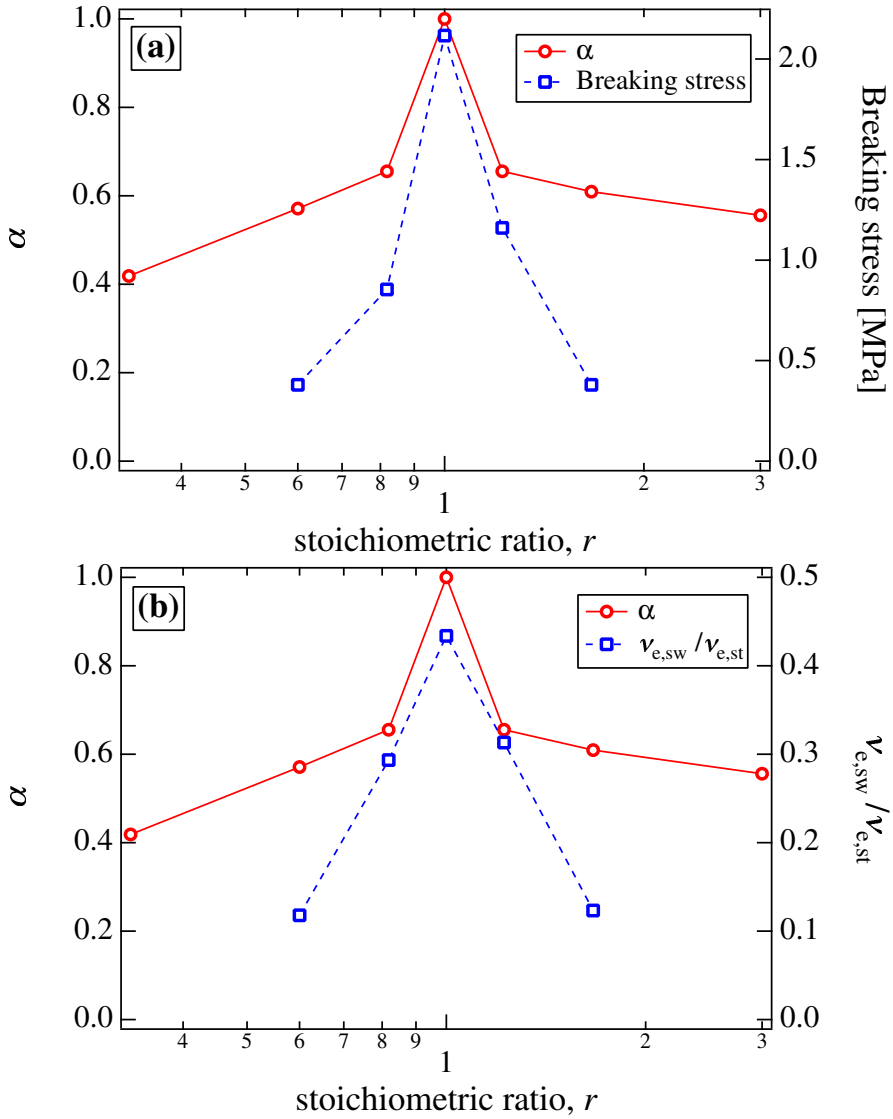

Figure 4.13: Plots of the ratio of gel component, α (solid line), as a function of the stoichiometric ratio, r. The right axes are (a) the breaking stress and (b) the ratio, $\nu_{\mathrm{e,sw}}/\nu_{rme,st}$. The χ value for $\nu_{\mathrm{e,sw}}$ is 0.475.

glutarate group for TNPEG) or electrostatic repulsive interaction between protonated trimethyleneamine groups for TAPEG at the end of arm chains, macromers do not overlap each other even at a concentration higher than ϕ_0^*. This leads to a formation of Tetra-PEG gels with a low degree of entanglements. Exclusive cross-end-coupling between amino and carboxyl groups of TAPEG and TNPEG macromers enables a formation of a tetrahedron-type network with a high yield and an extremely low degree of defects. All of these natures originating from a unique design of Tetra-PEG gels result in a formation of high-performance biocompatible gels with advanced mechanical properties.

4.5 Conclusion

Structure analyses of Tetra-PEG gels were carried out by means of swelling experiments and SANS, and the results were discussed by taking into account the mechanical properties of the same systems. The following facts are disclosed. (1) Tetra-PEG gels are stoichiometrically prepared irrespective of the initial polymer concentration, and their swelling behaviors are well predicted by the Flory-Rehner theory. (2) The mechanical moduli of Tetra-PEG gels, E and G, are proportional to the initial polymer concentration and is one order of magnitude larger than the corresponding gels made with similar tetra-arm PEG gels prepared with a low-molecular-weight coupling reagent. This indicates that cross-end-coupling of A- and B-type tetra-PEG is essential for gel preparation with extremely low defects. (3) The scattering functions of the macromers can be well reproduced by the scattering function for star polymers. (4) SANS functions of Tetra-PEG gels can be described by simple Ornstein-Zernike function without excess scattering component originating from cross-linking inhomogeneities. This means that Tetra-PEG gels are extremely homogeneous, and an “ideal” network free from defects is formed. (5) Preparation in non-stoichiometric composition leads to formation of defects in the polymer chain network and results in a significant depression of the mechanical properties. Structural models of macromer solutions and of Tetra-PEG gels, which account for the advanced mechanical properties of Tetra-PEG gels, are proposed.

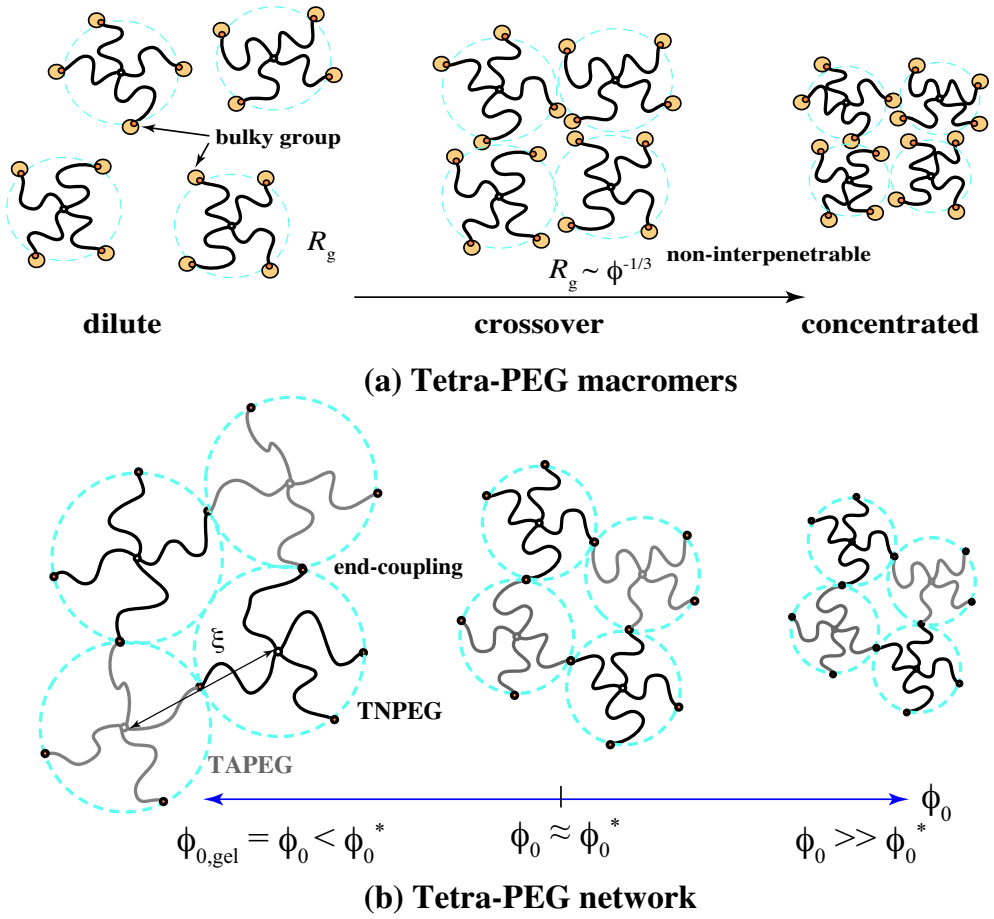

Figure 4.14: Schematic models showing the concentration-dependence of (a) macromer solutions and (b) Tetra-PEG gels. Due to the presence of bulky/hydrophobic groups at the end of arm chains, macromers are non-interpenetrable even at $\phi_0 > \phi_0^*$. By end-coupling of the end-groups exclusively between TAPEG and TNPEG, a regularly arranged Tetra-PEG gel is formed with a diamond-like architecture.

References

[1] Stein, R. S. *J. Polym. Sci.* 1969, **B7**, 657-660.

[2] Bueche, F. *J. Col. Interf. Sci.* 1970, **33**, 61-66.

[3] Shibayama, M.; Takata, S.; Norisuye, T. *Physica A* 1998, **249**, 245-252.

[4] Beltzung, M.; Herz, J.; Picot, C. *Macromolecules* 1983, **16**, 580-584.

[5] Norisuye, T.; Masui, N.; Kida, Y.; Shibayama, M.; Ikuta, D.; Kokufuta, E.; Ito, S.; Panyukov, S. *Polymer* 2002, **43**, 5289-5297.

[6] Okumura, Y.; Ito, K. *Adv.Mater.* 2001, **13**, (7), 485-487.

[7] Haraguchi, K.; Takehisa, T. *Adv. Mater.* 2002, **14**, 1120-1124.

[8] Gong, J. P.; Katsuyama, Y.; Kurokawa, T.; Osada, Y. *Adv. Mater.* 2003, **15**, (14), 1155-1158.

[9] Sakai, T.; Matsunaga, T.; Yamamoto, Y.; Ito, C.; Yoshida, R.; Suzuki, S.; Sasaki, N.; Shibayama, M.; Chung, U. *Macromoleules* 2008, **41**, 5379-5384.

[10] Flory, P. J., *Principles of Polymer Chemistry*; Cornell Univ.: Ithaca, 1953.

[11] Onuki, A. *Adv. Polym. Sci.* 1993, **109**, 63-121.

[12] Flory, P. J.; Rehner, J., Jr. *J. Chem. Phys.* 1943, **11**, 521.

[13] Shibayama, M.; Tanaka, T. *Adv. Polym. Sci.* 1993, **109**, 1-62.

[14] James, H. M.; Guth, E. *J. Chem. Phys.* 1947, **15**, 669-683.

[15] Mark, J. E.; Erman, B., *Rubberlike Elasticity A Molecular Primer*; Wiley: NY, 1988.

[16] Pearson, D. S. *Macromolecules* 1977, **10**, 696-701.

[17] Tanaka, T.; Hocker, L. O.; Benedek, G. B. *J. Chem. Phys.* 1973, **59**, 5151-5159.

[18] Einstein, A., *Theory of the opalescence of homogeneous liquids and mixtures of liquids in the vicinity of the critical state. In Colliod chemistry*, Alexander, J., Ed. Reinhold: New York, 1926; Vol. 1, p 323.

[19] Zimm, B. H. *J. Chem. Phys.* 1948, **16**, 1093-1099.

[20] Higgins, J. S.; Benoit, H. C., *Polymers and Neutron Scattering*; Clarendon Press: Oxford, 1994.

[21] Benoit, H. *J. Polym. Sci.* 1953, **11**, 507-510.

[22] Richter, D.; Farago, B.; Huang, J. S.; Fetters, L. J.; Ewen, B. *Macromoleules* 1989, **22**, 468-472.

[23] Ornstein, L. S.; Zernike, F. *Proc. Acad. Sci.* Amsterdam 1914, **17**, 793.

[24] Shibayama, M. *Macromol. Chem. Phys.* 1998, **199**, 1-30.

[25] Shibayama, M.; Isono, K.; Okabe, S.; Karino, T.; Nagao, M. *Macromolecules* 2004, **37**, 2909-2918.

[26] Okabe, S.; Nagao, M.; Karino, T.; Watanabe, S.; Adachi, T.; Shimizu, H.; Shibayama, M. *J. Appl. Cryst.* 2005, **38**, 1035-1037.

[27] Okabe, S.; Karino, T.; Nagao, M.; Watanabe, S.; Shibayama, M. *Nuclear Inst. and Methods in Physics Research, A* 2007, **572**, 853-858.

[28] Shibayama, M.; Nagao, M.; Okabe, S.; Karino, T. *J. Phy. Soc. Jpn.* 2005, **74**, 2728-2736.

[29] Hedden, R. C.; Saxena, H.; Cohen, C. *Macromolecules* 2000, **33**, 8676-8684.

[30] Mallam, S.; Horkay, F.; Hecht, A. M.; Geissler, E. *Macromolecules* 1989, **22**, 3356.

[31] Horkay, F.; Tasaki, I.; Basser, P. J. *Biomacromolecules* 2000, **1**, (1), 84-90.

[32] Lutolf, M. P.; Hubbell, J. A. *Biomacromolecules* 2003, **4**, 713-722.

[33] Debye, P.; Bueche, A. M. *J. Chem. Phys.* 1950, **18**, 1423-1425.

[34] Soni, V. K.; Stein, R. S. *Macromolecules* 1990, **23**, 5257-5265.

[35] Brandrup, J.; Immergut, E. H., *Polymer Handbook*; Wiley Interscience: N.Y., 1989.

[36] Burchard, W. *Adv. Polym. Sci.* 1999, **143**, 115-194.

[37] de Gennes, P. G., *Scaling Concepts in Polymer Physics*; Cornell University: Ithaca, 1979.

[38] Shibayama, M.; Takahashi, H.; Nomura, S. *Macromolecules* 1995, **28**, 6860-6864.

[39] Bastide, J.; Leibler, L. *Macromolecules* 1988, **21**, 2647.

Chapter 5

SANS and SLS Studies on Tetra-PEG Gels in As-prepared and Swollen States

5.1 Introduction

In chapter 5, a series of Tetra-PEG gels have been investigated by small-angle neutron scattering (SANS) and static light scattering (SLS). SANS experiments were carried out for the swollen gel in swelling equilibrium, as well as the precursor macromer solutions and the as-prepared gels.

It is well known that polymer gels have inhomogeneous structures.[1–6] Since these inhomogeneous structures are only "topologically frozen", a polymer gel in a solvent is an open system and is able to obey thermodynamics.[7] This is why a gel can change its volume depending on its environment and reach thermodynamic equilibrium.[8,9] Inhomogeneous structures in polymer gels are ascribed to an introduction of cross-links to a polymeric system, which fixes the topological architecture of the system. These inhomogeneities are often characterized by an upturn in the scattering intensity at low q-region in small-angle neutron scattering (SANS)[10] or a speckle pattern in laser light scattering,[11,12] where q is the magnitude of the scattering vector. There are various types of inhomogeneities, such as spatial, topological, connectivity, and mobility inhomogeneities as classified by shibayama et al.[13] A large number of studies on structural characterization of polymer gels have been carried out by using these properties.[6] Since the physical properties of gels, such as mechanical properties and optical properties, strongly depend on the structure, it is extremely important to clarify the relationship between structure and mechanical properties. The understanding

of cross-link inhomogeneities is vital from both scientific and engineering points of view since they affect the physical properties of the network polymer, such as mechanical and optical properties.[14] On the other hand, there has been a desire to prepare an "ideal" polymer network free from defects.[15] One of the theoretically promising methods to prepare a model network was end-coupling of telechelic polymer having a sharp molecular weight distribution by multi-functional cross-linker.[16–20] There has been no success to prepare defect-free networks so far.[21–23] No matter how precisely one controlled the architecture, the obtained "model network" had strong forward scattering at low q region and or exhibited double shoulder scattering curves. For example, Mendes et al. classified gel structures to (I) the one-correlation length gels, (II) the soft order gels that have a scattering maximum, and (III) the two-correlation length gels.[22] In chapter 4, we revealed that SANS functions of Tetra-PEG gels can be described by simple Ornstein-Zernike function without excess scattering component originating from cross-linking inhomogeneities. In this chapter, we discuss the structure of Tetra-PEG gels in as-prepared and swollen states with the scattering intensity data in a wide q range covering not only SANS ($0.003 \leq q \leq 0.2$ Å^{-1}) but also light scattering (LS) regime ($0.0008 \leq q \leq 0.002$ Å^{-1}).

5.2 Theoretical Background

5.2.1 Scattering functions for multi-arm polymer chains

The form factor of multi-arm star polymer chains, $P_{\mathrm{star}}(q)$ is given by[24,25]

$$P_{\mathrm{star}}(q) = \frac{2Z}{fu^2}\{u - [1 - \exp(-u)] + \frac{f-1}{2}[1 - \exp(-u)]^2\} \tag{5.1}$$

Here, f is the number of arms of the star polymer, Z is the degree of polymerization, and $u \equiv Za^2q^2/6$ with a being the segment length. Eq 5.1 is a "Debye function" for f-arm polymer chain. The inter-polymer interaction can be taken into consideration in terms of the Flory-Huggins interaction parameter, χ, and the scattering intensity is given by,

$$I(q) = \frac{(\Delta\rho)^2}{N_{\mathrm{A}}} \frac{V_2\phi P_{\mathrm{star}}(q)}{1 + (1-2\chi)\left(\frac{V_2}{V_1}\right)\phi P_{\mathrm{star}}(q)} \tag{5.2}$$

Here, N_{A} is the Avogadro's number, and ϕ is the volume fraction of the solute. V_1 and V_2 are the molar volumes of the solvent and the monomer unit of the solute,

respectively. $(\Delta\rho)^2$ is the scattering length density difference square between the polymer 2 and solvent 1.

$$(\Delta\rho)^2 = (\rho_2 - \rho_1)^2 = \left[\left(\frac{b_2}{\tilde{V}_2}\right) - \left(\frac{b_1}{\tilde{V}_1}\right)\right]^2 \tag{5.3}$$

where b_i and $\tilde{V}_i$ are the scattering length and the volume of the solvent ($i = 1$) and the monomeric unit of component ($i = 2$).

5.2.2 Scattering functions of polymer gels

According to de Gennes,[26] the scattering intensity function of polymer gels in swelling equilibrium is the same as that of polymer solutions at the same concentration and is given by

$$I(q) = \frac{(\Delta\rho)^2 RT\phi^2}{N_{\mathrm{A}} M_{\mathrm{OS}}} \frac{1}{1 + \xi^2 q^2} \tag{5.4}$$

Here, ξ is the correlation length of the network. R is the gas constant, and T is the absolute temperature. M_{OS} is the osmotic modulus of the gel given by[9]

$$M_{\mathrm{OS}} = \frac{RT\phi^2}{V_1}\left(\frac{1}{1-\phi} - 2\chi\right) + \nu_{\mathrm{e}} RT\left[\frac{1}{2}\left(\frac{\phi}{\phi_0}\right) + \left(\frac{\phi}{\phi_0}\right)^{1/3}\right] \tag{5.5}$$

where ν_{e} is the number density of the effective elastic chains in the network. In principle, the scattering function can be represented by the so-called Ornstein-Zernike function,[27] i.e., eq 5.4. However, it is known that scattering intensity functions of gels have significant forward scattering at low q-region due to cross-linking inhomogeneities. As a result, by adding an extra term, eq 5.4 is modified to[28]

$$I(q) = \frac{(\Delta\rho)^2 RT\phi^2}{N_{\mathrm{A}} M_{\mathrm{OS}}}\left[\frac{1}{1 + \xi^2 q^2} + \frac{A_{\mathrm{inhom}}}{\left(1 + \Xi^2 q^2\right)^2}\right] \tag{5.6}$$

The extra term A_{inhom} is dependent on the chemistry of gel preparation since it represents how the component polymer chains are topologically frozen by cross-linking.

5.3 Experimental Section

5.3.1 Sample preparation

Tetra-amine-terminated PEG (TAPEG) and tetra-NHS-glutarate-terminated PEG (TNPEG) were prepared from tetrahydroxyl-terminated PEG (THPEG) having equal

arm lengths. Here, NHS represents for N-hydroxysuccinimide. The details of TAPEG and TNPEG preparation are reported elsewhere.[29] The molecular weights (M_w) of TAPEG and TNPEG were matched to each other, and four sets of samples having different M_w's were prepared, i.e., M_w = 5k, 10k, 20k, and 40k g/mol. The sample code is given by the M_w, e.g., Tetra-PEG-5k being Tetra-PEG with $M_w = 5 \times 10^3$. The activity of the functional group was estimated using NMR. Tetra-PEG gels were synthesized as follows. Constant amounts of TAPEG and TNPEG (5-160 mg/mL) were dissolved in phosphate buffer (pH7.4) and phosphate-citric acid buffer (pH5.8), respectively. In order to obtain coherent neutron scattering from the polymers, these buffer solutions were prepared with deuterated water. In order to control the reaction rate, the ionic strengths of buffers were chosen to be 25 mM for lower macromer concentrations (5-100 mg/mL) and 75 mM for higher macromer concentrations (110-160 mg/mL) for Tetra-PEG-10k. The ionic strengths of buffers were chosen to be 50 mM for lower macromer concentrations (5-100 mg/mL) and 100 mM for higher macromer concentrations (110-160 mg/mL) for Tetra-PEG-5k, 20k 40k. Two solutions were mixed, and the resulting solution was poured into the mold. At least 12 hours were spent for completion of reaction before the following experiments.

5.3.2 Small-angle neutron scattering (SANS)

Small-angle neutron scattering experiments were carried out at two-dimensional SANS instrument, SANS-U,[30,31] the University of Tokyo, located at JRR-3 Research Rector, Japan Atomic Energy Agency, Tokai, Ibaraki, Japan. Monochromated cold neutron beam with the average neutron wavelength of 7.00 Å and 10 % wavelength distribution was irradiated to the samples. The scattered neutrons were counted with a two-dimensional position detector (Ordela 2660N, Oak Ridge, USA). The sample-to-detector distance was chosen to be 1 and 4 m for macromer (TAPEG) measurements and 2 and 8 m for Tetra-PEG-gel measurements. After necessary corrections for open beam scattering, transmission and detector inhomogeneities, the corrected scattering intensity functions were normalized to the absolute intensity scale with a polyethylene secondary standard. The details of the instrument are reported elsewhere.[?,30] Incoherent scattering subtraction was made with the method reported by Shibayama

et al.[32]

5.3.3 Static light scattering (SLS)

Static light scattering (SLS) measurements were performed by a static/dynamic compact goniometer (DLS/SLS-5000), ALV, Langen, Germany. A He-Ne laser with a power of 22 mW emitting a polarized light at $\lambda = 6328$ Å was used as the incident beam. SLS intensity functions were taken at 20 °C at scattering angles of $30° - 150°$.

5.4 Results and Discussion

5.4.1 Macromer solutions

Figure 5.1 shows the scattering intensity curves of (a) TAPEG-5k, (b) TAPEG-10k, (a) TAPEG-20k, and (d) TAPEG-40k macromer solutions in as-prepared state with various concentrations, ϕ ($= \phi_0$). The solid lines show the curve fits with eq 5.2, i.e., the scattering function for tetra-arm polymer chains. All observed SANS functions were well represented by eq 5.2. It should be noted that the interaction parameter, χ, has to be varied from 0.495 (TAPEG-5k) to 0.465 (TAPEG-40k) in order to reproduce the observed SANS intensity functions with eq 5.2.

The molecular weight-dependence of the interaction parameter χ is shown in Figure 5.2, which seems to be a decreasing function of M_w. The reasons for the M_w-dependence may be the presence of arm-end,[29] and the chain-end effect becomes insignificant by increasing M_w. As a matter of fact, the value of χ approaches the value of linear PEG chains[33] ($\chi = 0.43$ at $T = 20$ °C) by increasing M_w.

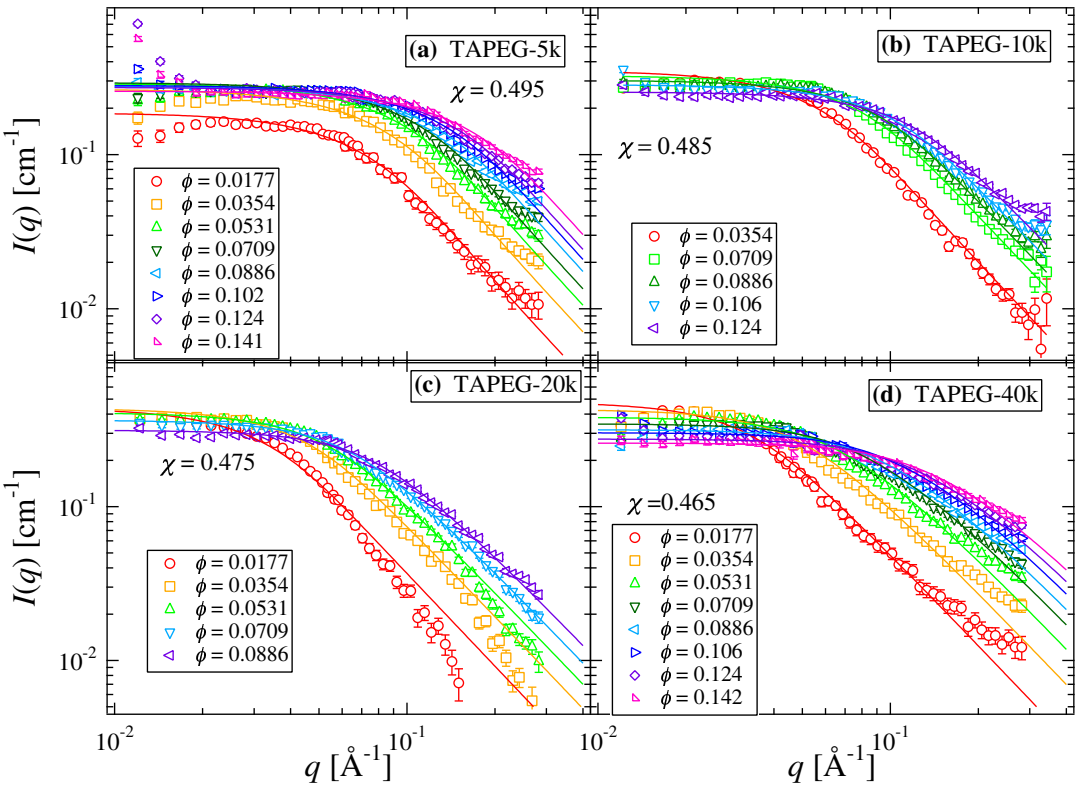

Figure 5.1: The scattering intensity curves of TAPEG macromer solutions, (a) TAPEG-5k, (b) TAPEG-10k, (c) TAPEG-20k, and (d) TAPEG-40k.

Figure 5.3 shows the M_w- and concentration-dependence of the radius of gyration, R_g of TAPEG. R_g seems to be a decreasing function of the initial polymer fraction, ϕ_0, as well as of M_w. The inset shows that R_g is roughly given by $R_g \sim \phi_0^{-1/3}$, indicating that a simple contraction occurs in Tetra-PEG chains as a function of ϕ_0. This exponent indicates that the Tetra-PEG chains behave as compressive elastic balls dependent on the concentration, and no inter-penetration occurs even at $\phi_0 > \phi_0^*$, where ϕ_0^* is the overlap concentration. The absence of inter-penetration may be due to the presence of a large number of end groups as discussed in the previous paper.[28] Regarding M_w-dependence, on the other hand, the plots of R_g vs ϕ_0 in the inset do not seem to be superimposed by shifting with an equal gap, although the M_w of the TAPEGs are in a series of two folds (i.e., 5k, 10k, 20k and 40k). Hence, there is a strong deviation from a power law, i.e., $R_g \sim M_w^{-\alpha}$ with $\alpha = 1/2$ (Θ-solvent) or 3/5 (good solvent). Figure 5.4 shows the M_w-dependence of R_g for the case of $\phi_0 = 0.0709$. The dashed and chain lines are calculated values by assuming $R_g \sim M_w^{-\alpha}$

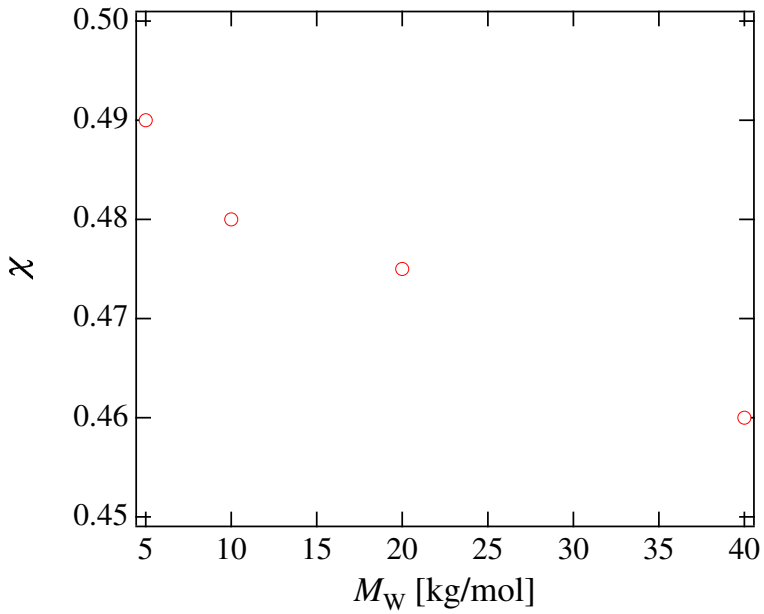

Figure 5.2: The molecular weight dependence of the apparent interaction parameter χ.

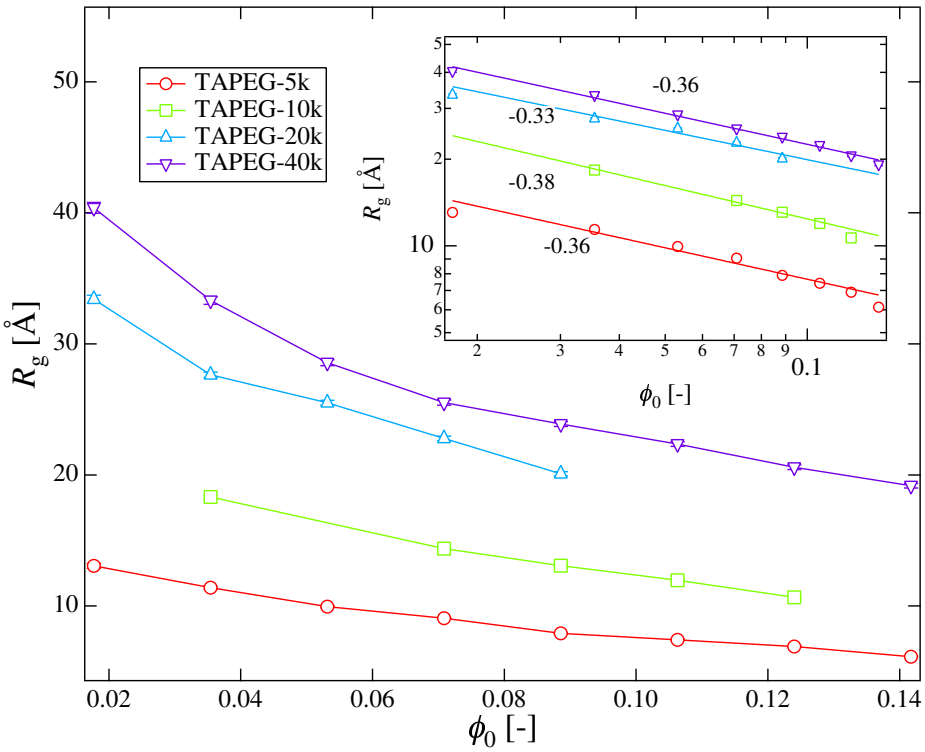

Figure 5.3: Polymer concentration-dependence of the radius of gyration, R_g, of TAPEGs having various M_w's. The inset shows the log-log plots.

with $\alpha = 1/2$ and $3/5$, respectively. Interestingly, a relation $R_g \sim M_w^{-1/2}$ is obtained for TAPEG-5k and TAPEG-40k, although a significant positive deviation is seen for TAPEG-10k and TAPEG-20k. The reason is not clear at this stage.

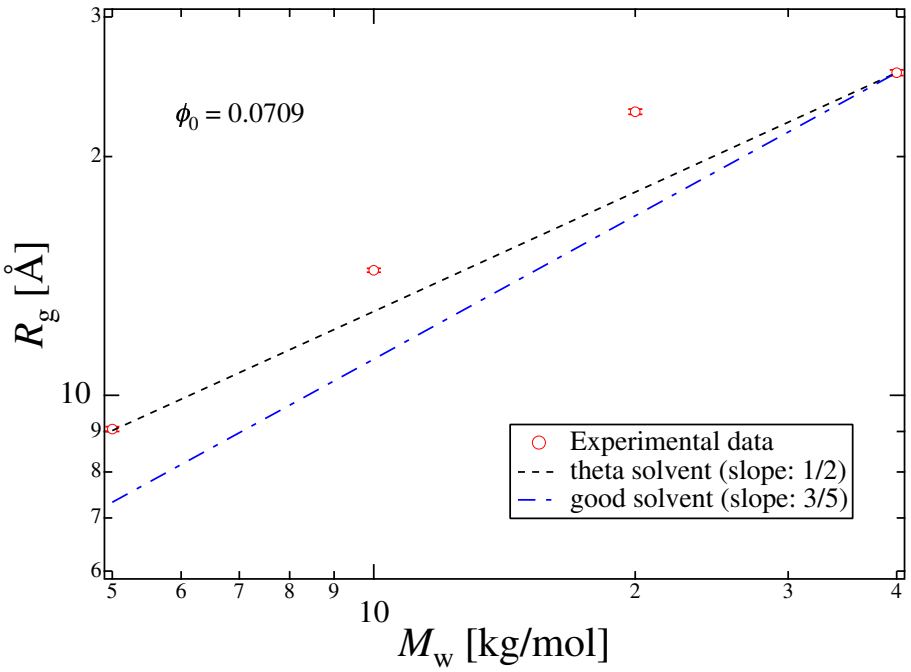

Figure 5.4: M_w-dependence of R_g for $\phi_0 = 0.0709$. The dashed and chain lines denote calculated values by assuming $R_g \sim M_w^{-\alpha}$ with $\alpha = 1/2$ and 3/5, respectively.

5.4.2 Tetra-PEG Gels in as-prepared state

Figure 5.5 shows SANS curves of as-prepared gels for (a) Tetra-PEG-5k gels, (b) Tetra-PEG-10k gels, (c) Tetra-PEG-20k gels, and (d) Tetra-PEG-40k gels. Note that these sub-figures correspond to those of Fig. 5.1. The solid lines are the fits with eq 5.4, i.e., the Ornstein-Zernike (OZ) function. In the case of as-prepared Tetra-PEG-5k gel, a strong upturn in $I(q)$ for $q \leq 0.01\text{Å}^{-1}$ is observed for $\phi_0 \geq 0.0531$, and a fitting with eq 5.4 is poor. However, for larger q, each $I(q)$ can be fitted with an OZ function. Unlike the case of Tetra-PEG-5k gels, no significant upturn in $I(q)$ is found at low q-region in Tetra-PEG-10k, -20k, and -40k in this q-region. It should be noted here the following. Polymer gels usually exhibit a strong upturn in low q-region due to the presence of inhomogeneities.[5,6] Even in the case of "ideal polymer networks" made by end-linking of telechelic polymer chains, significant inhomogeneities are reported.[22,23] Figure 5.6 shows concentration-dependence of the correlation length, ξ, for Tetra-PEG gels with various M_w's. Surprisingly, the larger M_w is, the smaller ξ is. If ξ represents the mesh size formed by cross-end-coupling

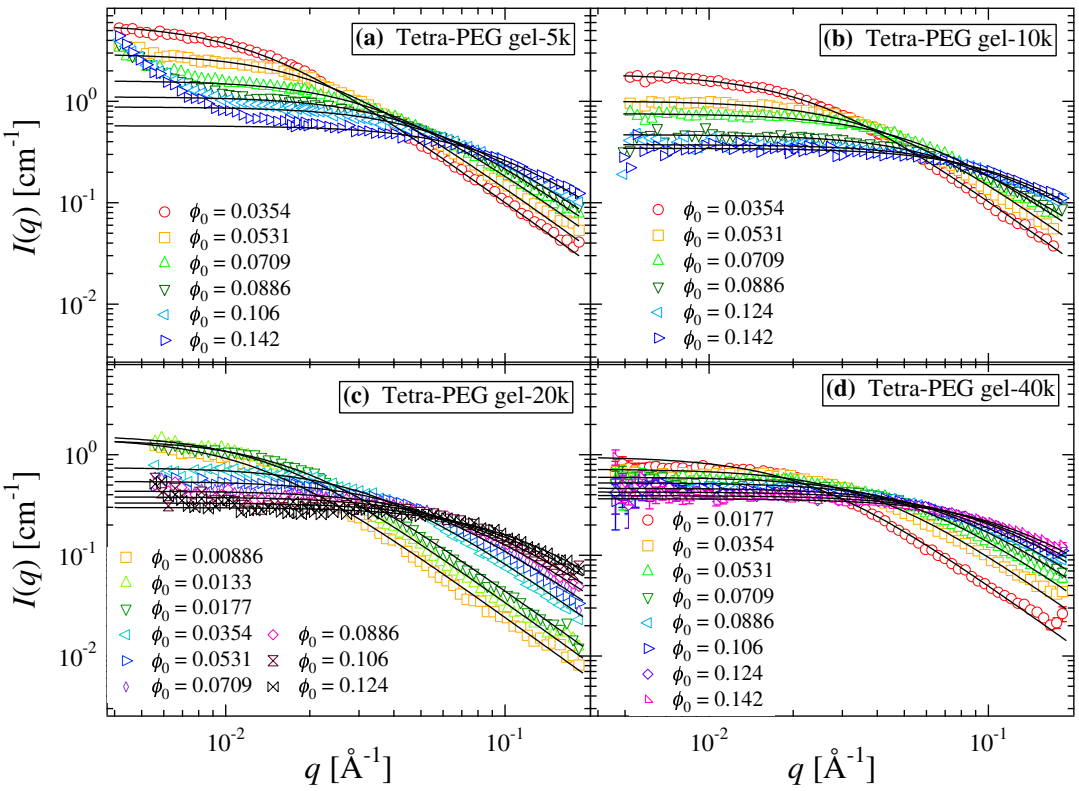

Figure 5.5: SANS curves of as-prepared gels for (a) Tetra-PEG-5k, (b) -10k, (c) -20k, and (d) -40k. The solid lines denote the results of curve fit with OZ functions.

of TAPEG and TNPEG, ξ should increase with M_w with a power of either 1/2 (Θ solvent) or 3/5 (good solvent). The experimental results, however, show the opposite behavior. The concentration-dependence of ξ is also quite different from that of the macromers. Though ξ seems to be well represented by a power-law function of ϕ_0 for each set of Tetra-PEG as shown in the inset, the exponents are much larger than -3/4 expected for a semidilute solution in a good solvent as well as for a gel in swelling equilibrium.[26] These exponents seem to decrease as M_w increases and approach the value, i.e., -3/4. As a matter of fact, Tetra-PEG-40k gels show $\xi \sim \phi_0^{-0.78}$, of which exponent is close enough to -3/4 (See, the inset of Figure 6). Hence, it is conjectured that the observed ξ for Tetra-PEG -40k gels represents the size of "mesh" of the polymer network. On the other hand, those for 5k, 10k, and 20k may represent additional concentration fluctuations, of which correlation lengths are much larger than the mesh size. This is probably due to formation of imperfect polymer network as schematically shown in Figure 5.7. That is, if an arm chain is not long enough, the arm chain is too rigid to undergo cross-end coupling reaction between TAPEG and TNPEG with a high yield. If this is the case, a large number of network defects are formed, leading to an observation of a larger mesh size characterized by the correlation length, ξ. The yield of cross-end coupling is expected to increase by increasing the initial polymer concentration, leading to a stronger concentration-dependence of ξ. This may be why the exponent is much larger than that expected for polymer network in a good solvent. However, these structural and kinetic constraints are suppressed by increasing M_w, leading to a recovery of the expected exponent.

5.4.3 Swollen gels in swelling equilibrium

Figure 5.8 show a series of SANS intensity functions for Tetra-PEG gels in swelling equilibrium for (a) Tetra-PEG gel-5k, (b) -10k, (c) -20k, and (d) -40k. As shown in these figures, $I(q)$s for the swollen gels are satisfactorily fitted with OZ functions irrespective of ϕ. Here, note that ϕ is the polymer volume fraction at swelling equilibrium, which is different from the polymer volume fraction at preparation, ϕ_0. As shown in these figures, cross-linking inhomogeneities seem to disappear by swelling, which is opposite to the case of randomly cross-linked conventional gels (statistical gels).[34–39] Note that in the case of conventional gels, cross-linking inhomogeneities

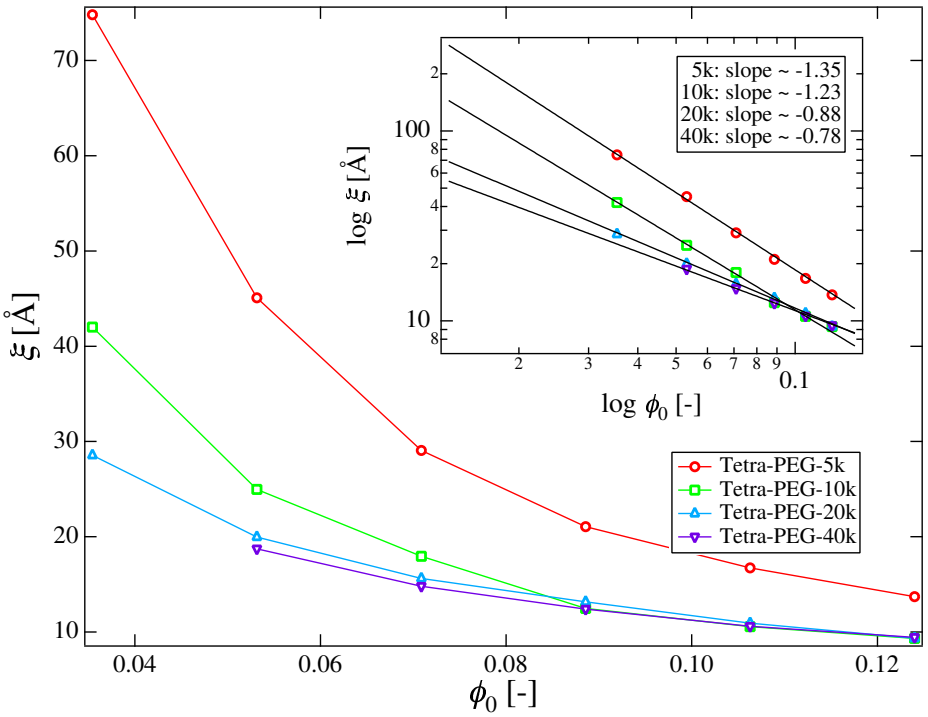

Figure 5.6: Concentration-dependence of the correlation length, ξ, for Tetra-PEG gels with macromer molecular weights of 5k, 10k, 20k, and 40k.

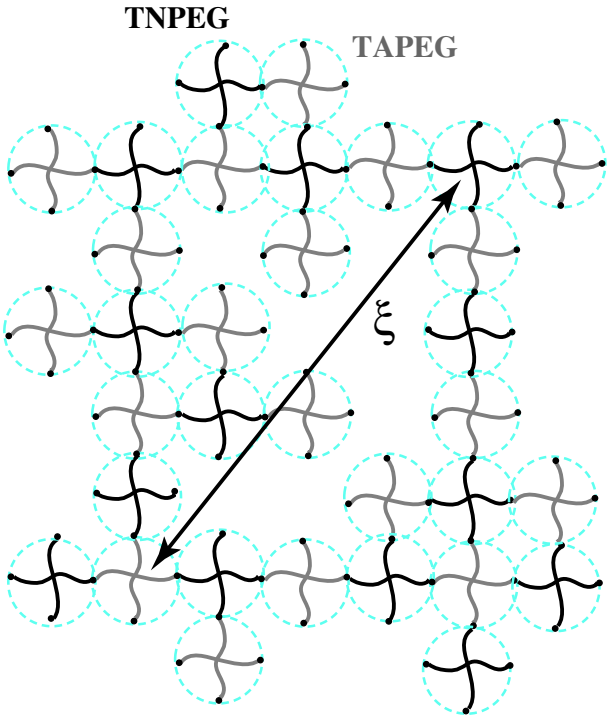

Figure 5.7: Schematical representation of the structure of Tetra-PEG-5k gels. Due to imperfect cross-end-coupling reaction, large voids are formed, which are characterized by ξ.

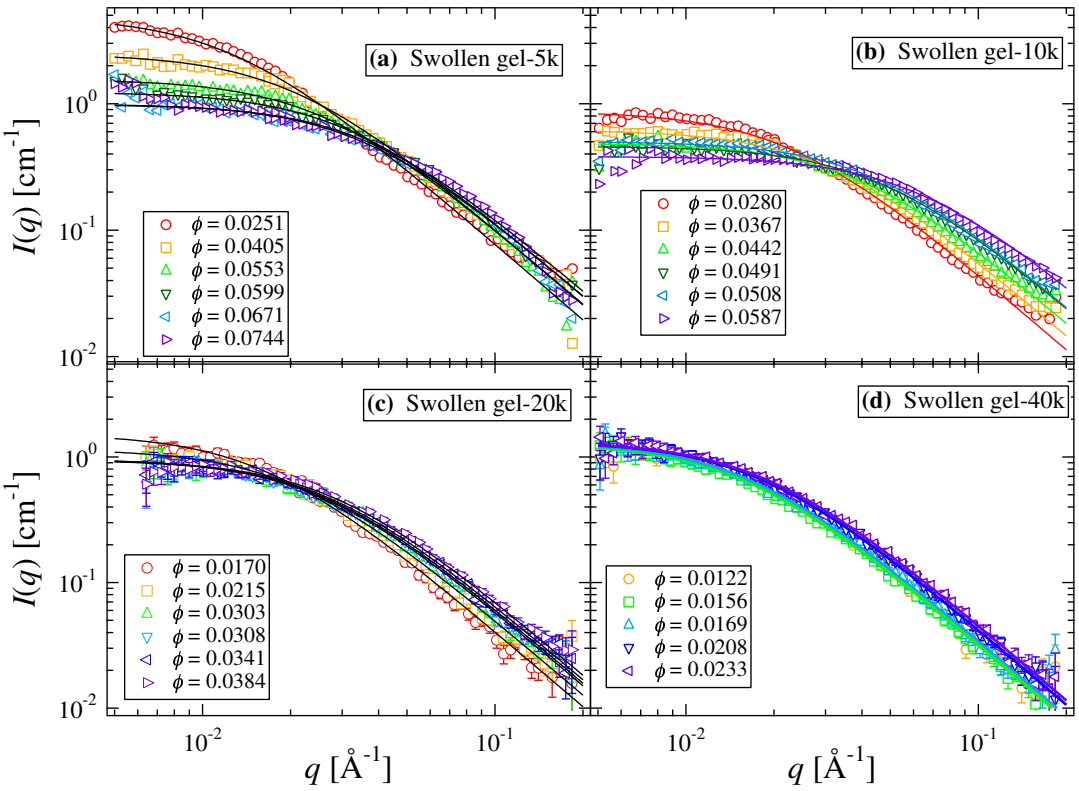

Figure 5.8: A series of SANS intensity functions for Tetra-PEG gels in swelling equilibrium for (a) Tetra-PEG gel-5k, (b) -10k, (c) -20k, and (d) -40k. The solid lines denote the results of curve fit with OZ functions.

are not explicit in as-prepared gels because cross-links are introduced so as to minimize the free energy. However, cross-linking inhomogeneities become explicit due to inhomogeneous swelling according to the difference in the local cross-link density as was explained by Bastide and Leibler.[34] Even in the case of statistical gels made by end-linking, swollen gels exhibit upturn in SANS.[23] Hence, the absence of an upturn in the SANS intensity functions observed in Tetra-PEG gels is quite unusual. Another interesting feature of Tetra-PEG gels is that the SANS intensity functions become ϕ-independent by increasing M_w. The reason for this unique behavior will be discussed later. Figure 5.9 shows ξ vs ϕ plots for swollen gels for (a) Tetra-PEG-5k, (b) -10k, (c) -20k, and (d) -40k (solid symbols with solid lines) as well as ξ vs ϕ_0 plots for as-prepared gels (open symbols and broken lines). Various interesting features can be extracted from this figure. First, ξ increases by swelling (i.e., the values of ξ move left and upward by changing ϕ_0 to ϕ). Second, different from the case of as-prepared

gels (Fig. 5.6), no clear relationship between ξ and ϕ is found in the swollen gels. Third, the ϕ-dependence of ξ becomes smaller by increasing M_w. For example, in the case of Tetra-PEG-40k, ξ and ϕ are collapsing into a small region of $\xi \approx 60$ Å and $0.01 < \phi < 0.02$ independent of ϕ_0. This tendency seems reasonable because a unique set of values of ξ and ξ is expected to exist in a gel at swelling equilibrium, i.e., (ξ_{eq}, ϕ_{eq}), for a network with a given set of M_w and ξ. This tendency weakens as M_w decreases. For example, in the case of Tetra-PEG-5k, ξ changed little with swelling and ξ scales with $\phi^{-1.01}$. Thus, a unique set of values of ξ and ϕ does not exist for Tetra-PEG-5k. Hence, it is concluded that Tetra-PEG-40k gel is closer to an ideal network than other gels with lower M_ws. Figure 5.10 schematically shows as-prepared Tetra-PEG-40k gels as a function of ϕ_0, and those in swelling equilibrium at the polymer volume fraction ϕ. In the case of as-prepared gels, the characteristic size of the network scales with ϕ_0^{γ}, where the exponent γ is close to -3/4 (See Figure 9). When the gels are swollen in water, they reach a unique swollen state depending on their molecular weights as shown schematically in the bottom of Figure 5.10. The presence of a unique swollen state independent of ϕ_0 suggests that cross-linking reaction occurs exclusively at the surface of Tetra-PEG macromers and no entanglement formation takes place. Hence, it is concluded that the cross-end-coupling employed in this system is an effective method to prepare an ideal network without defects or trapped entanglements.

5.4.4 Master curves

In the discussion of Figure 5, it was pointed out that a strong upturn was observed at low q region for Tetra-PEG-5k gel. In order to elucidate this anomaly in the low q region ($0.003 \leq q \leq 0.02$ Å^{-1}), we carried out static light scattering (SLS) in the region of $0.0008 \leq q \leq 0.002$ Å^{-1}. Figure 5.11(a) shows the result of SANS as well as SLS experiments. Though there is a small missing region between SANS and SLS data (marked by the dashed line), both sets of scattering intensity data seem to be smoothly connected to each other and a master curve is obtained. Note that the SLS data are shifted vertically so as to be connected with the corresponding SANS data. More interestingly, by scaling $I(q)/\phi_0\xi^2$ and ξq, all scattering intensity curves fall onto a single maser curve as shown in Figure 5.11(b). Similar behaviors were

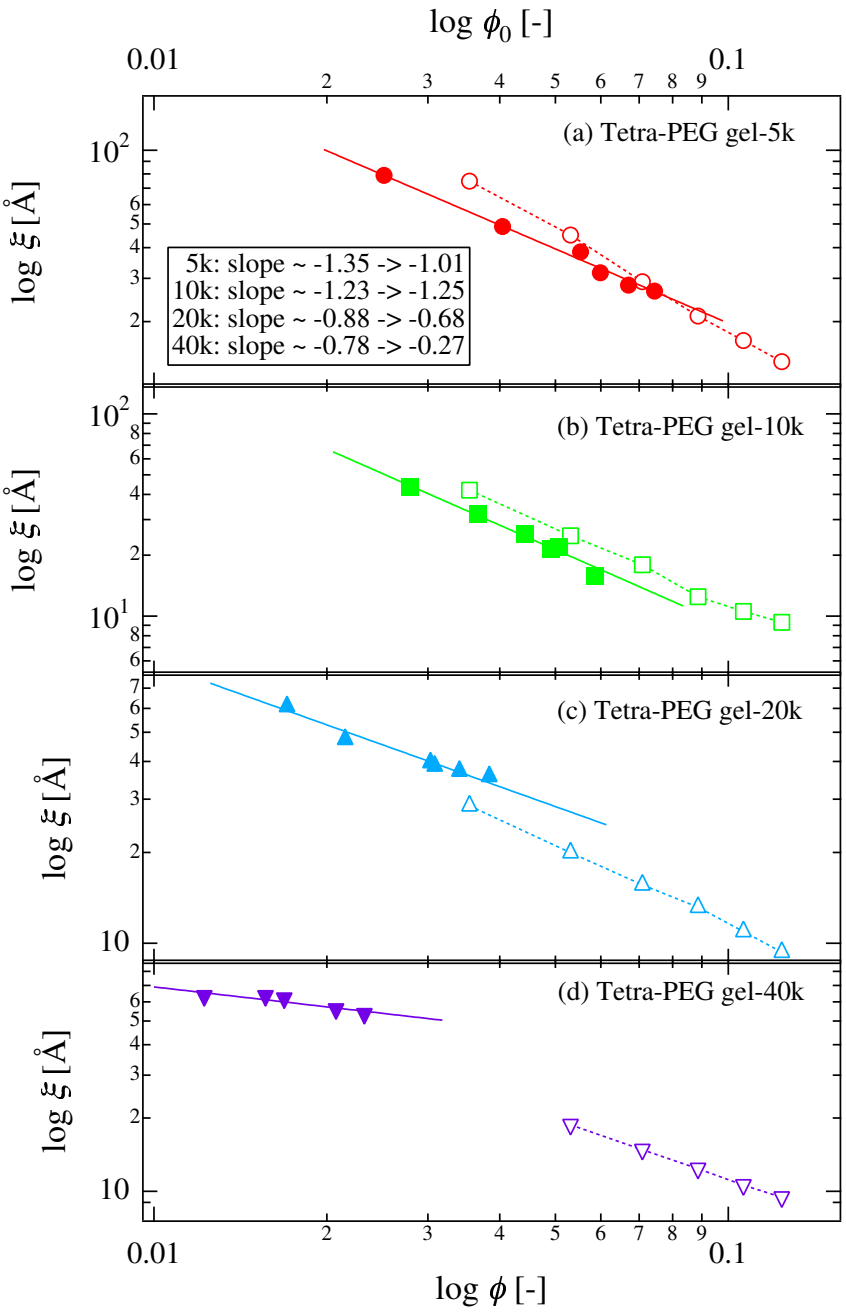

Figure 5.9: Concentration-dependence of ξ of swollen gels for Tetra-PEG gel-5k, -10k, -20k, and -40k (solid symbols with solid lines) as well as those of as-prepared gels (open symbols and broken lines).

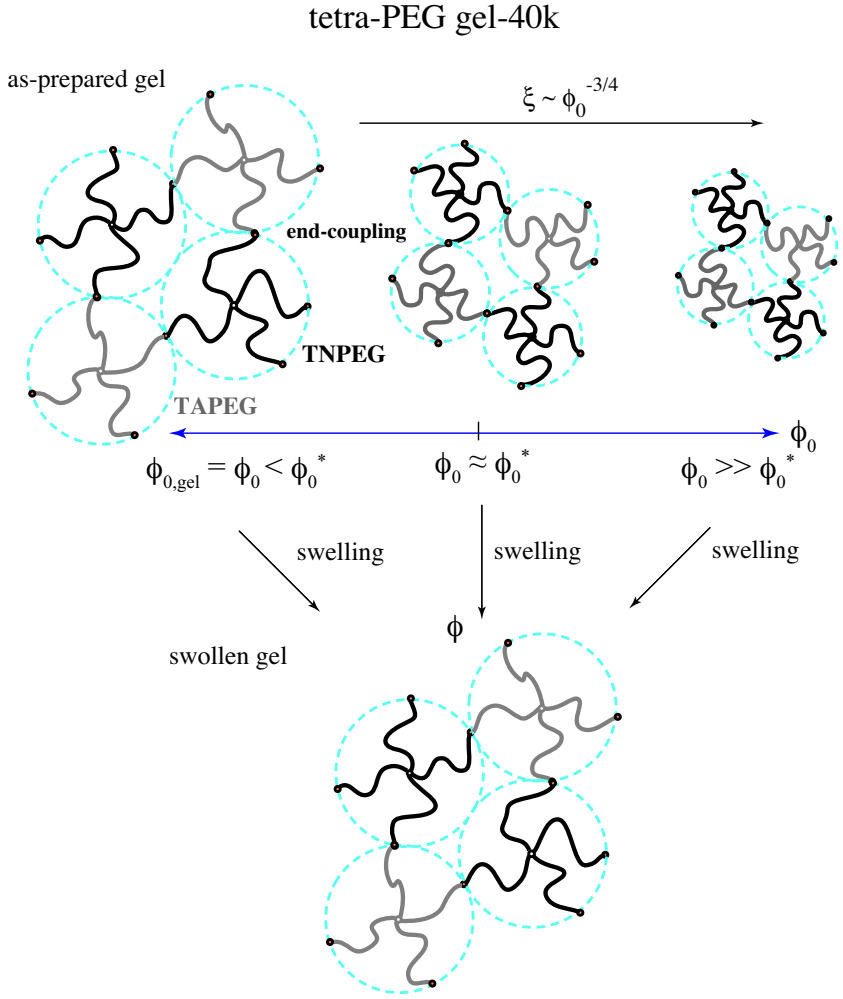

Figure 5.10: Schematic representation showing the change of network size as a function of ϕ_0 and of ϕ.

also observed in all the Tetra-PEG gels. This strongly indicates that Tetra-PEG gels have a self-similar structure with respect to the polymer concentration at preparation, ϕ_0. This figure also shows Tetra-PEG gels have two characteristic length scales, i.e., the correlation length, ξ, and the characteristic length of inhomogeneities, Ξ, given by eq 5.6. Now, let us discuss the origin of the inhomogeneities characterized by Ξ. It is more interesting to compare the master curves in the scattering intensity functions of Tetra-PEG gels having different M_{w}s. Figure 5.12 shows the plots of the master curves obtained for Tetra-PEG gel-5k (open circles), -10k (open squares), -20k (open triangles), and -40k (open rhombus). The curves denoted by crosses indicate the scattering intensity function of linear PEG chains ($M_{\mathrm{w}} = 102 \times 10^3$ at 10 °C) reported by Hammouda.[40] Surprisingly enough, the SANS function for the linear PEG chains is also nicely superimposed to the master curve by employing the reduced variables as shown in Figure 5.12. It is reported that this upturn corresponds to clustering of PEG chains in water with a typical size of 500 $\mathring{A}$, and the major reason of clustering is the presence of hydrophobic end groups, such as $-\mathrm{OCH_3}$. It is of particular interest that the behavior of the linear PEG is quite similar to Tetra-PEG gel-5k. This suggests that Tetra-PEG gel-5k has a clustered structure similar to linear PEG chains in water. This is probably due to clustering of arm PEG chains with unreacted end group. It is noted that the presence of such clustered (or aggregated) structure is typical in PEG aqueous solutions.[41–43] Figure 5.12 indicates that this clustered structure seems to be suppressed by increasing M_{w}. Hammouda et al. proposed two kinds of scattering functions different in the cluster term, i.e., Debye-Bueche type squared-Lorentz function[40] and a power-law functions,[42]

$$I(q) = \frac{A}{\left(1 + \Xi^2 q^2\right)^2} + \frac{B}{1 + \xi^2 q^2} \quad (\mathrm{Debye - Buechefunction}) \tag{5.7}$$

and

$$I(q) = A' q^{-\beta} + \frac{B}{1 + \xi^2 q^2} \quad (\mathrm{power - lawfunction}) \tag{5.8}$$

where A, B, and A' are numerical factors, and β is an scattering exponent. Note that the scattering form of eq 5.7 is exactly the same as that of eq 5.6 and is employed by many researchers including the authors.[6,7,44,45] This means that there exists a two-phase structure having a sharp boundary characterized by the so-called Porod law ($I(q) \sim q^{-4}$). On the other hand, eq 5.8 suggests the presence of a fractal structure characterized by mass fractal, $D = \beta$.[46–48] The scattering exponent at the

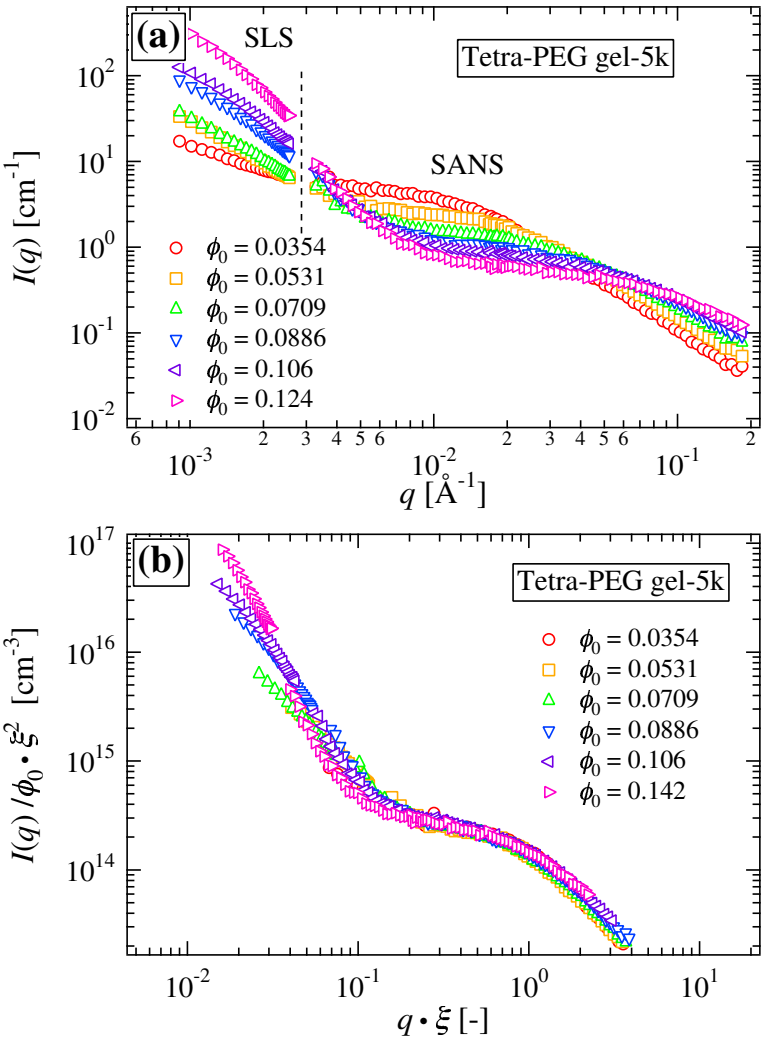

Figure 5.11: (a) SANS as well as SLS intensity functions for Tetra-PEG gel-5k prepared at various concentrations, ϕ_0s. The missing q region is indicated by the vertical dashed line. (b) Scaled plots, $I(q)/\phi_0\xi^2$ and ξq.

low q-region in Figure 5.11b is close to -2. Hence, the hypothesis of the presence of a two-phase structure with a sharp boundary does not seem to be applicable to Tetra-PEG gels. This exponent (-2) revealed in Tetra-PEG gels for $M_{\rm w} \geq 10$k may indicate that Tetra-PEG gels have two correlation lengths ξ and Ξ ($\gg \xi$) in SANS regime and in SLS regimes, respectively, and the scattering intensity is given by

$$I(q) = \frac{A_{\rm SLS}}{1+\Xi^2 q^2} + \frac{A_{\rm SANS}}{1+\xi^2 q^2} \quad \text{(anotherOZfunction)} \tag{5.9}$$

If this is the case, Tetra-PEG gels are one phase system having bimodal concentration fluctuations in submicrometers and a few tens of angstroms. We conjecture that the inhomogeneities characterized by ξ correspond to the distance between polymer-poor regions originating from imperfect cross-end-coupling reaction. Further investigations to elucidate this conjecture is in progress.

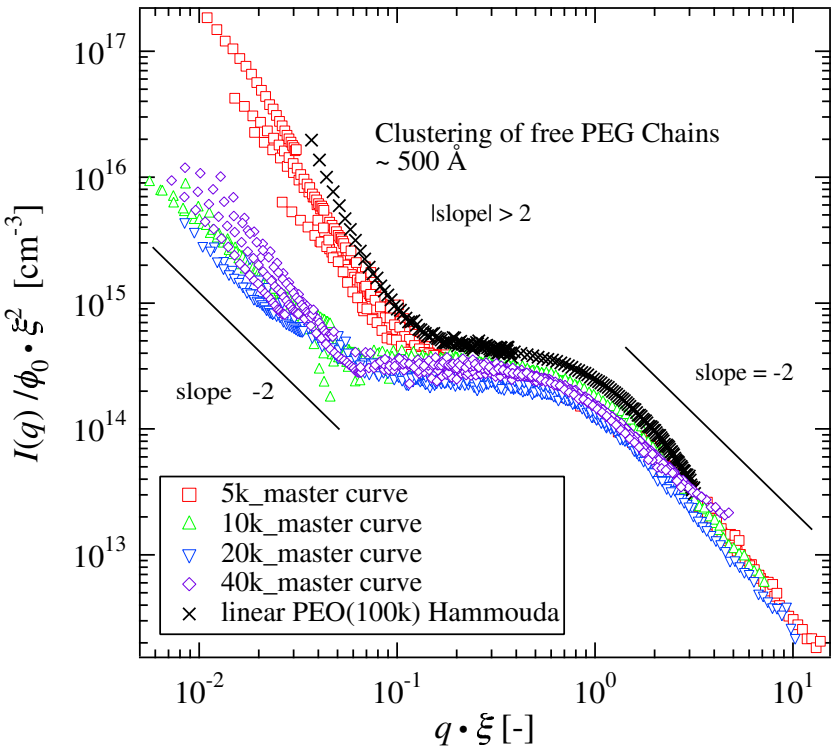

Figure 5.12: Scaled plots, $I(q)/\phi_0\xi^2$ and ξq, for Tetra-PEG gel-5k (open circles), -10k (open squares), -20k (open triangles), and -40k (open rhombus). Crosses indicate the reduced the scattering intensity function for linear PEG chains ($M_{\rm n} = 100$k) in water.

5.5 Conclusion

The structure of Tetra-PEG gels was investigated by small-angle neutron scattering (SANS) as well as static light scattering (SLS). The following facts are disclosed: (1) The TAPEG macromer solutions, consisting of tetra-arm polymer chains, are not interpenetrable due to the presence of end groups, and the individual chains behave as hard spheres. Hence, the radius of gyration, R_g scales with $\phi_0^{-1/3}$. (2) The structure factors of both as-prepared and swollen gels in SANS regime can be represented by Ornstein-Zernike type scattering functions and be superimposed to single master curves, irrespective of the molecular weight. (3) No inhomogeneities appeared even by swelling. (4) However, in SLS regime, a steep upturn was observed in SANS curves in as-prepared Tetra-PEG gels, indicating the presence of PEG chain clusters or defects. A master-curve relationship holds also in SLS regime for a gel having the same molecular weight, indicating a self-similar network structure in Tetra-PEG gels. (5) The upturn in scattering intensity is assigned to be a clustered structure as is often observed in PEG in water and/or network defects. The upturn is suppressed by increasing M_w due to a formation of more regular network structures with less inhomogeneities. It is concluded that Tetra-PEG gels have no noticeable entanglements, but have self-similar structures with respect to M_w, and form ideal tetrafunctional polymer networks, provided that M_w is high enough ($\sim 40 \times 10^3$).

References

[1] Stein, R. S. *J. Polym. Sci.* 1969, **B7**, 657-660.

[2] Pines, E.; Prins, W. J. *Polym. Sci., Polym. Phys. Ed.* 1972, **B10**, 719-724.

[3] Candau, S.; Bastide, J.; Delsanti, M. *Adv. Polym. Sci.* 1982, **44**, 27.

[4] Panyukov, S.; Rabin, Y. *Macromolecules* 1996, **29**, 7960.

[5] Bastide, J.; Candau, S. J., *Structure of Gels as Investigated by Means of Static Scattering Techniques. In The Physical Properties of Polymer Gels*, Cohen Addad, J. P., Ed. John Wiley: NY, 1996; Vol. Chapt. 9, p 143.

[6] Shibayama, M. *Macromol. Chem. Phys.* 1998, **199**, 1-30.

[7] Panyukov, S.; Rabin, Y. *Physics Report* 1996, **269**, 1-132.

[8] Flory, P. J.; Rehner, J., Jr. *J. Chem. Phys.* 1943, **11**, 521.

[9] Treloar, L. R. G., *The Physics of Rubber Elasticity.* Clarendon Press: Oxford, 1975.

[10] Mallam, S.; Horkay, F.; Hecht, A. M.; Geissler, E. *Macromolecules* 1989, **22**, 3356.

[11] Pusey, P. N.; van Megen, W. *Physica A* 1989, **157**, 705-741.

[12] Joosten, J. G. H.; Gelade, E. T. F.; Pusey, P. N. *Phys. Rev. A* 1990, **42**, 2161-2175.

[13] Shibayama, M.; Norisuye, T. *Bull. Chem. Soc. Jpn.* 2002, **75**, 641-659.

[14] Shibayama, M.; Takata, S.; Norisuye, T. *Physica A* 1998, **249**, 245-252.

[15] Mark, J. E.; Erman, B., *Rubberlike Elasticity A Molecular Primer.* Wiley: NY, 1988.

[16] Mark, J. E.; Sullivan, J. L. *J. Chem. Phys.* 1977, **66**, 1006-1011.

[17] Jong, L.; Stein, R. S. *Macromolecules* 1991, **24**, (9), 2323-2329.

[18] Sullivan, J. L.; Mark, J. E.; Hampton, P. G.; Cohen, R. E. *J. Chem. Phys.* 1978, **68**, 2010-2012.

[19] Mark, J. E.; Rahalkar, R. R.; Sullivan, J. L. *J. Chem. Phys.* 1979, **70**, 1794-1797.

[20] Llorente, M. A.; Mark, J. E. *J. Chem. Phys.* 1979, **71**, 682-689.

[21] Geissler, E.; Horkay, F.; Hecht, A. M.; Rochas, C.; Lindner, P.; Bourgaux, C.; Couarraze, G. *Polymer* 1997, **38**, 15.

[22] Mendes, E.; Hakiki, A.; Herz, J.; Boue ´ , F.; Bastide, J. *Macromolecules* 2004, **37**, 2643-2649.

[23] Sukumaran, S. K.; Beaucage, G.; Mark, J. E.; Viers, B. *Eur. Phys. J. E* 2005, **18**, 29-36.

[24] Benoit, H. *J. Polym. Sci.* 1953, **11**, 507-510.

[25] Richter, D.; Farago, B.; Huang, J. S.; Fetters, L. J.; Ewen, B. *Macromoleules* 1989, **22**, 468-472.

[26] de Gennes, P. G., *Scaling Concepts in Polymer Physics.* Cornell University: Ithaca, 1979.

[27] Ornstein, L. S.; Zernike, F. *Proc. Acad. Sci.*, Amsterdam 1914, **17**, 793.

[28] Matsunaga, T.; Sakai, T.; Akagi, Y.; Chung, U.; Shibayama, M. *Macromolecules* 2009, **42**, 1344-1351.

[29] Sakai, T.; Matsunaga, T.; Yamamoto, Y.; Ito, C.; Yoshida, R.; Suzuki, S.; Sasaki, N.; Shibayama, M.; Chung, U. *Macromoleules* 2008, **41**, 5379-5384.

[30] Okabe, S.; Karino, T.; Nagao, M.; Watanabe, S.; Shibayama, M. *Nuclear Inst. and Methods in Physics Research, A* 2007, **572**, 853-858.

[31] Okabe, S.; Nagao, M.; Karino, T.; Watanabe, S.; Adachi, T.; Shimizu, H.; Shibayama, M. *J. Appl. Cryst.* 2005, **38**, 1035-1037.

[32] Shibayama, M.; Nagao, M.; Okabe, S.; Karino, T. *J. Phy. Soc. Jpn.* 2005, **74**, 2728-2736.

[33] Lutolf, M. P.; Hubbell, J. A. *Biomacromolecules* 2003, **4**, 713-722.

[34] Bastide, J.; Leibler, L. *Macromolecules* 1988, **21**, 2647.

[35] Mendes, E. J.; Lindner, P.; Buzier, M.; Boue, F.; Bastide, J. *Phys. Rev. Lett.* 1991, **66**, 1595.

[36] Mendes, E.; Girard, B.; Picot, C.; Buzier, M.; Boue, F.; Bastide, J. *Macromolecules* 1993, **26**, 6873.

[37] Mendes, E.; Oeser, R.; Hayes, C.; Boue, F.; Bastide, J. *Macromolecules* 1996, **29**, 5574.

[38] Shibayama, M.; Shirotani, Y.; Hirose, H.; Nomura, S. *Macromolecules* 1997, **30**, (23), 7307.

[39] Shibayama, M.; Shirotani, Y.; Shiwa, Y. *J. Chem. Phys.* 2000, **112**, 442-449.

[40] Hammouda, B.; Ho, D.; Kline, S. *Macrmolecules* 2002, **35**, 8578-8585.

[41] Zhou, P.; Brown, W. *Macrmolecules* 1990, **23**, 1131-1139.

[42] Hammouda, B.; Ho, D. L.; Kline, S. *Macrmolecules* 2004, **37**, 6932-6937.

[43] Polik, W. F.; Burchard, W. *Macrmolecules* 1983, **16**, 978-982.

[44] Wu, W.; Shibayama, M.; Roy, S.; Kurokawa, H.; Coyen, L. D.; Nomura, S.; Stein, R. S. *Macromolecules* 1990, **23**, 2245-2251.

[45] Onuki, A. *J. Phys. II France* 1992, **2**, 45-61.

[46] Bouchaud, E.; Delsanti, M.; Adam, M.; Daoud, M.; Durand, D. *J. Physique* 1986, **47**, (8), 1273-1277.

[47] Adam, M.; Delsanti, M.; Munch, J. P.; Durand, D. *J. Physique* 1987, **48**, (10), 1809-1818.

[48] Adam, M.; Lairez, D., *Sol-Gel Transition. In Physical Properties of Polymeric Gels*, Cohen Addad, J. P., Ed. John Wiley & Sons: New York, 1996; p 87.

Chapter 6

SANS Studies on Tetra-PEG Gel under Uniaxial Deformation

6.1 Introduction

Elucidation of the deformation mechanism of polymer networks and/or polymer gels has been one of the most intriguing problems in polymer science for a number of decades.[1–7] The framework of rubber elasticity was constructed on the basis of randomly cross-linked Gaussian chain networks. There are a number of theories and models to describe the deformation of polymer networks, such as affine network model,[3,8] junction-affine network model,[9] phantom network model,[1,2,10] slip-link model,[11] and tube model.[12,13] Pioneering works on the phantom chain model by James and Guth in 1940s[1,2] and the scattering function for phantom chains proposed by Pearson[10] have been examined by a large number of investigators. Extensive discussions on deformation mechanism of polymer networks were given by Flory in 1976.[5] Small-angle neutron scattering (SANS) is recognized to be one of the most suitable means to elucidate the relationship between the microscopic and macroscopic behaviors of deformation because polymer chains in a polymer network can be selectively labeled and the change of polymer conformation can be studied as a function of macroscopic deformation.[14,15] Benoit et al. performed a pioneering work on deformation of polymer network with SANS.[9] They performed SANS experiments on branch-labeled and labeled-chain networks of polystyrene. The former gave the information of the inter-cross-link distance and the latter did the radius of gyration of labeled chains. They reported that both the change of the inter-cross-link distance and that of the radius of gyration were far below than those predicted by affine or junction-affine models.

In 1980s, a number of SANS investigations were carried out on deformed polymer networks. Ullman proposed scattering functions from labeled chains in polymeric networks for swollen and stretched polymer networks and compared them with those obtained by SANS experiments.[16–18] One of the important findings was that the chain deformation was less than that calculated from the phantom network model. Beltzung and coworkers reported the behavior of dry poly(dimethylsiloxane) networks submitted to uniaxial extension.[14] Boue et al. discussed the structure and dynamics of polymer networks under deformation.[15] These authors also concluded that knowledge of the chain deformation on the level of the mesh size of the network failed to provide all the necessary information to precisely correlate the molecular processes with the macroscopic response of the network samples.

These examples clearly indicated that quantitative discussions on the deformation of polymer networks had not been available because of the lack of "ideal" polymer network suitable for quantitative comparison of polymer chain deformation between the theories and experiments. Here, the "ideal" network means a polymer network consisting of monodisperse polymer chains without any defects, such as loops and dangling chains, and no trapped-entanglements. Recently, we developed near-"ideal" polymer networks called Tetra-PEG gels with negligible fractions of dangling chains and entanglements.[19–22] Here, we report a series of small-angle neutron scattering (SANS) results on deformed Tetra-PEG gels and discuss the deformation mechanism. Focuses are placed on (1) the relationship of spatial inhomogeneities and the gel structure and (2) deformation mechanism of Tetra-PEG gels.

6.2 Theoretical Background

6.2.1 Deformation models of polymer networks

If a polymer network is partially labeled with deuterated polymer chains, the change of the radius of gyration of the labeled chains, R_g, are given as a function of the macroscopic deformation ratio, λ. There are several deformation models for polymer networks as introduced in Introduction. Depending on the theories, the relationship between macroscopic and microscopic deformation is different as follows,

(i) affine network model

$$\frac{R_{\mathrm{g,para}}}{R_{\mathrm{g},0}} \equiv \alpha_{\mathrm{aff,para}} = \lambda, \frac{R_{\mathrm{g,perp}}}{R_{\mathrm{g},0}} \equiv \alpha_{\mathrm{aff,perp}} = \lambda^{-1/2} \tag{6.1}$$

where $R_{\mathrm{g},0}$ is the radius of gyration of the labeled chains in undeformed state. $R_{\mathrm{g,para}}$ and $R_{\mathrm{g,perp}}$ are those in the parallel and perpendicular directions in deformed state, respectively. However, in reality, the microscopic deformation of polymer network is different from that in macroscopic deformation due to thermal motions of polymer chains and other reasons. Well-known deformation models are junction-affine and phantom models;

(ii) junction-affine network model

$$\frac{R_{\mathrm{g,para}}}{R_{\mathrm{g},0}} \equiv \alpha_{\mathrm{j-aff,para}} = \left(\frac{1+\lambda^2}{2}\right)^{1/2}, \frac{R_{\mathrm{g,perp}}}{R_{\mathrm{g},0}} \equiv \alpha_{\mathrm{j-aff,perp}} = \left(\frac{1+\lambda}{2\lambda}\right)^{1/2} \tag{6.2}$$

(iii) phantom network model[10]

$$\begin{aligned} \frac{R_{\mathrm{g,para}}}{R_{\mathrm{g},0}} &\equiv \alpha_{\mathrm{ph,para}} = \left(\frac{f+2+(f-2)\lambda^2}{2f}\right)^{1/2} \\ \frac{R_{\mathrm{g,perp}}}{R_{\mathrm{g},0}} &\equiv \alpha_{\mathrm{ph,perp}} = \left(\frac{f+2+(f-2)\lambda^{-1}}{2f}\right)^{1/2} \end{aligned} \tag{6.3}$$

Here, f is the functionality of the cross-links. Evaluation of the ratio of the radius of gyrations after to before deformation allows one, in principle, to discuss the deformation mechanism of polymer networks.

6.2.2 SANS functions for "ideal" polymer networks

According to the de Gennes's C^* theorem, the scattering function for polymer gels is the same as that of the corresponding semi-dilute polymer solutions. Hence, by taking into account an excess scattering form gel inhomogeneities, $A_{\mathrm{ex}}(q)$, the scattering intensity from a gel, $I(q)$, is given by[23]

$$I(q) = \frac{(\Delta\rho)^2 RT\phi^2}{N_{\mathrm{A}} M_{\mathrm{OS}}} \left[\frac{1}{1+\xi^2 q^2} + A_{\mathrm{ex}}(q)\right] \tag{6.4}$$

where N_{A} is the Avogadro's number, $\Delta\rho$ is the scattering density difference, R is the gas constant, T is the absolute temperature, ϕ is the polymer volume fraction,

M_{OS} is the longitudinal modulus, and q is the magnitude of the scattering vector. ξ is the correlation length. $A_{ex}(q)$ is the excess scattering intensity dependent on the structure of inhomogeneities in the gel.[24] When $A_{ex}(q) = 0$, eq 6.4 is nothing but the so-called Ornstein-Zernike (OZ) function. The characteristic size of polymer network is given by the "blob" with size of ξ. When a gel is deformed, the blob is expected to be deformed to an ellipsoid with their principal axes to be ξ_{para} and ξ_{perp} in the direction of parallel and perpendicular directions, respectively. If the polymer network is fully labeled, e.g., hydrogeneous polymer network in deuterated solvent, deformation of the polymer network is observed as a deformation of blobs.[25,26] Hence,

$$\xi_{para} = \alpha_{para}\xi_0, \quad \xi_{perp} = \alpha_{perp}\xi_0 \tag{6.5}$$

By SANS experiments for deformed polymer networks, one would expect the microscopic deformation ratios, α_{para} and α_{perp} as a function of macroscopic deformation ratio, λ.

6.3 Experimental Section

6.3.1 Sample preparation

Tetra-amine-terminated PEG (TAPEG) and tetra-NHS-glutarate-terminated PEG (TNPEG) were prepared from tetrahydroxyl-terminated PEG (THPEG) having equal arm lengths. Here NHS represents *N*-hydroxysuccinimide. The details of TAPEG and TNPEG preparation are reported elsewhere.[19] Equal amounts of TAPEG and TNPEG were dissolved in phosphate buffer (pH 7.4) and phosphate-citric acid buffer (pH 5.8), respectively, and the resulting solution was poured into the mold with the size of 60 mm long × 45 mm wide × 3 mm thick. Note that buffer solutions were prepared with deuterated water in order to reduce the incoherent scattering from H-containing materials. To control the reaction rate, the ionic strengths of the buffers were chosen to be 100 mM. At least 12 h were spent for the completion of the reaction before the following experiments. The molecular weights (M_w) of TAPEG and TNPEG were matched to each other, and two sets of macromers having different Mw values were prepared, that is, M_w = 20k and 40k g/mol. The sample code is given by the M_w, for example, Tetra-PEG gel-20k being Tetra-PEG with $M_w = 20 \times 10^3$ g/mol. Constant amounts of TAPEG and TNPEG (M_w = 20k g/mol, 100 mg/mL,

and M_w = 40k g/mol, 140 mg/mL) were dissolved in phosphate buffered D_2O (pH 7.4) and phosphate-citric acid buffered D2O (pH 5.8), respectively. The specimens were used in as-prepared state.

6.3.2 Stretching measurement

The stretching measurement was carried out on dumbbell-shaped films using a mechanical testing apparatus (CR-500DX-SII rheometer; Sun Scientific Co., Tokyo, Japan) at a crosshead speed of 0.1 mm/sec. The sample thickness for the stretching measurement was 1 mm.

6.3.3 Small-angle neutron scattering

SANS experiments were performed at the two-dimensional SANS instrument (SANS-U), Neutron Science Laboratory, the University of Tokyo.[27,28] The neutron wavelength was 7.0 Å. The monochromatization was attained with a mechanical velocity selector, and the wavelength distribution was ca. 10%. The sample-to-detector distances (SDD) were 2 and 8 m, which cover the q-range of 0.005 - 0.2 $Å^{-1}$. The scattered neutrons were collected with a two-dimensional detector (model 2660N, Ordela).

Deformation SANS experiments were carried out for reed-shape samples held on a stretching device equipped in a laboratory-made stretching chamber. The initial cross-head distance was 20 mm. Though there is a possibility of a biaxial deformation, we employed the reed-shaped specimens under the limitation of experimental conditions, such as, the limitation of sample size, the space of SANS sample stage (smaller is better), and the necessary neutron beam size (larger is better). The humidity of the sample environment was kept constant by placing a bottle of water near the sample in a shielded-stretching chamber throughout the experiment. After loading a gel sample, the humidity and temperature were equilibrated within 5 min. The stretching was driven by a stepping motor. The stretching rate was 70 mm/min. Whenever the samples were stretched, SANS experiments were started after waiting for 10 min. The observed scattered intensity functions were corrected for air scattering, incoherent scattering, and transmission and then were rescaled to the absolute intensity, $I(q)$, with a polyethylene secondary standard. Incoherent scattering

intensity subtraction was made with the T-method reported elsewhere.[29]

6.4 Results and Discussion

6.4.1 Stress-elongation curves of Tetra-PEG gels

First of all, let us show the stress-elongation curves of Tetra-PEG gel-20k and -40k before beginning to discuss the SANS results, where λ is the stretching ratio. Figure 6.1(a) and (b) show the photographs of Tetra-PEG gel-40k at $\lambda = 1.0$ and $\lambda = 5.0$ on the laboratory-made stretching device for SANS experiments. As shown in Fig 6.1(b), Tetra-PEG gels can be deformed like a stripe of rubber. Figure 6.1 (c) shows the stretching stress-elongation curves of Tetra-PEG gel-20k (100 mg/mL) and -40k (140 mg/mL). These concentrations were the same as those in the SANS experiments. The stretching ratios that SANS measurements were carried out are marked by arrows in the figure (λ = 1.0, 1.5, 2.0, 2.5, 3.0, and 5.0). The stretching ratios of $\lambda = 2.5$ for Tetra-PEG gel-20k and $\lambda = 5.0$ for Tetra-PEG gel-40k are close to the cross-over from Gaussian to Non-Gaussian region. Therefore, the molecular chains in the network were stretched large enough.

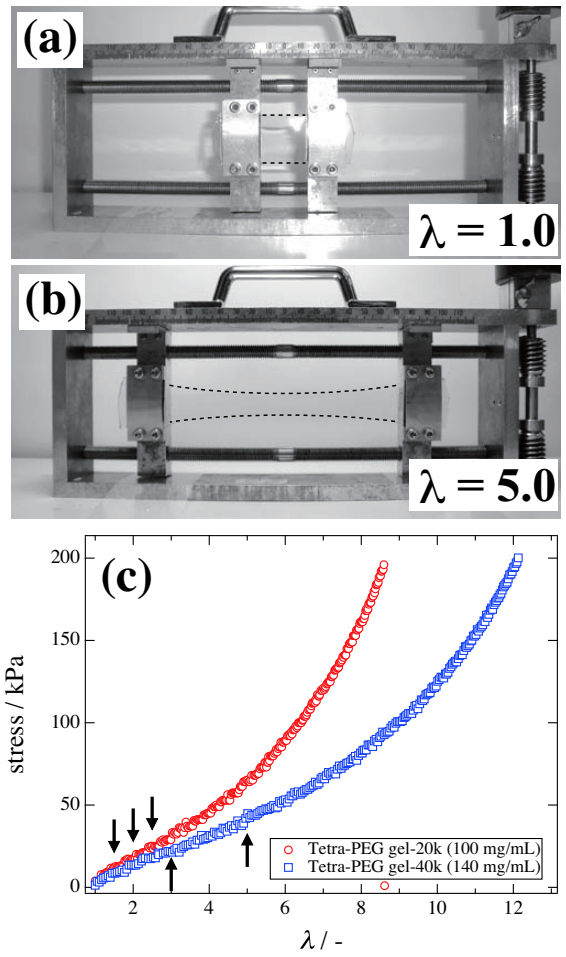

Figure 6.1: Photographs of Tetra-PEG gel-40k in (a) nonstretched state ($\lambda = 1.0$) and (b) stretched state ($\lambda = 5.0$). (c) Stretching stress-elongation curves of Tetra-PEG gel-20k and -40k. The stretching ratios at which SANS experiments were carried out are marked by arrows.

6.4.2 Tetra-PEG gel-20k

Figure 6.2 shows two dimensional (2D)-SANS scattering patterns obtained for uniaxially deformed Tetra-PEG gel-20k (100 mg/mL). The stretching ratios were $\lambda =$ 1.0, 1.5, 2.0, and 2.5. The stretching direction was horizontal. The upper and lower figures show SANS patterns taken at SDD = 8 m and 2 m, respectively. As shown in the figure, both scattering patterns (SDD = 8 m and 2 m) had isotropic patterns at $\lambda = 1.0$. When the samples were stretched, anisotropic patterns appeared in both low-q (8m SANS data) and high-q regions (2m SANS data). Note that the 8m-SANS patterns showed a two-lobe pattern in the stretching direction at $\lambda = 2.0$ and 2.5 (the

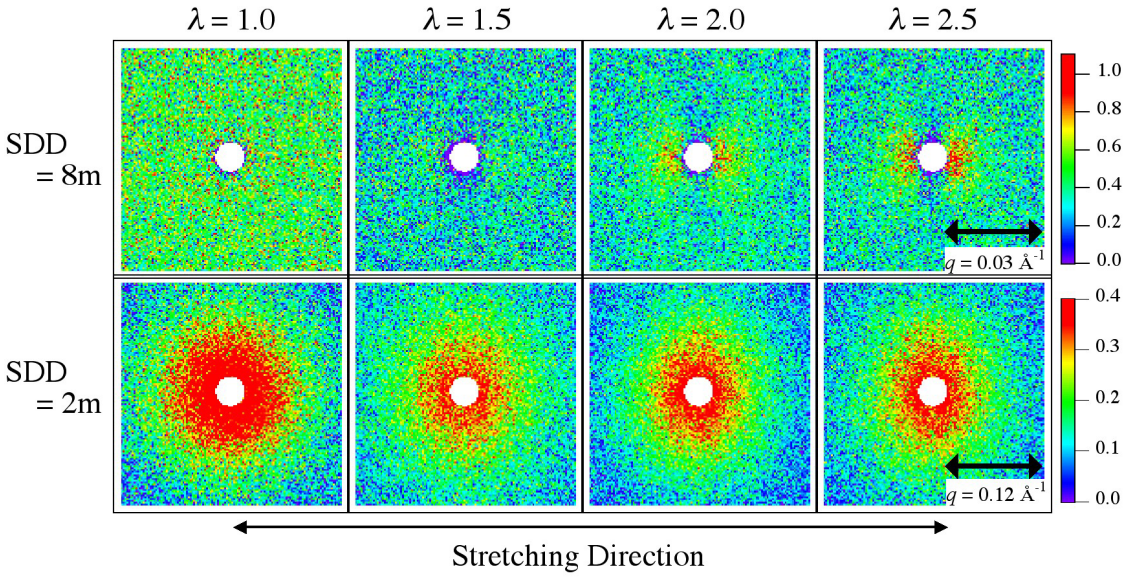

Figure 6.2: 2D SANS patterns of Tetra-PEG gel-20k (100 mg/mL) at SDD = 8m (top) and 2m (bottom). Stretching ratios are $\lambda = 1.0$, 1.5, 2.0 and 2.5.

so-called abnormal butterfly pattern). On the other hand, the 2m-SANS patterns became slightly elliptic with their long axis perpendicular to the stretching direction (the so-called a normal butterfly pattern). It is noteworthy that marked anisotropic patterns (called "abnormal butterfly patterns") are commonly observed in polymer gels due to spatial inhomogeneities even with the elongation ratio of less than $\lambda = 2$.[26,30–32] Therefore, the result shown in Figure 6.2 is rather surprising. In the case of Tetra-PEG gels, furthermore, no inhomogeneities were observed even in swollen gels as discussed in our previous paper.[23] Hence, this is the first time to observe anisotropic inhomogeneities in a Tetra-PEG gel network.

Figure 6.3 shows the sector averaged scattering intensities in the parallel and perpendicular directions for Tetra-PEG gel-20k (Figure 6.2). Here, the sector average was taken with the sector angle of $\pm$ 10° with respect to the parallel and perpendicular directions. The SANS curve for unstretched sample (circles) was obtained by taking circular averaging; the dashed line indicates a theoretical fit with eq 6.4 by setting $A_{\mathrm{ex}}(q) = 0$ and the obtained ξ value was 13 Å. As shown here, there is a clear difference in the low-q region, i.e., an upturn in the intensity for $q \leq 0.02$ Å^{-1} in the parallel direction (open triangles) and a suppression in the perpendicular direction (filled triangles). On the other hand, a different type of anisotropy was observed in

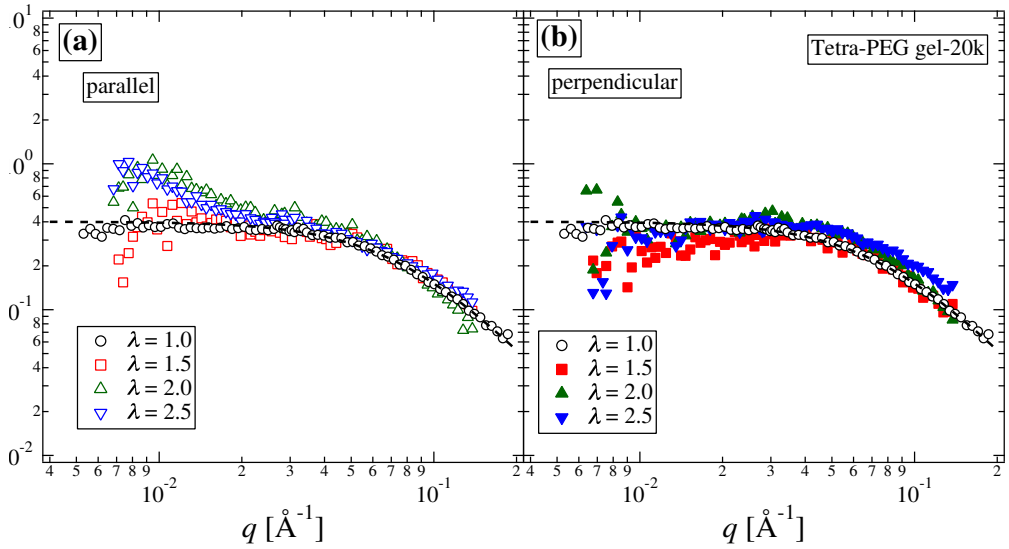

Figure 6.3: Sector averaged scattering intensities ($\pm 10°$) for Tetra-PEG gel-20k at different stretching ratios (a) parallel and (b) perpendicular direction to the stretching direction. The dashed line indicates the curve fit with OZ function.

high-q region ($q \geq 0.04$ Å^{-1}), i.e., an elliptic pattern in the perpendicular direction. Since this q-region corresponds to the thermal fluctuations of polymer chains in a blob, it is deduced that polymer chains are somewhat stretched in the stretching direction.

In order to characterize the anisotropy in the SANS patterns, annular averages for two different q values were calculated. Figure 6.4 shows an azimuthal-angle plot of the scattering intensities at $q = 0.010$ Å^{-1} (0.0084 Å$^{-1} < q < 0.012$ Å^{-1}) and $q = 0.072$ Å^{-1} (0.054 Å$^{-1} < q < 0.089$ Å^{-1}) with various stretching ratios. ψ is the azimuthal angle on the 2D detector plane and $\psi = 0$ is defined as the stretching direction. The azimuthal angle was taken with an interval of 10°. $q = 0.010$ Å^{-1} and 0.072 Å^{-1} correspond to representative anisotropic regions of the low-q and high-q, respectively. It is needless to mention that the unstretched sample gives a ψ-independent pattern. As shown in the figure, both q-regions show ψ dependence by increasing stretching ratio. Note that there is a phase difference by 90°. This means that the anisotropy directions of low-q and high-q are opposite. We employed the following Gaussian equations for the curve fitting.

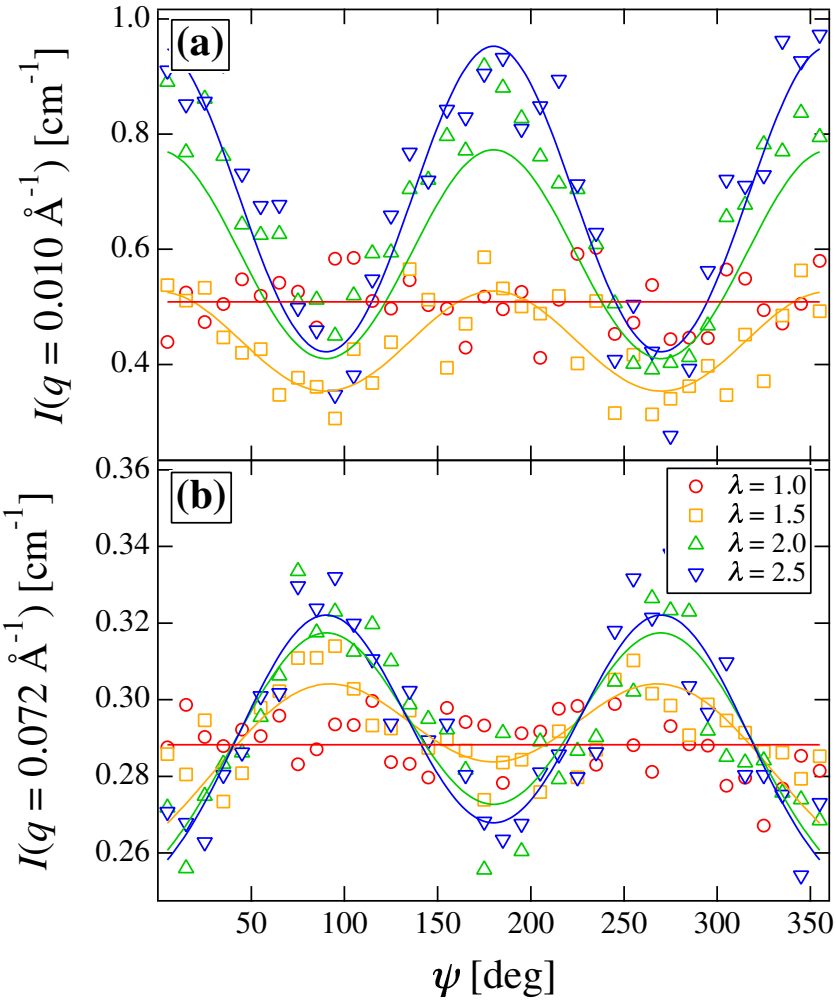

Figure 6.4: Azimuthal plots of SANS intensities for Tetra-PEG gel-20k at (a) $q = 0.010$ Å^{-1} and (b) $q = 0.072$ Å^{-1}. $\lambda = 2.0$.

$$I(\psi) = A\sum_{i=0}^{2}\exp\left[-\frac{(\psi - 180i)^2}{2\sigma^2}\right] + B \quad (\text{at low}q) \tag{6.6}$$

$$I(\psi) = A\sum_{i=0}^{2}\exp\left[-\frac{(\psi - 90(2i-1))^2}{2\sigma^2}\right] + B \quad (\text{at high}q) \tag{6.7}$$

where A is the amplitude (height) of the modulation, σ^2 is the variance, and B is the baseline. Here, the full width at half maximum ($FWHM$) of Gaussian is defined by $FWHM = 2(2ln2\sigma)^{1/2}$. In the case of strong anisotropy, A and $FWHM$ become larger and smaller, respectively. Here, we define the degree of anisotropy with the ratio of $A/FWHM$ and discuss it as a function of the stretching. Note that parallel and perpendicular orientations are indicated by positive and negative signs,

respectively. Figure 6.5 shows the degree of anisotropies at the different scattering intensities $I(q = 0.010\ \text{Å}^{-1})$ and $I(q = 0.072\ \text{Å}^{-1})$. It is clearly shown that the degree of anisotropy increased with increasing stretching ratio, λ, and the anisotropies in the low-q (inhomogeneities; defects) and high-q (blob; polymer chains) regions behave oppositely.

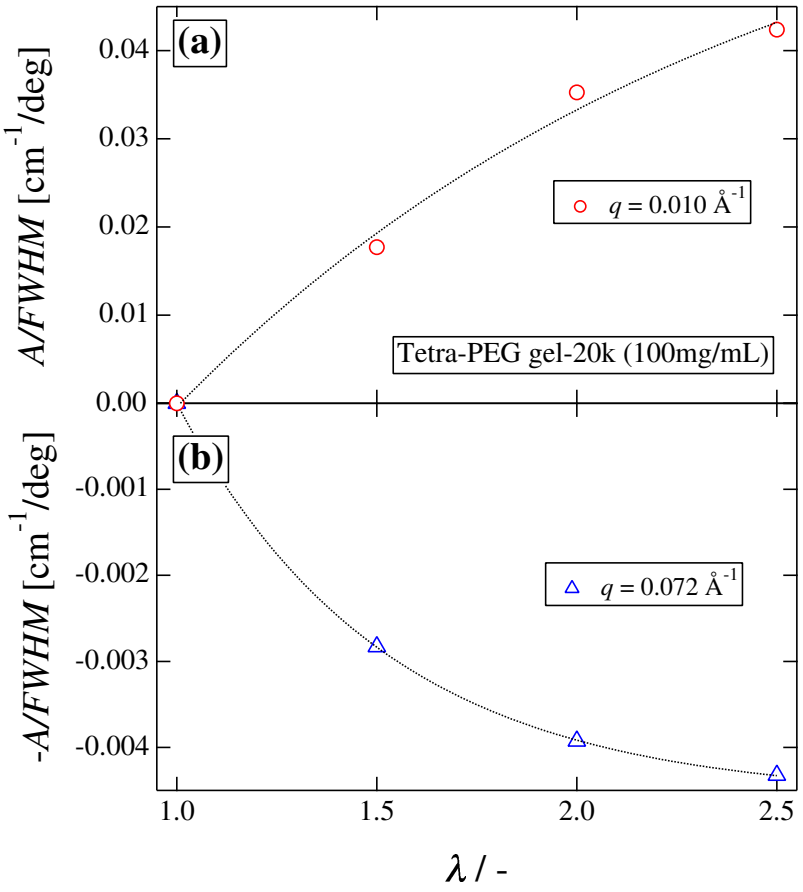

Figure 6.5: The degree of anisotropy at low- and high-q regions for Tetra-PEG gel-20k evaluated with eqs 6.6, 6.7. The dotted lines are for the eye.

6.4.3 Nonstoichiometric Tetra-PEG gel-20k

In the case of Tetra-PEG gels, it is of particular importance to match the concentration of TAPEG and TNPEG for obtaining defect-free polymer networks and achieving optimal mechanical properties.[21] If a stoichiometric condition is broken, the mechanical properties drastically deteriorate as reported elsewhere.[21] In order to investigate the effect of defects (dangling chains) in polymer networks under deformation, we intentionally introduced dangling chains by preparing nonstoichiometric Tetra-PEG gels with the following compositions; [TAPEG]/[TNPEG] = 1.1 : 0.9, 1.2 : 0.8, and 1.3 : 0.7. Figure 6.6 shows the azimuthal plots of scattering intensities for nonstoichiometric 100 mg/mL Tetra-PEG gel-20k. All samples were measured at $\lambda = 2.0$. As shown in the figure, anisotropic scattering patterns were obtained at all compositions similar to the case of the stoichiometric gel ([TAPEG]/[TNPEG] = 1.0 : 1.0).

Figure 6.7 shows the degree of anisotropy obtained from the curve fitting with eqs 6.6 and 6.7 for nonstoichiometric Tetra-PEG gels. We expected that the degree of anisotropy would increase for the low-q region because of an introduction of defects. This is because inhomogeineities are known to be amplified by deformation, such as stretching or swelling.[30,33] Interestingly, however, the degrees of anisotropy of both two ranges were suppressed with increasing asymmetry in the composition. The reasons why the degree of anisotropy decreased are explained as follows. By introducing defects (i.e., dangling chains), deformation is localized around the defect regions and perfect network regions become less deformed by stretching with the cost of a larger deformation of the defect regions. As a result, the anisotropy of high-q region (i.e., blob deformation) becomes small. Similarly, the anisotropy of low-q region is also suppressed because of the same reason at the high-q region, despite the number of defects increases. Note that such decrease in the degree of anisotropy by introducing defects may apply only to near-"ideal" network like Tetra-PEG gels.[22] Strong inhomogeneities observed in the literature,[24] on the other hand, may be ascribed to densely cross-linked zones in a network. That is, conventional gels having a large fraction of various types of defects, such as dangling chains, trapped entanglements, loops, would show an increase in anisotropy when deformed by further introducing defects.

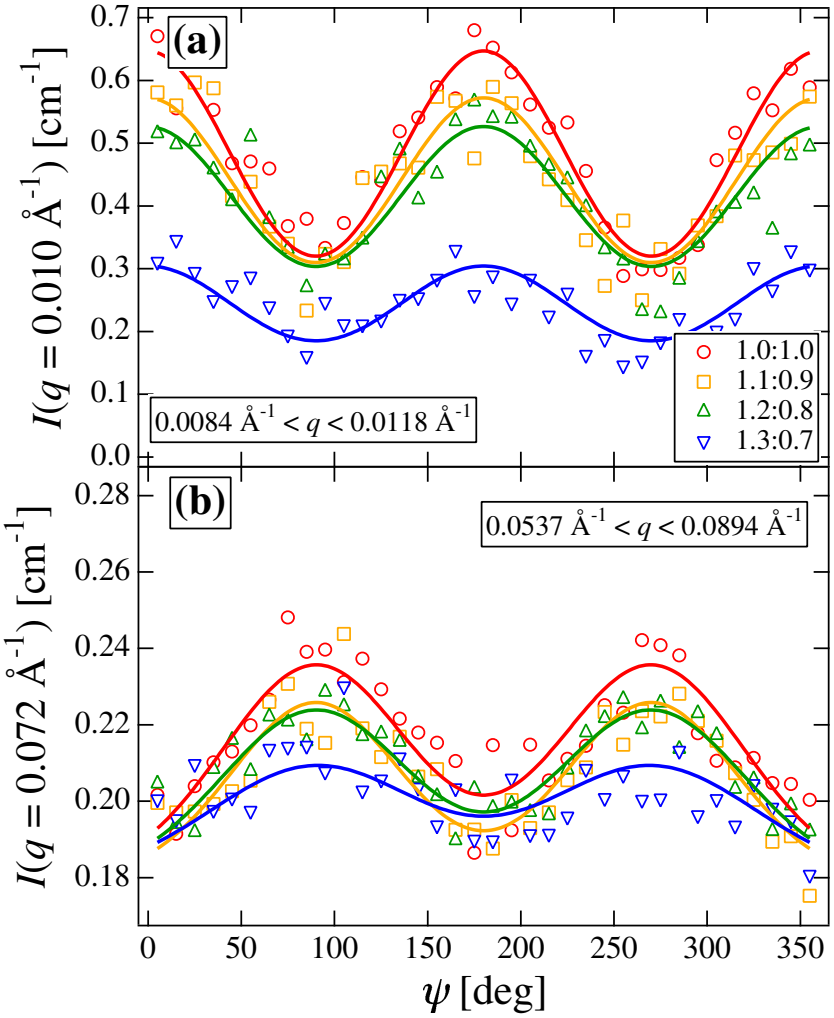

Figure 6.6: Azimuthal plots of SANS for nonstoichiometric gels at (a) $q = 0.010$ Å^{-1} and (b) $q = 0.072$ Å^{-1}. $\lambda = 2.0$.

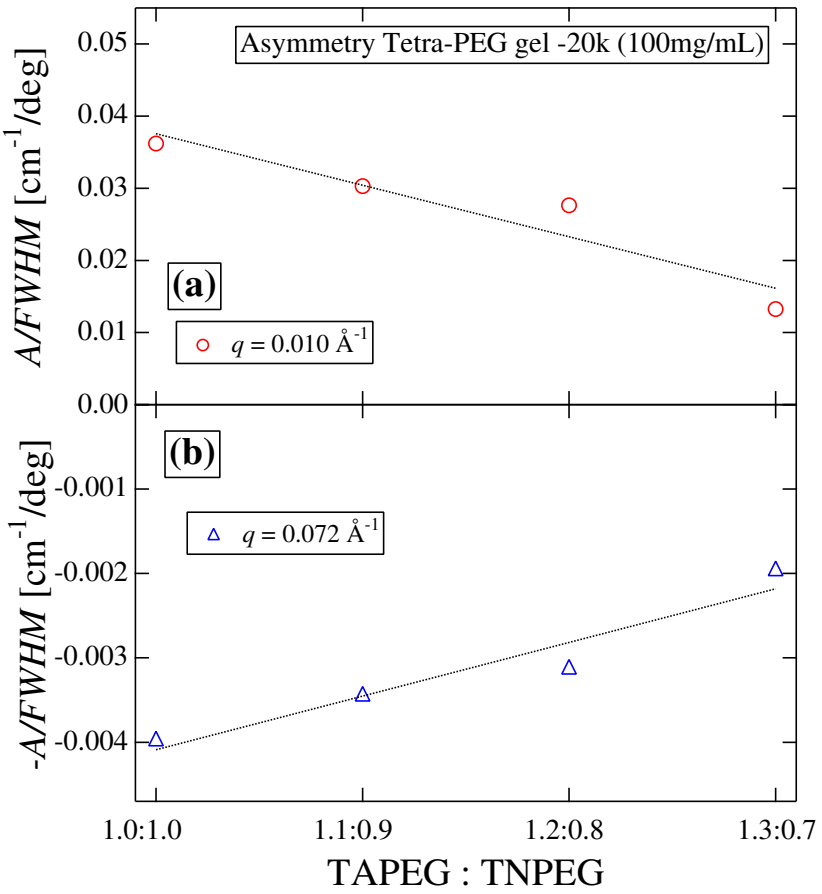

Figure 6.7: The degree of anisotropy at low- and high-q regions for nonstoichiometric Tetra-PEG gel-20k evaluated with eqs 6.6 and 6.7. The dotted lines are for the eye.

6.4.4 Tetra-PEG gel-40k

Figure 6.8 shows the SANS 2D patterns for Tetra-PEG gel-40k (140 mg/mL) under uniaxial deformation. The stretching ratios were $\lambda = 1.0, 3.0$, and 5.0. At SDD = 2m, the scattering patterns at $\lambda = 1.0$ were isotropic. However, to a surprise, anisotropy in the SANS patterns for deformed gels is hard to recognize in Figure 6.8. A careful observation leads to acknowledge that the scattering patterns at SDD = 8m differ substantially from that of Tetra-PEG gel-20k (See Fig. 6.2). No anisotropy was detected at all at stretching ratios up to $\lambda = 5.0$ at least in the low-q region.

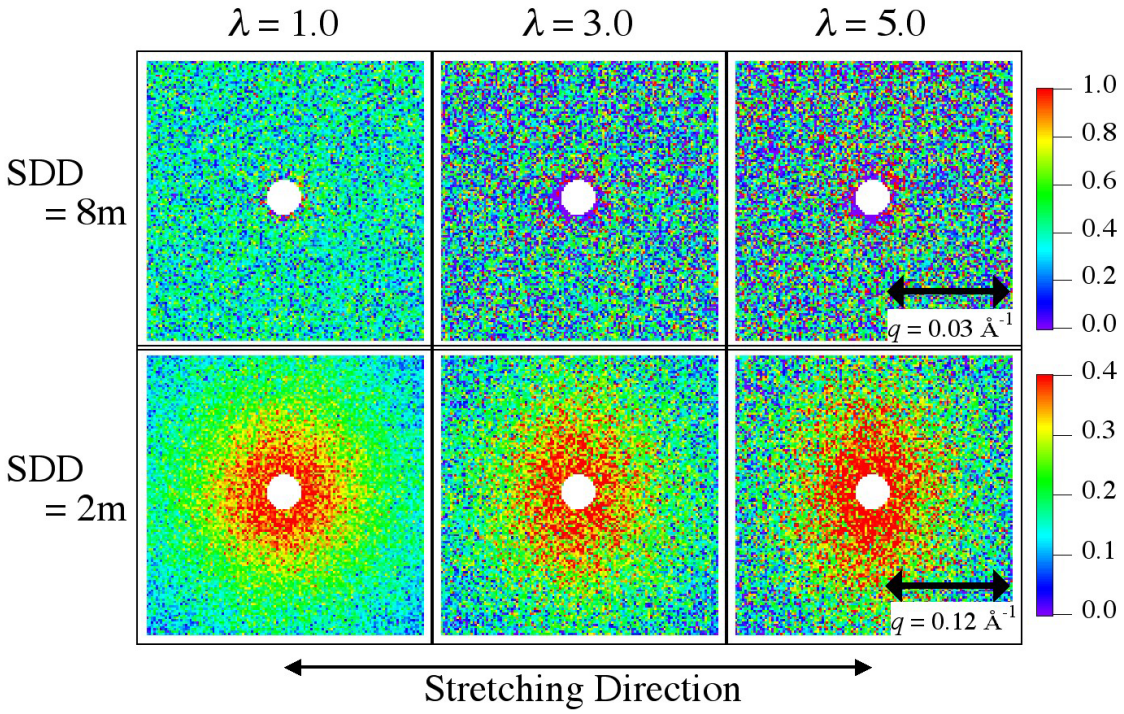

Figure 6.8: SANS 2D patterns for Tetra-PEG gel-40k at SDD = 8m (top) and 2m (bottom). Stretching ratios are $\lambda = 1.0$, 3.0, and 5.0.

Figure 6.9 shows the sector averaged scattering intensities in the parallel and perpendicular directions to the stretching direction for Figure 6.8. Here, the sector average was taken similarly to the case of Tetra-PEG gel-20k. It should be noted that no noticeable inhomogeneities were observed in deformed gel at the low-q region ($q = 0.010$ Å^{-1}). Since we reported in the previous paper that Tetra-PEG gel-40k is closer to an ideal network than other Tetra-PEG gels with lower M_w's based on the

results of the swelling and SANS experiments,[23] it can be concluded that Tetra-PEG gel-40k forms a very homogeneous network. The SANS functions can be fitted with eq 6.4 (again with $A_{ex}(q) = 0$) with $\xi = 9.0$ Å. This value is of the order of the monomer segment length of PEG. This means that the concentration fluctuations in Tetra-PEG gel-40k are of the order of monomer.

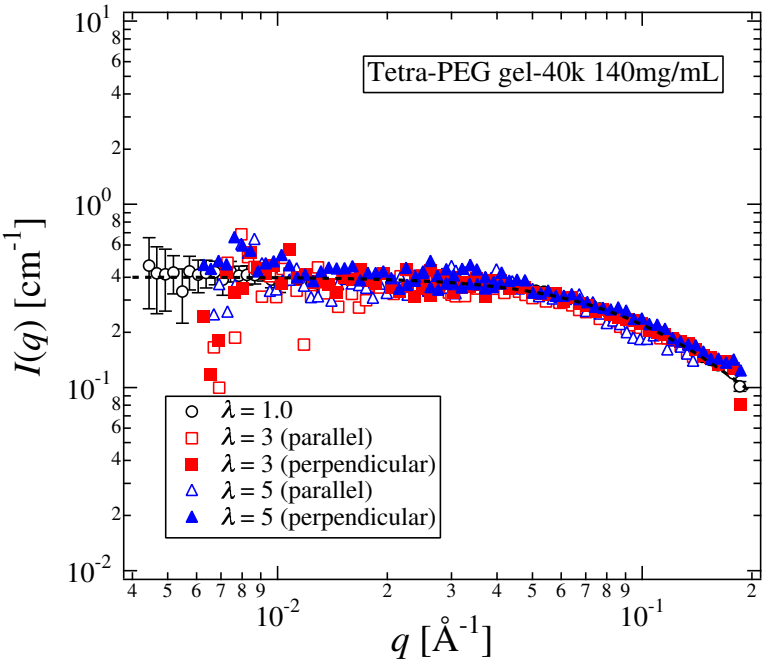

Figure 6.9: Sector averaged scattering intensities (±10°) for Tetra-PEG gel-40k at different stretching ratios. The dashed line indicates the curve fit with OZ function.

In order to elucidate the anisotropy of thermal fluctuation at high-q region, we obtained an azimuthal plot for Tetra-PEG gel-40k. Figure 6.10 shows the result. It is clear from the figure that the anisotropy of Tetra-PEG gel-40k was much less than that of Tetra-PEG gel-20k (Fig. 6.4). Figure 6.11 shows the variation of the degree of anisotropies at low- and high-q. The degree of anisotropy at high-q was about a half of that of Tetra-PEG gel-20k when compared at the same value of λ.

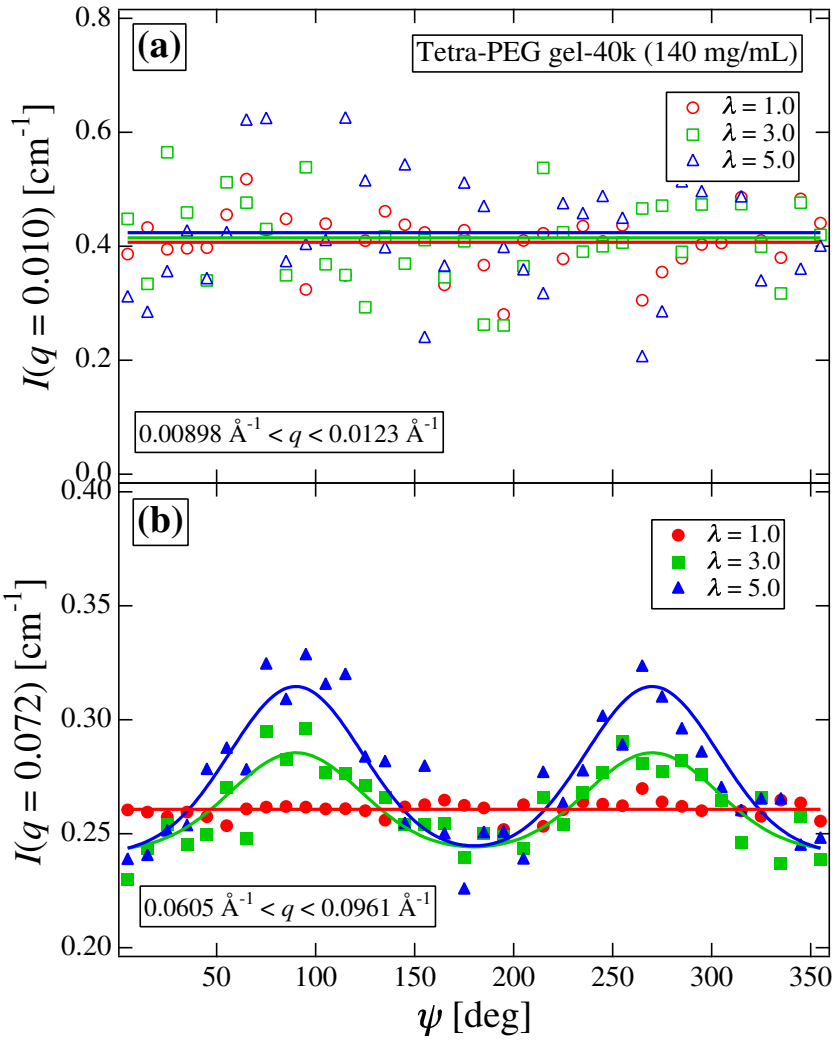

Figure 6.10: Azimuthal plots of SANS intensities for Tetra-PEG gel-40k at (a) $q = 0.010$ Å^{-1} and (b) $q = 0.072$ Å^{-1}. $\lambda = 1.0$, 3.0, and 5.0.

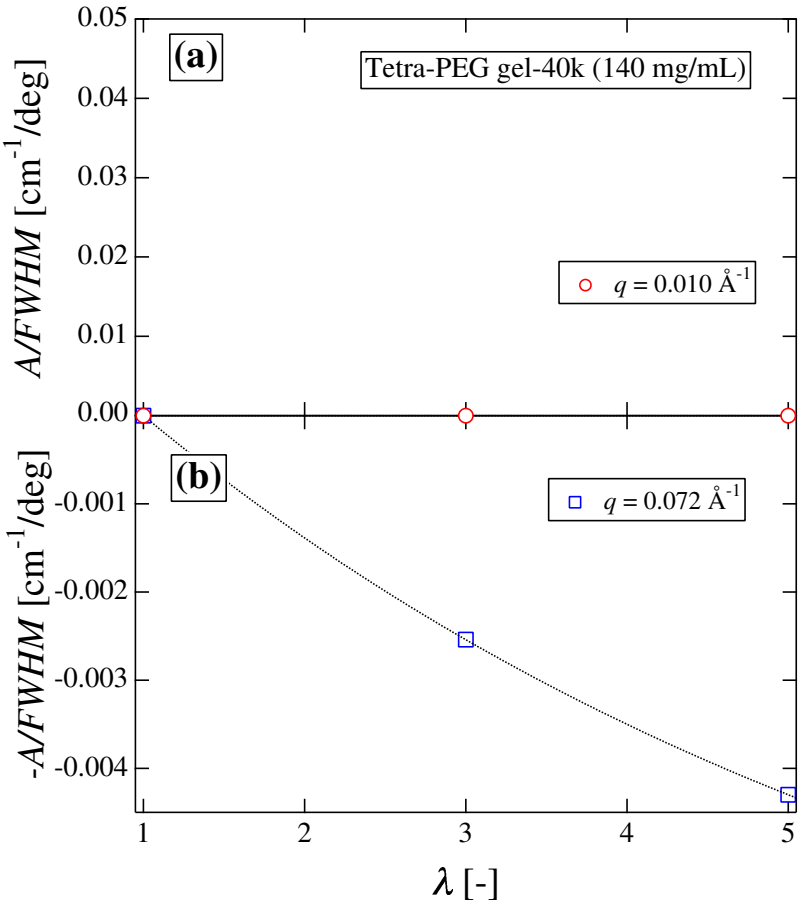

Figure 6.11: The degree of anisotropy at low- and high-q regions for Tetra-PEG gel-40k evaluated with eqs 6.6 and 6.7. The dotted lines are for the eye.

6.4.5 Deformation mechanism of Tetra-PEG gels

The difference in the network structures between Tetra-PEG gels-20k and -40k is depicted schematically in Figure 6.12. The difference in the microscopic deformation behaviors is ascribed to the degree of perfection of the network. These seem to cause an emergence of inhomogeneities upon stretching. On the other hand, such inhomogeneities do not appear in Tetra-PEG gels-40k. Now, let us discuss the deformation mechanism of polymer networks.

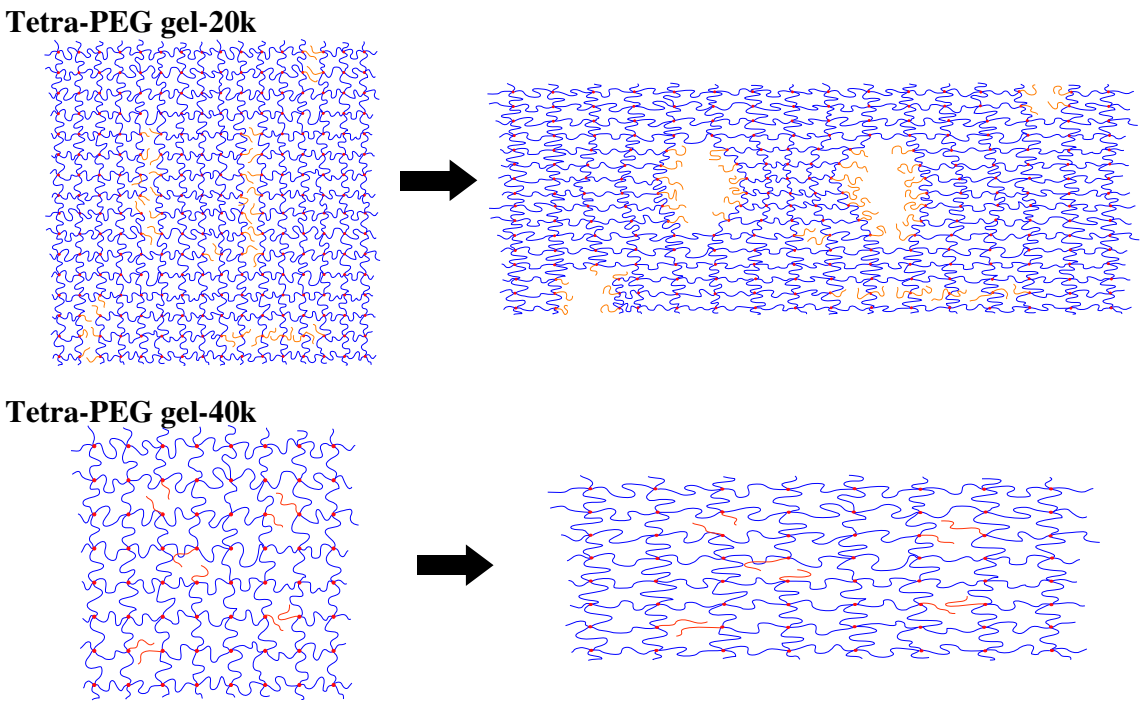

Figure 6.12: Schematic models of uniaxial deformation for Tetra-PEG gel-20k and Tetra-PEG gel-40k.

In the literature, there are many discussions on the relationship between the macroscopic and microscopic deformation,[14–17] where the change of the radius of gyration, R_g, was plotted as a function of the macroscopic deformation ratio. However, the length parameter studied in polymer gels is, in most cases, the correlation length, which is a measure of the range of thermal concentration fluctuations. If the correlation length carries some information of network inhomogeneities, it shows anisotropic change by stretching deformation as were studied by Geissler et al.,[34] Mendes et al.,[26,31] and by Shibayama et al.[32] When the deformation mechanism is discussed

for polymer gels, the anisotropy in the correlation length is often plotted, similar to the case of R_g, as a function of the macroscopic deformation ratio by using the relationship of eq 6.5.[26,32] Figure 6.13 shows the plot of the microscopic deformation ratios, $\alpha_{\rm para}$ and $\alpha_{\rm perp}$, as a function of macroscopic deformation ratio, λ. As shown here, the variation of the experimental values, i.e., $\alpha_{\rm para}$ and $\alpha_{\rm perp}$, for Tetra-PEG gels were negligibly small, and none of the polymer network models did not work at all. Mendes et al. observed strong anisotropy in SANS functions, i.e., abnormal butterfly pattern, for fully-labeled networks and concluded that these patterns could not be explained by the classical theories of network deformation.[26] Then, they tried to fit the anisotropic SANS functions with those predicted by various theories, such as heterogeneous model,[25] thermal heterogeneous model by Onuki,[35] the strain-concentration coupling model by Rabin and Bruinsma.[36,37] However, the agreement was rather poor.

Now let us discuss the scientific significance of this finding. In the case of Beltzung and coworkers, the "phantom-like" is ascribed not only to thermal motions of cross-links as well as the polymer chain segments but also to (i) imperfect cross-linking reaction and (ii) "constraint" of network chains, i.e., a high population of spatial neighbor cross-links within a domain characterized by topological neighbor cross-links. Regarding (ii), it is meaningful to discuss the ratio of the spatial to topological neighbor cross-links, Γ, i.e., the number of spatial neighbors per topological neighbors. Γ can be evaluated by,[5,14]

$$\begin{aligned} \Gamma &= \frac{4\pi}{3} n^{1/2} \qquad \text{(for bulk polymer network)} \\ \Gamma &= \frac{4\pi}{3} \phi n^{4/5} \qquad \text{(for swollen gel)} \end{aligned} \tag{6.8}$$

where n is the degree of polymerization between neighboring cross-links and ϕ is the polymer volume fraction. The value of Γ is of the order of a few tens to hundreds for bulk polymer networks, while of the order of unity for highly swollen gels. Therefore, fluctuations of polymer chains in bulk network are strongly suppressed by spatial neighbors. On the other hand, the disagreement in the behavior of the correlation length between the theory and the experiments for fully-labeled polymer networks must be mainly ascribed to the ill-formed networks with large inhomogeneities in these gels.

In the case of Tetra-PEG gels, on the other hand, it is reported that there are no entanglements in the blob defined by the topological neighbors.[20,22] Furthermore, the concentrations of Tetra-PEG gels employed in this work is rather high (e.g., 100 mg/mL for Tetra-PEG gel-20k and 140 mg/mL for Tetra-PEG gel-40k) in order to attain a large stretching ratio, e.g., $\lambda = 5.0$. In this concentration range, the measure of concentration fluctuations (i.e., the correlation length) is 13 or 9.0 Å, which is much smaller than the radius of gyration of Tetra-PEG macromers (20.1 Å, 20.6 Å, respectively for Tetra-PEG-20k (100 mg/mL) and Tetra-PEG-40k (140 mg/mL))[23] and very close to the monomer size. Hence, only thermal fluctuations around the neighborhood of the monomer itself may be possible. As a result, the concentration fluctuations observed as the correlation length is solely due to segmental thermal fluctuations in the solvent irrespective of the stretching ratio. This is a piece of strong evidence of near-"ideal" polymer network. Comparison of the mechanical properties between experiments and theories will be reported in the forthcoming paper.

6.5 Conclusion

The deformation mechanism of polymer networks was investigated by using near-"ideal" polymer network, Tetra-PEG gels. Tetra-PEG gel-20k showed slight change in the scattering intensity by deformation. An upturn in the intensity was observed at low-q region, indicating emergence of inhomogeneities. On the other hand, Tetra-PEG gel-40k did not show any anisotropy at low-q region. Though a very small anisotropy appeared by stretching the gel by 5 times, essentially no anisotropy was observed in Tetra-PEG gel-40k. On the other hand, thermal concentration fluctuations were observed due to a segmental motion around its mean position irrespective of the stretching ratio. In any case, this is the first time, to our knowledge, that deformation mechanism of polymer networks is discussed with a well-defined polymer network and no anisotropy is observed in SANS for largely deformed gel. Intentional introduction of dangling chains to polymer network resulted in lowering in network inhomogeneities. This was explained with the suppression of deformation of the majority of the network with the cost of local deformation of the defect regions.

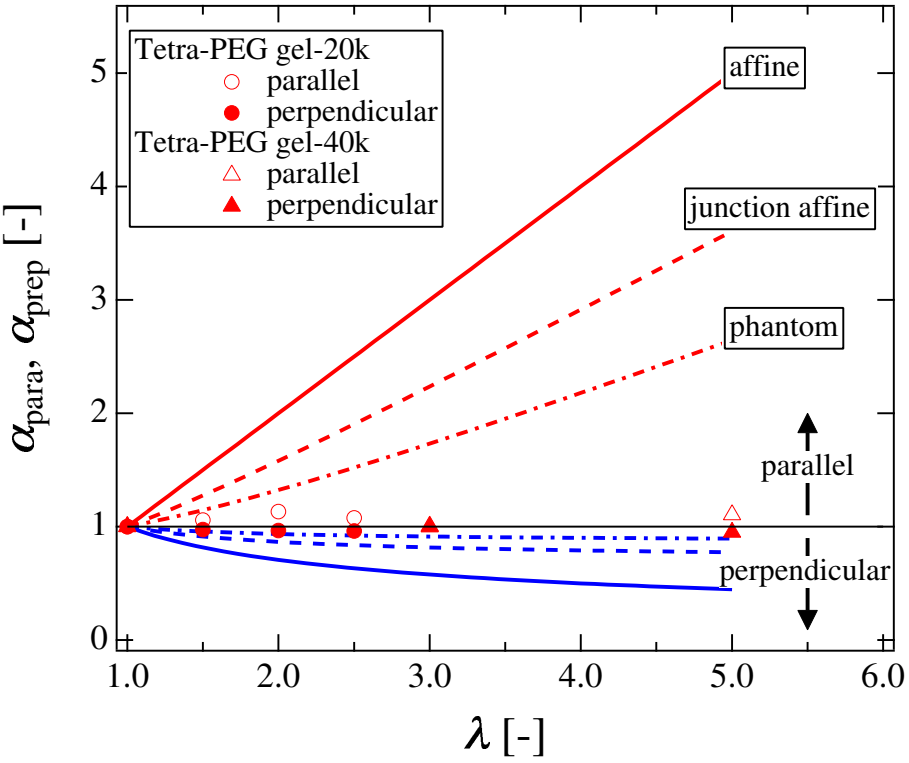

Figure 6.13: Variation of microscopic stretching ratios as a function of macroscopic stretching ratio, for affine (solid line), junction-affine (dashed line), phantom chain (chain line), and Tetra-PEG gels (circles and triangles).

References

[1] Guth, E.; James, H. M. *Rubb. Chem. Techn.* 1941, **14**, 596.

[2] James, H. M.; Guth, E. *J. Chem. Phys.* 1947, **15**, 669-683.

[3] Flory, P. J.; Rehner, J., Jr. *J. Chem. Phys.* 1943, **11**, 521.

[4] James, H. M.; Guth, E. *J. Chem. Phys.* 1953, **21**, 1039-1049.

[5] Flory, P. J.; Gordon, M.; McCrum, N. G. *Proc. R. Soc. Lond. A* 1976, **351**, 351-380.

[6] Treloar, L. R. G., *The Physics of Rubber Elasticity.* Clarendon Press: Oxford, 1975.

[7] Mark, J. E.; Erman, B., *Rubberlike Elasticity A Molecular Primer.* Wiley: NY, 1988.

[8] Flory, P. J., *Principles of Polymer Chemistry.* Cornell Univ.: Ithaca, 1953.

[9] Benoit, H.; Decker, D.; Duplessix, C.; Picot, C.; Rempp, P. *J. Polym. Sci., Polym. Phys. Ed.* 1976, **14**, 2199-2128.

[10] Pearson, D. S. *Macromolecules* 1977, **10**, 696-701.

[11] Ball, R. C.; Edwards, S. F.; Doi, M.; Warner, M. *Polymer* 1981, **22**, 1010-1018.

[12] Doi, M.; Edwards, S. F., *The Theory of Polymer Dynamics.* Oxford Univ. Press: Oxford, 1986.

[13] Gaylord, R. *J. Polym. Bull.* 1982, **8**, 325-329.

[14] Beltzung, M.; Picot, C.; Herz, J. *Macromolecules* 1984, **17**, 663.

[15] Boue, F.; Bastide, J.; Buzier, M., SANS Probing of Statics and Dynamics of Polymer Networks Under Deformation: Relation Between the Scatterings of Labeled Paths and Labeled Free Chains Dissolved in the Network. In *Molecular Basis of Polymer Networks*, Baumgartner, A.; Picot, C. E., Eds. Springer: Berlin, 1989; pp 65-81.

[16] Ullman, R. *Macromolecules* 1982, **15**, 582-588.

[17] Ullman, R. *Macromolecules* 1982, **15**, 1395-1402.

[18] Tsay, H. M.; Ullman, R. *Macromolecules* 1988, **21**, 2963-2972.

[19] Sakai, T.; Matsunaga, T.; Yamamoto, Y.; Ito, C.; Yoshida, R.; Suzuki, S.; Sasaki, N.; Shibayama, M.; Chung, U. *Macromoleules* 2008, **41**, 5379-5384.

[20] Akagi, Y.; Matsunaga, T.; Shibayama, M.; Chung, U.; Sakai, T. *Macromolecules* 2010, **43**, 488-493.

[21] Matsunaga, T.; Sakai, T.; Akagi, Y.; Chung, U.; Shibayama, M. *Macromolecules* 2009, **42**, 1344-1351.

[22] Sakai, T.; Matsunaga, T.; Akagi, Y.; Kurakazu, M.; Chung, U.; Shibayama, M. *Macromol. Rapid Comm.* 2010, **31**, 1954-1959.

[23] Matsunaga, T.; Sakai, T.; Akagi, Y.; Chung, U.; Shibayama, M. *Macromolecules* 2009, **42**, 6245-6252.

[24] Shibayama, M. *Macromol. Chem. Phys.* 1998, **199**, 1-30.

[25] Bastide, J.; Leibler, L.; Prost, J. *Macromolecules* 1990, **23**, (6), 1821.

[26] Mendes, E.; Oeser, R.; Hayes, C.; Boue, F.; Bastide, J. *Macromolecules* 1996, **29**, 5574.

[27] Okabe, S.; Nagao, M.; Karino, T.; Watanabe, S.; Adachi, T.; Shimizu, H.; Shibayama, M. *J. Appl. Cryst.* 2005, **38**, 1035-1037.

[28] Okabe, S.; Karino, T.; Nagao, M.; Watanabe, S.; Shibayama, M. *Nuclear Inst. and Methods in Physics Research, A* 2007, **572**, 853-858.

[29] Shibayama, M.; Matsunaga, T.; Nagao, M. *J. App. Cryst.* 2009, **42**, 621-628.

[30] Mendes, E. J.; Lindner, P.; Buzier, M.; Boue, F.; Bastide, J. *Phys. Rev. Lett.* 1991, **66**, 1595.

[31] Mendes, E.; Schosseler, F.; Isel, F.; Boue, F.; Bastide, J.; Candau, S. J. *Europhys. Lett.* 1995, **32**, 273.

[32] Shibayama, M.; Kawakubo, K.; Ikkai, F.; Imai, M. *Macromolecules* 1998, **31**, 2586-2592.

[33] Bastide, J.; Leibler, L. *Macromolecules* 1988, **21**, 2647.

[34] Geissler, E.; Horkay, F.; Hecht, A. M. *J. Chem. Phys.* 1995, **102**, 9129-9132.

[35] Onuki, A. *J. Phys. II France* 1992, **2**, 45-61.

[36] Rabin, Y.; Bruinsma, R. *Europhys. Lett.* 1992, **20**, 79.

[37] Bruinsma, R.; Rabin, Y. *Phys. Rev. E* 1994, **49**, 554.

Chapter 7

Highly Elastic and Deformable Hydrogel Formed from Tetra-arm Polymers

7.1 Introduction

If a polymer network were an infinite series of uniform meshes connected by cross-links and had no inhomogeneities, the macroscopic properties of the network would be precisely controlled by the polymerization degree and the first order structure of the mesh chains. Such a perfectly cooperative network is called an "ideal" network. In reality, however, inhomogeneities do exist and affect the cooperativeness between the meshes, compromising the macroscopic properties. The spatial inhomogeneity is an inhomogeneous distribution of polymer segments in the network, and is observed as an excess scattering in small-angle light scattering (SALS) as well as small-angle neutron scattering (SANS) measurements.[1–3] The connectivity inhomogeneity includes dangling chains and elastically redundant loops, while the topological inhomogeneity includes trapped entanglements. The connectivity and topological inhomogeneities are generally discussed in the context of the theory of tree-like structure and elastically effective chains.[4,5] Because the connectivity and topological inhomogeneities have the opposite effect on the elastically effective chains, these contribution cannot be decomposed. Therefore, the understanding of the rubber elasticity remains a controversial issue in polymer science. In the history of the development of polymer networks, primitive randomly cross-linked networks were formed by radical polymerization using monomers and cross-linkers or by the vulcanization of polymer melts (Figure 7.1(a), top). Although these cross-linking methods are easy to perform and

have been used widely up to now, they yield networks with a large number of inhomogeneities.[6] In an attempt at realizing an ideal network, model networks were formed by using a modular construction method, that is, by using monodispersed chain extenders and multifunctional cross- linkers (Figure 7.1(b), middle).[7,8] Due to the use of the preprogrammed and monodispersed chain extenders, the degree of polymerization between chemical cross-links was precisely controlled. However, it was revealed that the obtained model networks did contain a substantial number of inhomogeneities.[9,10]

Tetra-PEG modules are superior to the conventional modules in the following ways: (i) Tetra-arm modules behave as impenetrable space-filled spheres in the solution; (ii) each Tetra- arm module contains one node and four chain extenders within its structure; and (iii) the amine-terminated Tetra-arm module has electrostatic repulsive amine groups that promote the homogeneous mixing of two Tetra-arm modules. These advantages contribute to the elimination of the inhomogeneities in the Tetra network. The SANS results suggested that practically no spatial inhomogeneity exists in the regions up to 200 nm in size.[11,12] The spatial inhomogeneity did not appear even under the equilibrium swelling condition, which has generated obvious spatial inhomogeneity in other polymer networks. Furthermore, the gelation process is well described by the reaction rate equation between the amine and activated-ester.[13] These results strongly suggest that the Tetra network is distinct from the other conventional model networks and is much closer to an ideal network. The ideal network structure is expected to have high mechanical properties, because the cooperativeness of the network equalizes the stress distribution. In this paper, we investigate representative mechanical properties of the Tetra network to compare with those of the ideal network.

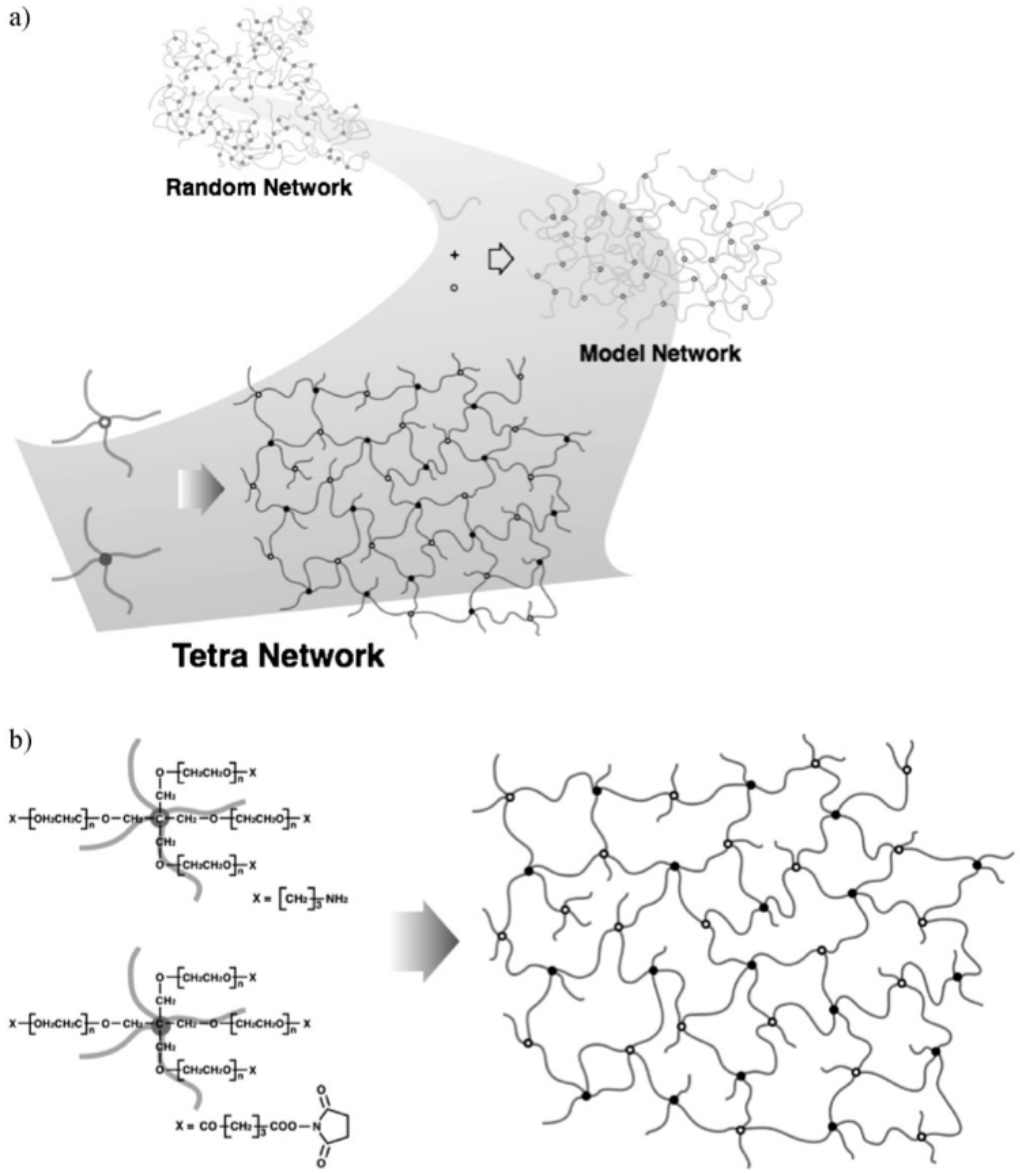

Figure 7.1: (a) Evolution of polymer networks toward an ideal network. (b) Scheme of fabrication process of Tetra network.

7.2 Experimental

7.2.1 Rheological Property of the Tetra Network

Constant amounts of Tetra-amine-terminated PEG (TAPEG) and tetra-NHS-glutarate-terminated PEG (TNPEG) ($10 - 80$ mg/mL) with $M_{\mathrm{w}} = 10$k g/mol were dissolved in phosphate buffer (pH 7.4) and phosphate-citric acid buffer (pH 5.8), respectively.

In order to control the reaction rate, the ionic strengths of the buffers were set to 25×10^3 M.[11] The two solutions were mixed in a 50mL Falcon tube for 10s using the voltex mixer (Delta mixer Se-08, Taitec, Japan). Then, the resultant solution was poured into the interstice of the double cylinder of a rheometer (MCR501, Anton Paar, Austria). The storage modulus (G'), loss modulus (G''), and loss tangent ($\tan \delta$) were measured at 12 h after mixing at a constant strain (1%) and a constant frequency (1 Hz) at 20 $^\circ C$ with a double cylinder geometry with 26.7 and 28.9-mm diameter cylinders. In the bouncy test, constant amounts of TAPEG and TNPEG (160 mg/mL) with Mw = 10k g/mol were dissolved in phosphate buffer (pH 7.4) and phosphate-citric acid buffer (pH 5.8), respectively. The ionic strengths of the buffers were set to 100×10^3 M.[11] Two solutions were mixed, and the resulting solution was poured into the sphere-shaped mold. After 12 h from the mixing, the sphere-shaped gel was dropped from the height of 15 cm, and monitored by the high-speed camera.

7.2.2 Stretching Property of the Tetra Network

Constant amounts of TAPEG and TNPEG (160 mg/mL) with M_w = 20k g/mol were dissolved in phosphate buffer (pH 7.4) and phosphate-citric acid buffer (pH 5.8), respectively. The ionic strengths of the buffers were set to 100×10^3 M.[11] Two solutions were mixed, and the resulting solution was poured into the mold. At least 12 h were allowed for the completion of the reaction before the following experiment was performed. The specimens were used in as-prepared state. The stretching measurement was carried out on dumbbell-shaped films using a mechanical testing apparatus (CR-500DX-SII rheometer; Sun Scientific Co., Tokyo, Japan) at a cross-head speed of 0.1 mm/s.

7.2.3 Compression Property of the Tetra Network

Constant amounts of TAPEG and TNPEG (160 mg/mL) with M_w = 20k g/mol were dissolved in phosphate buffer (pH 7.4) and phosphate-citric acid buffer (pH 5.8), respectively. The ionic strengths of the buffers were set to 100×10^3 M.[11] Two solutions were mixed, and the resulting solution was poured into the mold. At least 12

h were allowed for the completion of the reaction before the following experiment was performed. The specimens were used in as-prepared state. The compression test was carried out on cylinder-shaped (15 mm in diameter and 7.5 mm in height) specimens using a mechanical testing apparatus (INSTRON 3365; Instron Corporation, Canton, MA) at a velocity of 1.05 mm/min.

7.3 Results and Disscusion

7.3.1 Rheological Property of the Tetra Network

First, we measured the dynamic mechanical response of the Tetra network-10k, where 10k indicates that the molecular weight of the Tetra-arm module is 10 kg/mol, i.e., the length of each arm is 2.5 kg/mol. The storage modulus (G'), loss modulus (G''), and loss tangent (tan δ) are shown as a function of the initial polymer fraction (ϕ_0) (Figure 7.2(a)). Theoretically, the value of G' is proportional to the concentration of elastically effective chains.[14] G'' is positively correlated with the connectivity and topological inhomogeneities.[15,16] The tan δ represents the G'' normalized by G', i.e., G'' /G', and is expected to be zero for the ideal network. When the initial concentration of the Tetra-arm module was above 12 mg/mL ($\phi_0 = 0.011$), the elasticity appeared; namely, the gelation threshold was reached. As the ϕ_0 increased above the gelation threshold, G' increased, while tan δ decreased, suggesting the proceeding of the network formation and the elimination of connectivity inhomogeneities. At a concentration approximately above 30 mg/mL ($\phi_0 = 0.027$), the G'' and tan δ became extremely low, below the lower measurable limit of the rheometer (tan $\delta \sim 10^{-4}$). The value of tan δ was by one to three orders smaller than that of the other model networks and ringing gels;[16,17] that is, practically no external energy applied to the network was dissipated, and the Tetra network had extremely small connectivity and topological inhomogeneities. Indeed, when a sphere-shaped Tetra network whose structure consisted of 84% water was dropped onto a hard floor, it sprang back near the initial height (the reflection coefficient ~ 0.84) in a similar fashion to a power ball made of vulcanized polybutadiene (Figure 7.3). Furthermore, when the Tetra network was tapped with a finger, a ringing sound was emitted in the same manner as for ringing gels, suggesting that thousands of oscillations were permitted before

the deformation energy was dissipated into frictional energy.[17]

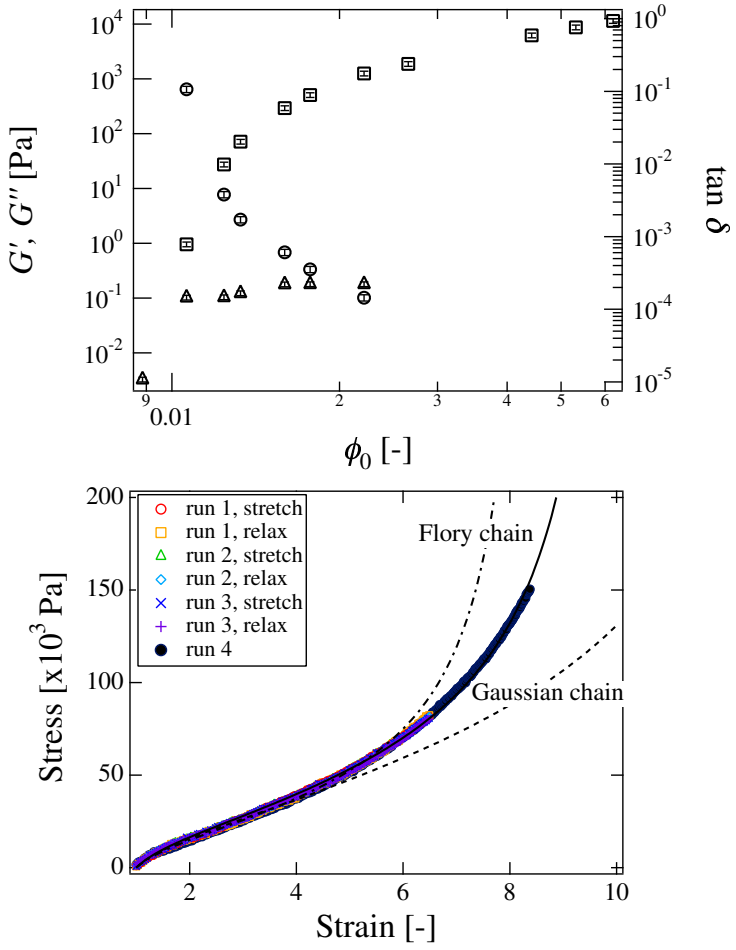

Figure 7.2: G', G'', and tan δ of Tetra network 10k as a function of ϕ_0. The square, triangle, and circle represents the G', G'' (left axis), and tan δ (right axis), respectively. (b) Stretching stress-strain curve of Tetra network 20k ($\phi_0 = 0.14$). The solid line, dashed line, and chain lines represent the fitting result by Equation 7.2 using R_0 as a free parameter, the fitting result assuming the Gaussian chain, and the fitting result assuming the Flory chain, respectively.

7.3.2 Stretching Property of the Tetra Network

We performed a stretching test of the Tetra network-20k ($\phi_0 = 0.14$). Initially, the Tetra network was stretched to $\lambda = 6.5$ and released; this stretch and release was repeated three times, and then the network was stretched to the limit (Figure 7.2(b)). The average value of $\lambda_{\max}$ was 8.1 and the maximum value was 9.9. Then, we tried to

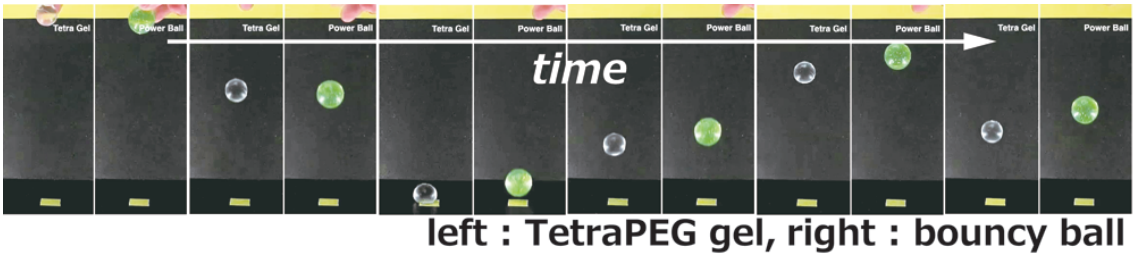

Figure 7.3: Stroboscopic photos of (left) Tetra-PEG ball and (right) a commercial power ball.

describe the stress-strain (SS) curve of the Tetra network by assuming that it consists of uniformly packed "elastic blobs". Here, the elastic blobs are defined as individual Tetra-arm modules behaving as nanoscopic rubber balls capable of complete shape recovery against deformation. Considering the finite extensibility of the polymer chain, the force applied to the single chain (F) is represented using the inverse-Langevin equation as

$$F = \frac{kT}{b} L^{-1}\left(\frac{R_0\lambda}{Nb}\right), \tag{7.1}$$

where R_0 is the initial end-to-end distance of a polymer, N (= 230) the polymerization degree between neighboring cross-links, and λ is the strain. If the incompressibility of a network is taken into account, the relationship between the stress (σ) and the strain (λ) of a polymer network constructed by ν inverse-Langevin elastic blobs is represented by

$$\sigma = \frac{\nu kT}{3}\frac{R_0}{b}\left[L^{-1}\left(\frac{R_0\lambda}{Nb}\right) - \lambda^{-3/2}L^{-1}\left(\frac{R_0\lambda^{-1/2}}{Nb}\right)\right]. \tag{7.2}$$

According to the literature, b was set to 3.3 Å.[18] The solid line represents a curve fit with Equation 7.2. Surprisingly, the SS curve of the Tetra network is nicely fitted with Equation 7.2 using the intrinsic fitting parameters. The resultant R_0 was 7.1 nm; it was in the range between the Gaussian (5.0 nm) and the Flory (8.6 nm) limit, suggesting that elastic blobs take the intermediate conformation between the two models. This result is also in good agreement with our previous SANS result showing that the Tetra-arm module takes a more contracted configuration than the Flory chain.[12] The $\lambda_{\max}$ (= Nb/R_0) obtained from the fitting result was 10.6, corresponding well to our experimental result and that of single polymer chain ($\lambda_{\max} \sim 11.4$) having similar degree of polymerization ($N \sim 200$).[19] It should be

noted that the SS curves for conventional polymer networks, in general, cannot be represented by Equation 7.2 using the intrinsic fitting parameters.[20] This is probably because the exact value of N cannot be defined due to a variety of inhomogeneities, or because trapped entanglements act as pseudo cross-links, or because the polymers are likely to be crystallized in the larger l region, or all. Thus, when a large strain is applied to conventional networks, weak regions are broken at a lower elongation ratio, and the crystallized regions are unlikely to be relaxed to the initial state, so that hysteresis is observed.[21] In contrast, no hysteresis was observed in the Tetra network, even when the specimens were repeatedly stretched to $\lambda = 6.5$ and released. These results strongly suggest that the Tetra network has an extraordinarily uniform network structure, and that its elasticity can be represented by uniformly packed elastic blobs.

7.3.3 Compression Property of the Tetra Network

Finally, a compression test was performed on the Tetra network-20k ($\phi_0 = 0.14$). Figure 7.4(a) and (b) shows a typical result. The compression breaking strength of polymer hydrogels is one of the most important properties for biomedical use, because compression is the deformation mode most often experienced in the body. The average maximum breaking stress was 25 MPa, and the average compression modulus was 99.7 kPa. Approximately half of the specimens were not broken at approximately 100% compression strain and 27 MPa of stress, which is the upper measurable limit of the mechanical apparatus. Although the compression modulus was one or two order smaller than that of native articular cartilage, the breaking stress surpasses that of the native articular cartilage ($\sim$10 MPa),[22] and is comparable to that of the high-performance hydrogels having unique double network structures with high-mechanical strength.[23]

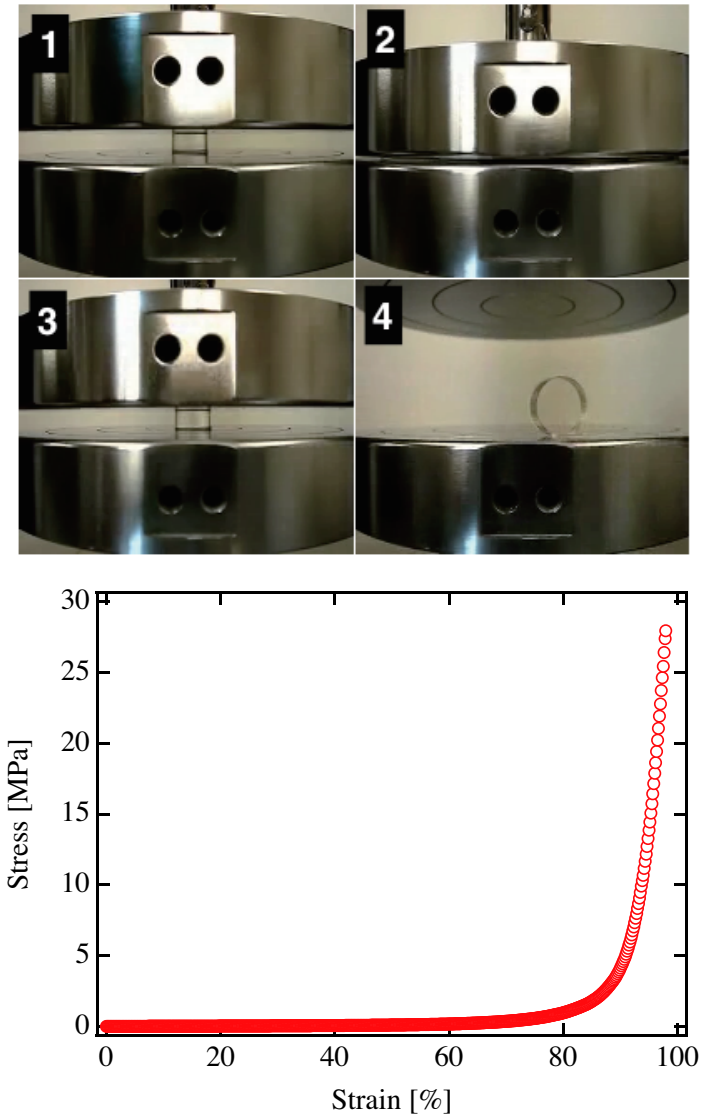

Figure 7.4: (a) Photograph demonstrating the compression test of the Tetra network. (b) The compression stress-strain curve of Tetra network 20k ($\phi_0 = 0.14$).

7.4 Conclusion

The major findings of this study on the Tetra network are as follows: (i) the value of tan δ was extremely low ($\sim 10^{-4}$); (ii) the stress-strain relationship could be described by the theoretical equation for the ideal network; and (iii) the maximum breaking strength was extremely high ($\sim$ 27 MPa). It is noteworthy that the stress-strain relationship on a macroscopic scale corresponded well to that of elastic blobs on a microscopic scale. In other words, each mesh chain equivalently and cooperatively contributed to the elasticity. This unique cooperativity was caused by the near-absence of the spatial inhomogeneities and trapped entanglements. Thus, to our knowledge, the Tetra network is closer to an ideal network than any other conventional model networks. Because the Tetra network can be treated as uniformly packed elastic blobs, we can translate the knowledge of the single polymer chains seamlessly into the design of polymer materials. We strongly believe that the Tetra network will contribute not only to the design of advanced polymer materials but also to further development of the theory of rubber elasticity.

References

[1] J. Bastide, L. Leibler, *Macromolecules* 1988, **21**, 2647.

[2] E. Mendes, R. Oeser, C. Hayes, F. Boue, J. Bastide, *Macromolecules* 1996, **29**, 5574.

[3] M. Shibayama, Y. Shirotani, Y. Shiwa, *J. Chem. Phys.* 2000, **112**, 442.

[4] M. Rubinstein, S. Panyukov, *Macromolecules* 2002, **35**, 6670.

[5] K. Dusek, V. Vojta, Br. *Polym. J.* 1977, **9**, 164.

[6] E. Mendes, A. Hakiki, J. Herz, F. Boue, J. Bastide, *Macromolecules* 2004, **37**, 2643.

[7] J. E. Mark, *Rubberlike Elasticity a Molecular Primer*, Wiley, New York 1988.

[8] G. Hild, *Prog. Polym. Sci.* 1998, **23**, 1019.

[9] M. Shibayama, H. Takahashi, S. Nomura, *Macromolecules* 1995, **28**, 6860.

[10] W. Michalke, M. Lang, S. Kreitmeier, D. Goritz, *J. Chem. Phys.* 2002, **117**, 6300.

[11] T. Matsunaga, T. Sakai, Y. Akagi, U. I. Chung, M. Shibayama, *Macromolecules* 2009, **42**, 6245.

[12] T. Matsunaga, T. Sakai, Y. Akagi, U. I. Chung, M. Shibayama, *Macromolecules* 2009, **42**, 1344.

[13] M. Kurakazu, T. Katashima, M. Chijiishi, K. Nishi, Y. Akagi, T. Matsunaga, M. Shibayama, U. I. Chung, T. Sakai, *Macromolecules* 2010, **43**, 3935.

[14] N. R. Langley, K. E. Polmanteer, *J. Polym. Sci. Polym. Phys.* 1974, **12**, 1023.

[15] S. F. Edwards, H. Takano, E. M. Terentjev, *J. Chem. Phys.* 2000, **113**, 5531.

[16] M. A. Villar, E. M. Valles, *Macromolecules* 1996, **29**, 4081.

[17] M. Gradzielski, H. Hoffmann, G. Oetter, *Colloid Polym. Sci.* 1990, **268**, 167.

[18] A. Harada, J. Li, M. Kamachi, *Macromolecules* 1993, **26**, 5698.

[19] Y. Sakai, T. Ikehara, T. Nishi, K. Nakajima, M. Hara, *Appl. Phys. Lett.* 2002, **81**, 724.

[20] R. D. Groot, A. Bot, W. G. M. Agterof, *J. Chem. Phys.* 1996, **104**, 9202.

[21] C. O. Horgan, R. W. Ogden, G. Saccomandi, *Proc. R. Soc. Lond.* 2004, **460**, 1737.

[22] H. Abe, K. Hayashi, M. Sato, *Data Book of Mechanical Properties of Living Cells, Tissues, and Organs*, Springer, Berlin 1996.

[23] J. P. Gong, Y. Katsuyama, T. Kurokawa, Y. Osada, *Adv. Mater.* 2003, **15**, 1155.

Summary

The relationship between structure and physical properties of Tetra-PEG gels was investigated from the viewpoint of inhomogeneities in network structure. Especially, we focused on the structural analysis for Tetra-PEG solutions and Tetra-PEG gels as a model network by using a small-angle neutron scattering (SANS) technique. The details of the respective chapters are summarized below.

In Chapter 2, a simple but reasonably-accurate method for incoherent scattering intensity evaluation for H-containg materials is proposed. This method (the T-method) requires only transmission and thickness of the sample and is given by,

$$\left(\frac{\mathrm{d}\Sigma}{\mathrm{d}\Omega}\right)_{\mathrm{inc}} = \frac{1}{4\pi}\frac{1-T}{tT}. \tag{7.3}$$

In order to apply, the following three conditions have to meet, (1) negligible absorption, (2) incoherent scattering is predominant, and (3) inapplicable to strong coherent scattering, such as critical phenomena. It is needless to mention that absolute intensity calibration is inevitable to apply this method for quantitative analyses of SANS data. It is demonstrated that multiple scattering of incoherent scattering from H-atoms cannot be ignored for most cases of SANS measurements. The validity and applicability of the T-method were carefully examined for (1) mixtures of H_2O and D_2O (strong incoherent scatterers), (2) nanoemulsion (strong coherent scatterers), (3) gels (weak coherent scatterers), and (4) a concentrated surfactant system (strong coherent scatter with inter-particle interference), and were found to be quite successful, particularly for H-rich samples of sample thicknesses being 0.1 cm to 0.4 cm. This method might not work for systems with critical concentration fluctuations because forward scattering is extraordinarily dominated not by incoherent scattering but by coherent scattering. In this dissertation, the subtraction of incoherent scattering intensity for all SANS data was carried out by means of the T-method.

In Chapter 3, we successfully designed and fabricated a novel homogeneous hydrogel by combining two symmetrical tetrahedron-like macromonomers of the same size. Tetra-PEG gel was prepared through a highly stoichiometrical and symmetrical gelation process. The breaking strength was extremely high, being comparable to that of native articular cartilage.We conclude that Tetra-PEG gel has an extremely homogeneous network structure. To the best of our knowledge, this is the first successful fabrication of a homogeneous chemical hydrogel having high mechanical strength. Since the mechanical properties of ideal networks can be modified by increasing the length between cross-linking points, we plan to further increase the mechanical properties of Tetra-PEG gel by controlling the PEG arm length.

In Chapter 4, structure analyses of Tetra-PEG gels were carried out by means of swelling experiments and SANS, and the results were discussed by taking into account the mechanical properties of the same systems. The following facts are disclosed. (1) Tetra-PEG gels are stoichiometrically prepared irrespective of the initial polymer concentration, and their swelling behaviors are well predicted by the Flory-Rehner theory. (2) The mechanical moduli of Tetra-PEG gels, E and G, are proportional to the initial polymer concentration and is one order of magnitude larger than the corresponding gels made with similar tetra-arm PEG gels prepared with a low-molecular-weight coupling reagent. This indicates that cross-end-coupling of A- and B-type tetra-PEG is essential for gel preparation with extremely low defects. (3) The scattering functions of the macromers can be well reproduced by the scattering function for star polymers. (4) SANS functions of Tetra-PEG gels can be described by simple Ornstein-Zernike function without excess scattering component originating from cross-linking inhomogeneities. This means that Tetra-PEG gels are extremely homogeneous, and an "ideal" network free from defects is formed. (5) Preparation in non-stoichiometric composition leads to formation of defects in the polymer chain network and results in a significant depression of the mechanical properties. Structural models of macromer solutions and of Tetra-PEG gels, which account for the advanced mechanical properties of Tetra-PEG gels, are proposed.

In Chapter 5, the structures of Tetra-PEG gels in as-prepared and swollen states

were investigated by small-angle neutron scattering (SANS) as well as static light scattering (SLS). The following facts are disclosed: (1) The TAPEG macromer solutions, consisting of tetra-arm polymer chains, are not interpenetrable due to the presence of end groups, and the individual chains behave as hard spheres. Hence, the radius of gyration, R_g scales with $\phi_0^{-1/3}$. (2) The structure factors of both as-prepared and swollen gels in SANS regime can be represented by Ornstein-Zernike type scattering functions and be superimposed to single master curves, irrespective of the molecular weight. (3) No inhomogeneities appeared even by swelling. (4) However, in SLS regime, a steep upturn was observed in SANS curves in as-prepared Tetra-PEG gels, indicating the presence of PEG chain clusters or defects. A master-curve relationship holds also in SLS regime for a gel having the same molecular weight, indicating a self-similar network structure in Tetra-PEG gels. (5) The upturn in scattering intensity is assigned to be a clustered structure as is often observed in PEG in water and/or network defects. The upturn is suppressed by increasing M_w due to a formation of more regular network structures with less inhomogeneities. It is concluded that Tetra-PEG gels have no noticeable entanglements, but have self-similar structures with respect to M_w, and form ideal tetrafunctional polymer networks, provided that M_w is high enough ($\sim 40 \times 10^3$).

In Chapter 6, the deformation mechanism of polymer networks was investigated by using near-"ideal" polymer network, Tetra-PEG gels. Tetra-PEG gel-20k showed slight change in the scattering intensity by deformation. An upturn in the intensity was observed at low-q region, indicating emergence of inhomogeneities. On the other hand, Tetra-PEG gel-40k did not show any anisotropy at low-q region. Though a very small anisotropy appeared by stretching the gel by 5 times, essentially no anisotropy was observed in Tetra-PEG gel-40k. On the other hand, thermal concentration fluctuations were observed due to a segmental motion around its mean position irrespective of the stretching ratio. In any case, this is the first time, to our knowledge, that deformation mechanism of polymer networks is discussed with a well-defined polymer network. Intentional introduction of dangling chains to polymer network resulted in lowering in network inhomogeneities. This was explained with the suppression of deformation of the majority of the network with the cost of local deformation of the defect regions.

In Chapter 7, we discussed the relationship between microscopic structure and macroscopic mechanical properties of Tetra-PEG gels. The major findings are as follows: (i) the value of tan δ was extremely low ($\sim 10^4$); (ii) the stress-strain relationship could be described by the theoretical equation for the ideal network; and (iii) the maximum breaking strength was extremely high ($\sim$ 27 MPa). It is noteworthy that the stress-strain relationship on a macroscopic scale corresponded well to that of elastic blobs on a microscopic scale. In other words, each mesh chain equivalently and cooperatively contributed to the elasticity. This unique cooperativity was caused by the near-absence of the spatial inhomogeneities and trapped entanglements. Thus, to our knowledge, theTetra-PEG gel network is closer to an ideal network than any other conventional model networks. Because the Tetra-PEG gel network can be treated as uniformly packed elastic blobs, we can translate the knowledge of the single polymer chains seamlessly into the design of polymer materials. We strongly believe that the Tetra-PEG gel network will contribute not only to the design of advanced polymer materials but also to further development of the theory of rubber elasticity.

In conclusion, Tetra-PEG gels may be valuable in application for practical use. For biomedical applications, hydrogels are required to meet three criteria at the same time: high-mechanical properties, biocompatibility and an easy fabrication process. Tetra-PEG gel has successfully satisfied all three criteria. First, it has attained high-mechanical properties using symmetrical tetrahedron-like constitutional polymers to form an extremely homogeneous structure. Second, Tetra-PEG gel uses biocompatible tetrahedron-like PEG with mutually reactive terminal groups; its gel formation reaction does not use or produce any toxic substance. Third, Tetra-PEG gel can be fabricated within a few minutes through in situ gelation by simply mixing two macromonomer solutions. Because of these combined merits, we strongly believe that Tetra-PEG gel and its derivatives may be useful in the biomedical field. Tetra-PEG gel will not only be useful as a biomaterial but may also contribute to the understanding of ideal networks. Furthermore, as we may be able to apply this strategy regardless of polymer species, we believe that this strategy will have a strong impact on the field of gel research.

List of Publications

Original Papers

1. M. Shibayama, T. Matsunaga, and M. Nagao, "Evaluation of Incoherent Scattering Intensity by Transmission and Sample thickness" *Journal of Applied Crystallography A*, **42**, 621-628 (2009)
   (**chapter 2**)

2. T. Sakai, T. Matsunaga, Y. Yamamoto, C. Ito, R. Yoshida, S. Suzuki, N. Sasaki, M. Shibayama, and U. Chung, "Design and fabrication of a high-strength hydrogel with ideally homogeneous network structure from tetrahedron-like macromonomers", *Macromolecules*, **41**, 5379-5384 (2008)
   (**chapter 3**)

3. T. Matsunaga, T. Sakai, Y. Akagi, U. Chung, and M. Shibayama, "Structure characterization of Tetra-PEG Gel by Small-angle Neutron Scattering", *Macromolecules*, **42**, 1344-1351 (2009)
   (**chapter 4**)

4. T. Matsunaga, T. Sakai, Y. Akagi, U. Chung, and M. Shibayama, "SANS and SLS Studies on Tetra-Arm PEG Gels in As-Prepared and Swollen States", *Macromolecules*, **42**, 6245-6252, (2009)
   (**chapter 5**)

5. T. Matsunaga, H. Asai, Y. Akagi, T. Sakai, U. Chung, and M. Shibayama, "SANS Studies on Tetra-PEG Gel under Uniaxial Deformation", *Macromolecules*, acceptted.

6. T. Sakai, Y. Akagi, T. Matsunaga, M. Kurakazu, U. Chung and M. Shibayama, "Highly Elastic and Deformable Hydrogel Formed from Tetra-arm Polymers",

Macromolecular Rapid Communication, **31**, 1954-1959 (2010)
(**chapter 7**)

Other publications

- T. Matsunaga and M. Shibayama, "Gel point determination of gelatin hydrogels by dynamic light scattering and rheological measurements", *Physical Review E, Rapid Communication*, **76**, 030401 (2007)
- T. Matsunaga, H. Endo, M. Takeda, and M. Shibayama, "Microscopic Structure Analysis of Clay-Poly(ethylene oxide) Mixed Solution in a Flow Field by Contrast-Variation Small-Angle Neutron Scattering", *Macromolecules*, **43**, 5075-5082 (2010)